QUANTITATIVE EVALUATION OF REJUVENATORS TO RESTORE EMBRITTLEMENT TEMPERATURES IN OXIDIZED ASPHALT MIXTURES USING ACOUSTIC EMISSION SOURCE LOCATION TECHNIQUES

BY

ZHE SUN

THESIS

Submitted in partial fulfillment of the requirements
for the degree of Master of Science in Systems and Entrepreneurial Engineering
in the Graduate College of the
University of Illinois at Urbana-Champaign, 2016

Urbana, Illinois

Adviser:

Professor Henrique Reis

ABSTRACT

Asphalt rejuvenator was designed to be an asphalt additive to revitalize, provide sealing and restore the properties of aged asphalt concrete. Its penetration depth into asphalt concrete, and its ability of restoring asphalt's embrittlement temperature was quantitatively investigated in this study using acoustic emission analysis and source location techniques. Four asphalt specimens, which have been oven-aged for 36 hours, were tested using the same acoustic emission approach after two, four, six, and eight weeks dwell time after being rejuvenated. Iterative and non-iterative acoustic emission source location approaches were used to determine the location of cracks inside the specimens in a low temperature environment. It was observed that the rejuvenator penetrated half of the height of the asphalt specimen at the end of the fourth week while the top half portion of the rejuvenated asphalt specimen has a lower embrittlement temperature than the bottom half portion. After four weeks of dwell time, the rejuvenator-treated samples had recuperated the embrittlement temperatures to the virgin condition. The rejuvenator kept acting upon the binder after four weeks of dwell time. At the end of the sixth week, the embrittlement temperature was observed to be homogeneous across the height of the specimen, and after eight weeks the specimen had an embrittlement temperature about 7 degrees lower than the embrittlement temperature of the virgin specimen. Furthermore, the concepts developed here were shown to be applicable to acoustic emission analysis on real pavements by installing the sensors only at the top surface of pavements.

To Father and Mother.

ACKNOWLEDGMENTS

I would like to express my deepest appreciation to my adviser, Professor Henrique Reis, who provided me the opportunity to work in the Non-Destructive Testing and Evaluation Laboratory at the University of Illinois at Urbana-Champaign. Thank you for your kind support and patient guidance throughout my academic study, as well as numerous insightful advise to improve my work and help me find my way through life's obstacles. I would not have been able to achieve this milestone of my life without your knowledge and help.

Thanks so much to my colleagues and lab mates: Ms. Megan McGovern, Mr. Nicholas Farace and Mr. Behzad Behnia for the encouragements and lots of help. You have made the experience in this lab so much fun and memorable. Thank you all for giving me such a meaningful and rewarding lifetime experience.

TABLE OF CONTENTS

LIST OF TABLES

LIST OF FIGURES

CHAPTER 1: INTRODUCTION

1.1 Problem Statement

In the United States, there are many ongoing efforts to develop more efficient maintenance strategies for asphalt pavements to help achieve both economic and environmental goals. It has been estimated that about 96% of the approximately 2.4 million miles of paved roads in the country are surfaced with asphalt [2]. A sustainable maintenance of these roadways becomes an issue of great importance. The popularity of asphalt concrete derives from the fact that it delivers a smooth, quiet surface, and can be rapidly constructed, particularly during rehabilitation, i.e., resurfacing, operations. Immediately after construction, asphalt is a remarkably tough and resilient material. This is mainly due to the fact that asphalt concrete is comprised of a highly ductile and healable matrix, i.e. asphalt binder, combined with hard aggregate particles, i.e., mineral sands and crushed stones, which provides stiffness and strength to the system. When compared to Portland cement Concrete, asphalt concrete can possess 5, 10, or even 20 times more fracture energy due to its ductile binder matrix and toughness-adding aggregate structure. Although traffic loads and thermal cycles tend to cause micro-damage in the asphalt binder system under certain conditions, this damage can be healed provided the binder retains sufficient fluidity. As a result, even as the pavement develops minor rutting and distributed micro-damage, pavement serviceability and smoothness can remain at a very high level for many years of service.

Figure 1.1: Oxidative aging of asphalt concrete pavements. With increasing oxidative aging in the top material layer, the pavement becomes increasingly more susceptible to damage accumulation due to mechanical and environmental loads.

However, with exposure to air and moisture content, asphalt binder ages with time, particularly near the pavement surface, which causes the binder to lose its ductility and resilience. Oxidative hardening leads to stiffness and embrittlement of asphalt binders, see Figure 1.1, which reduces healing capacity, and increases the rate of micro-crack propagation. Furthermore, the pavement system is more prone to coalesced micro-crack formation, and may begin to develop surface-initiated fatigue cracking. In addition, the brittle pavement surface will be prone to channeling cracks, such as thermal and block cracks, see Figure 1.2. Fatigue, thermal, and block cracking lead to an exponential decline

in pavement serviceability and a resulting exponential increase in maintenance costs to restore pavement condition. Furthermore, in a recent study conducted by Islam and Buttlar [3], a rough pavement network was found to add an additional user cost of over $300 per vehicle per 12,000 miles driven. The encouraging news from the study was that properly timed maintenance treatments, resulting in moderately smooth pavement over its life, yields approximately a 50-to-1 return on investment. Life extension has also been linked to sustainability benefits (reduced energy and emissions in the life cycle of the pavement from cradle to grave).

Figure 1.2: Thermal cracking (left) and block cracking (right) on asphalt concrete pavements in Illinois.

In-situ field aging or long-term aging is the dominant source of material property gradation through the pavement thickness. Figure 1.3 shows the predictions made using a binder aging prediction model by Mirza and Witczak [1] for an eight-year-old asphalt pavement subjected to central Illinois climactic conditions. Figure 1.3 illustrates the highly graded material properties caused by oxidative hardening through the pavement thickness. The time required to reach an unacceptable level of embrittlement near the pavement surface depends upon a number of factors, and varies from pavement to pavement, even within a given region and mixture type. Reliable tools are therefore needed to characterize the steeply graded properties of an aged asphalt pavement [4], and intelligently select the best maintenance strategy to restore the pavement to a crack-resistant state, which may include optimizing the relative amount of milling and surface replacement and/or the use of rejuvenators.

1.2 Research Objectives

Asphalt concrete used in pavements mainly consists of two parts: asphalt binder and aggregates particles with various sizes. Asphalt binder acts as a thermoplastic and viscoelastic adhesive to hold the aggregates together [5]. The major cause of asphalt concrete failures is the weakening of the adhesive bonding between aggregates and asphalt binder due to moisture damages, mechanical stresses and oxidative aging [6]. The loss of ductility and resilience due to oxidative aging will lead to an increase in the asphalt binder stiffness and a lower resistance of fracture. As a result, damages are more likely to occur in regions which undergo oxidative hardening. In order to restore the crack-resistant property

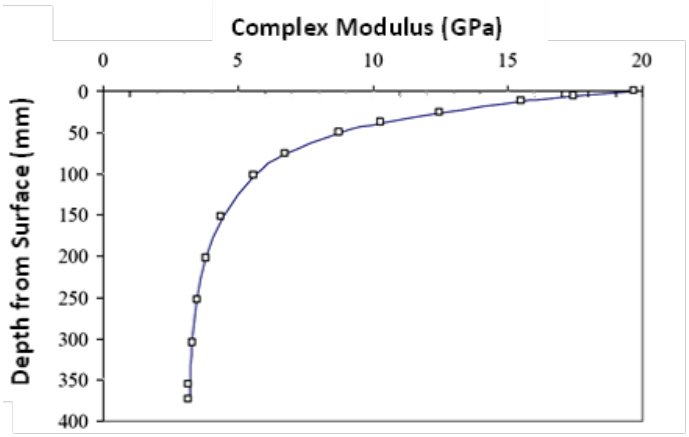

Figure 1.3: Asphalt Concrete Complex Modulus after Eight-Years in Service, as predicted using Mirza and Witczaks global aging model [1].

of asphalt concrete and prevent the occurrence of further damage, measures such as pavement surface milling and the application of rejuvenators are usually taken by the pavement engineers.

The use of rejuvenators is currently becoming popular in pavement maintenance. It is an asphalt additive and modifier to revitalize, provide sealing and restore the physical and chemical properties of the aged asphalt concrete [7]. Rejuvenators address the issue of oxidative hardening by softening the aged asphalt binder through restoring the asphaltenes to maltenes ratio [8]. Theoretically, after applying a layer of rejuvenator over the top surface of pavement, the rejuvenator will be able to penetrate the top surface and diffuse through the asphalt concrete to chemically react with the asphalt binder. Under the reaction with rejuvenator, material properties of the aged asphalt concrete can be restored to its original status, i.e., the virgin condition. For instance, the asphalt binder could be softened to have higher adhesive properties so that the asphalt concrete is less stiff and more susceptible to thermal cracking. Currently there is no standardized method to evaluate the performance of rejuvenators when applied in the field, especially its ability of diffusion and penetration in the asphalt concrete, except using visual inspection described in the past studies by Brown et al. [9].

The aim of this study is to show that Acoustic Emission (AE) techniques can be a powerful tool to characterize the low-temperature behavior of the rejuvenated asphalts, so that the restorative effectiveness of rejuvenators can be evaluated. Specifically, a pre-determined amount of rejuvenator was applied on the top surfaces of four 36 hours oven-aged asphalt concrete specimens. These four specimens were put into a cooler to simulate a cold temperature environment, and tested using the same acoustic emission approach after two, four, six, and eight weeks of dwell time. The characteristics of the AE emission events were gathered and studied. The locations of the thermal cracks were also determined using AE source location techniques by backtracking the AE waves using their arrival times at

each of the AE sensors. The embrittlement temperature of each specimen was then determined using the AE analysis and source location results. By comparing the embrittlement temperatures of the rejuvenator-treated asphalt samples to the untreated ones, the depth of rejuvenator penetration and rejuvenator's restorative effectiveness is able to be quantitatively examined.

1.3 Description of Experimentation

Conventionally the performance grading of asphalt binders are examined based on AASHTO standard protocols [10–12]. These standard protocols require conducting standardized laboratory testing on the binder specimens using specified testing instruments, and some of the tests such as Disk-shaped Compact Tension (DC(T)) test require specially shaped asphalt concrete specimens. These tests are time-consuming and expensive to conduct, and the results obtained using different testing methods usually involve a high variance. As a volumetric NDT evaluation method for asphalt, AE-based evaluation can provide efficient real-time evaluation of the material properties for the asphalt concrete, and it also provides the possibility to conduct rapid field testing on pavement using portable AE instrumentation without requiring additional test sample preparation. Past studies using AE techniques to evaluate physical properties, especially the embrittlement temperature, of asphalt binder samples and asphalt concrete mixture specimens can be found in [13–18].

Asphalt binder and aggregates have different coefficients of thermal expansion, thus upon being subjected to low temperature, aggregates and binder deform at different rates as the temperature varies. When the tensile stress of the asphalt mixture exceeds the binder strength, thermal cracking happens within the asphalt concrete and strain energy is released as elastic stress waves. These waves are picked up using AE piezoelectric sensors and are characterized as AE events. In this study, an AE event is defined as an AE signal received by an AE sensor with a minimum voltage of 0.2 V and a minimum energy of $4V^2 - \mu s$.

Current evaluation of asphalt embrittlement temperature using the AE-based approach usually involves counting the number of AE events and monitoring the increasing rate of AE events. One of the commonly used AE approaches is proposed in the study conducted by Buttlar et al., which defines the embrittlement temperature as the temperature when the first major AE event occurs with energy higher than 100 $V^2 - \mu s$ [15]. The embrittlement temperatures of asphalt specimens with different aging levels estimated using the event rate criterion were shown to be close to the embrittlement temperatures obtained using the energy level criterion. The embrittlement temperature results found using the AE approaches have been proved to agree with the results produced by standard tests [13]. The AE-based approach to estimate embrittlement temperatures has the potential to replace the AASHTO standard protocols to

specify performance grading of asphalt binders and asphalt concrete mixtures at low-temperature because of its many advantages.

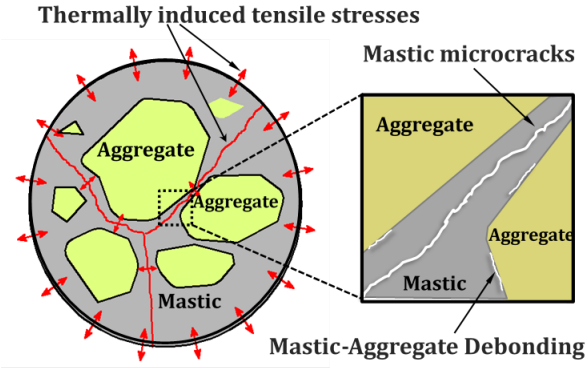

Figure 1.4: Schematic illustration of two main types of microdamage within asphalt concrete, i.e., mastic microcrack and mastic-aggregate debonding.

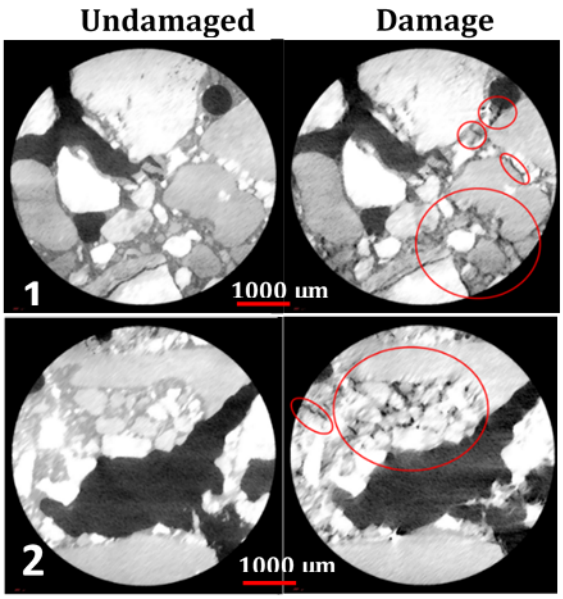

Figure 1.5: X-ray Computed Micro-Tomography Imaging of crack damage induced by cooling. On the left are the images before cooling and on the right are the images after cooling. Both photographs show microcracks in the mastic microcrack and mastic-aggregate debonding.

In first part of this study, the embrittlement temperature of the asphalt mixture is quantitatively evaluated by observing the AE event and AE event rate response caused by the increasing thermal stresses, which develop as the specimen cools because of the different coefficients of thermal expansion between the aggregates and the binder. When the magnitude of the tensile stresses reaches the local binder strength, cracks occur, releasing strain energy in the form of transient stress waves, i.e., acoustic emission events, which are detected using piezoelectric sensors. Here, the temperature at which the event-rate is equal or above 5 events per second (with event energy equal or above 4 $V^2 - \mu s$)

is termed as the mixture's embrittlement temperature. Figure 1.4 shows a schematic diagram of the two main types of thermally-induced microdamage in asphalt concrete, i.e., microcracks in the mastic and mastic aggregate debonding where mastic is the mixture of asphalt binder and fines. To visualize this type of micro-damage, x-ray computer micro-tomography imaging was taken of asphalt concrete specimens before and after cooling. Figure 1.5 shows the results of the micro-tomography imaging where mastic micro-cracking and mastic-aggregate debonding are observed. The length of the observed microcracks and debonding varied between 28 and 750 μm.

In addition to evaluating the embrittlement temperature based on AE event count and AE event rate, the second part of this study addresses the relationship between the cooling temperature and the location of the thermal cracks, and makes uses of this relationship to propose a method to estimate the embrittlement temperatures based on the source location results. The embrittlement temperatures of the original and oven-aged asphalt specimens are investigated first, then compared with the embrittlement temperatures of the rejuvenator-treated specimens. The restoration effect of asphalt rejuvenator are then evaluated using the comparison results. Based on previous studies, the specimens treated by the rejuvenator are expected to have higher resistance to thermal damages and would crack at a lower temperature than the untreated specimens.

1.4 Paper Overview

Chapter 2 provides a set of literature reviews which are relevant to this study. A concise history of the usage of rejuvenators in the U.S. is presented first, followed by a brief review of different acoustic emission techniques. An overview of conventional AE source location methods is also provided.

Chapter 3 provides the detailed explanations of various source location methods. The concepts of basic source location calculation procedures are described, and the application of these methods on characterizing properties of asphalt concrete is discussed.

Chapter 4 provides a detailed description of the sample preparation steps and the laboratory experimentation procedures.

Chapter 5 assesses the accuracy of the source location algorithms described in Chapter 3 by conducting experiments on a large rectangular asphalt specimen. Source location results calculated using the algorithms are compared with authentic locations of the AE sources.

Chapter 6 quantitatively evaluates the embrittlement temperatures of the asphalt concrete specimens using an acoustic

emission approach. This chapter also investigates the relationship between AE source locations and asphalt embrittlement temperatures. The restoration effect of asphalt rejuvenator is then evaluated using the source location results.

Chapter 7 examines the AE source location results when the sensors are only installed on one surface of the asphalt concrete.

Chapter 8 - Conclusion and future recommendations

CHAPTER 2: LITERATURE REVIEW

2.1 Literature Review on Asphalt Rejuvenator

The hard, oxidized nature of reclaimed asphalt binder is a major concern when incorporating recycled materials into Hot Mix Asphalt (HMA) mixtures. Oxidation, the main mechanism behind asphalt aging, changes certain chemical properties of the asphalt; specifically, the ratio between asphaltenes and maltenes. Asphaltenes are known for their insolubility in pentane and function as the bodying agents in the form of asphalt and bitumen products. Asphaltenes do not have a specific chemical formula due to the fact that the chemical composition of asphaltenes can vary depending on the source. Maltenes are the residual components in the asphalt after the asphaltene is removed from the mixture [19–21]. Maltenes exist in various types: polar compounds/nitrogen bases (peptizers for the asphaltenes), acidiffins (solvent for the peptized asphaltenes), and paraffins (saturated hydrocarbons that act as a gelling agent). The asphaltenes to maltenes ratio influences the rheology of bitumen; as oxidation occurs, polar compounds and acidiffins are converted into asphaltenes thus increasing the ratio, resulting in a stiffer, more brittle asphalt binder. The reaction rate of oxidation can be accelerated at high temperatures and/or high exposure to ultraviolet light. The amount of asphalt oxidation is proved to be directly related to the exposure time with air, thus, stockpiling asphalt materials may result in higher amount of oxidation. Regardless of the reasons for oxidation, products have been produced to counteract the effects of oxidation. Depending on the use of the product (preventative/corrective maintenance or recycling), these products have been called many different names [22], such as service life extenders, softening agents, rejuvenator seals, and recycling agents/additives. For consistency, any such product will typically be referred to as a rejuvenator.

A rejuvenator, as the name implies, is a product that aims to restore the physical and chemical properties of aged bitumen. Rejuvenators address the issue of oxidative hardening by softening the aged asphalt via the restoration of the original asphaltenes to maltenes ratio discussed above [7, 8, 20]. Some examples of rejuvenators are refined tallow, waste vegetable or frying oils, waste motor oils, lube extracts, extender oils, emulsions, soft virgin binders, and bio-binders [21, 23, 24]. Rejuvenators are generally applied to the surface of existing pavements; therefore, it is essential for the rejuvenator to have the ability to penetrate the surface and diffuse through the aged asphalt. If the rejuvenator lacks this ability, not only will the aged asphalt be unaffected, but the unabsorbed rejuvenator will reduce skid resistance [8, 9]. To avoid creating slick, over-coated surfaces, it is often good practice to apply rejuvenators in several coats at a lower application rate [20]. During the diffusion process, the rejuvenator first forms a low-viscosity

layer around the layer of aged binder which coats the aggregate. Then, the rejuvenator starts to diffuse into the aged binder, thus softening it. Eventually, all the rejuvenator penetrates into the aged binder and the inner layer becomes less viscous and the outer layer becomes more viscous as the mixture approaches a state of equilibrium [8, 9]. Oliver [25] found that the rate of diffusion can be increased by adding diluents or by increasing temperature. Thus, the environment in which the rejuvenator is applied is a critical consideration, especially in terms of application rate. After a sufficient dwell time, the performance of the rejuvenator can be evaluated.

Research efforts are still being carried out towards developing a quantitative understanding of the effect of rejuvenators [7, 26–29]. Many past studies regarding the use of rejuvenators including using rejuvenators in conjunction of hot in-place recycling (HIPR) techniques [25, 30–32], recycled asphalt pavement (RAP) [7] and recycled asphalt shingles (RAS) [29] have been proposed. A microscopic level investigation on rejuvenators conducted by Nahar et al. demonstrated that there are many different types of rejuvenating products available, and some fulfill their function of softening hard asphalt better than others [23]. Regardless, it is clear that the intended purpose of these products make them very desirable to be in used in tandem with recycled materials [33–35]. Based upon these studies, the effectiveness of rejuvenators is still an active area of research. For a more detailed literature review on the recent studies of asphalt rejuvenators, the reader is encouraged to refer to [36].

2.2 Literature Review on Acoustic Emission Techniques

Acoustic emission (AE) is a passive inspection technique that analyzes the acoustic waves generated within the material for defect detection and analysis of solid. AE has become a popular non-destructive evaluation tool nowadays due to the advances in high-speed digital AE instrumentation technology. The current AE monitoring system is advanced enough to allow high-frequency data acquisition with short data processing time. In addition, the development in acoustic emission sensors with high sensitivity and AE waveform analytical software also contributes to the increasing usage of AE techniques [37]. AE techniques have been widely used in material performance evaluation and health monitoring in large structures, pipes and vessels for a number of years.

These acoustic waves are usually generated by a rapid release of energy from moving dislocations, cracks, fiber breaks, disbands, etc. [38]. Common sources of acoustic emission are consisted of fracture of crystallites, crack nucleation and growth, mechanical dislocation, fracture inside a material, material phase transformation, electrical discharges, etc. [39]. The application of AE analysis to characterize solid material properties has gained popularity in recent decades. Many acoustic emission studies are related to the engineering inspection of steels, concrete and composites.

A concise review on using AE as a tool for the composite-materials studies was provided by Hamstad in 1986 [40]. AE can be an useful approach to study the material properties due to its high-sensitivity and real-time capability while studying any mechanism which generates sound waves. AE waves generated within the composite structures are shown to have correlation to the growth of damage that leads to changes in many measured properties of composites. Charentenay et al. showed that AE monitoring can be used to distinguish different stages of delamination: no cracking and initiation, microcracking and stable cracking growth [41]. The correlation between AE and the stress/strain level was shown by Old et al. [42]. Sim et al. conducted interrupted tension tests of 0/90-deg glass/epoxy laminates and demonstrated the cumulative AE counts are correlated with the decreasing dynamic modulus and the increasing damping [43]. The cumulative AE counts in composite materials were also shown to be correlated with the compliance change and the resonant frequency [44, 45]. Conducting AE tests during tensile tests for chopped strand mat/polyester also showed that the curing effects of composite materials are correlated with the AE event counts [46].

Recently AE techniques have been extensively applied to concrete structures as a non-destructive evaluation method. AE parameters such as AE event count, AE wave amplitude, AE energy and spectral analysis are shown to be strongly correlated with the failure process of materials. A study conducted by Ohtsu et al. in 1991 uses a pull-out test of an anchor-bolt from a concrete block and a cylinder-tensile test to show that the type and orientation of the cracks within a concrete structure can be determined using AE analysis [47]. A similar study in 1997 by Grosse et al. has shown that three-dimensional localization and frequency domain analysis on AE events can be used to investigate the crack classification produced by steel concrete interaction. Relative moment tensor inversion method using a cluster analysis technique was employed to characterize the fracture mechanisms of concrete. The results obtained in the investigation were proved to be promising. This study also suggested that AE measurements could provide a better way of assessing the damage of concrete [48]. AE techniques have been proved to be an effective tool to study the freezing and thawing effects in concrete materials [49].

AE techniques have also been applied to the evaluation of asphalt concrete properties. Seo et al. conducted a study in 2008 to show that the degree of accumulative AE energy and count can be used as a parameter to characterize the fatigue damage and healing ability in asphalt concrete [50]. In this study, a series of uniaxial tensile cyclic tests with and without rest period were conducted and AE parameters including emission counts were acquired. Test results indicated that the accumulative AE energy and the AE event count are useful to assess the initiation and propagation of fatigue damages. It can also be used to quantify the beneficial effects of the rest period on the performance of asphalt concrete. The frequency-amplitude analysis showed that crack formations coincide with the peaks of maximum AE amplitude (Amax) with higher frequencies. The healing effect of asphalt was shown to be best described by Amax with lower frequencies during the rest period. In addition, the test results demonstrated that the Kaiser effect does not

hold for fatigue in asphalt concrete.

Previous studies by Arnold et al. [51] and McGovern et al. [52] used AE analysis as a tool to analyze the behavior of asphalt material under low temperatures. Similar AE analyses on asphalt concrete were also carried out by emphasizing the number of globally monitored AE event counts received by sensors [13] and the spectral analysis on the AE signals [53].

A recent study done by Behzad et al. in 2010 utilizes the usage of accumulative AE emission counts to determine the embrittlement temperature of asphalt mixtures [54]. The embrittlement temperature was defined in this study as the temperature at which the first AE event above a certain energy threshold value occurs. Behzad evaluated the correlation among different binder types, aging levels, binder thicknesses and asphalt embrittlement temperatures. The testing methods proposed in this study and the evaluation results were able to help pavement engineers to determine when a pavement surface has become vulnerable to thermal cracking in a certain climate.

2.3 Literature Review on Acoustic Emission Source Location Methods

One of the most useful applications of AE is to locate sources of energy release inside a structure, which is often referred as the AE source location technique. AE source location facilitates the process of inspecting where a structure has developed damages and what area internally it is affecting without having to destructively damage the material to locate the defect. AE source location is significantly useful for monitoring structural health under extreme conditions, especially at low temperature or high pressure environment [55].

Zonal location method is the simplest form of source location. The sensors are sparsely installed on the surface of the monitoring structure, and each AE sensor has a specific monitoring range depending on its sensitivity to the AE signals. The area enclosed by the sensors forms the critical monitoring area, which is divided into multiple zones, and each zone is associated with the closest sensor to it. After the sensors receive the AE signals, the specific zone associated with the first triggered sensor will be divided into multiple sub-zones. This process continues until the location of the source is determined to be located inside the last determined sub-zone, which is either an area or volume. Zonal location method does not have specific requirement on the minimum number of sensors to be triggered, and does not rely on the straight wave path assumption. This method is commonly used for two dimensional source location in plate or thin wall structures such as tanker cars for trains [56]. As for more complicated structures, zonal location method has inhibit computation limits and is susceptible to many sources of error.

More sophisticated source location methods have been developed in the past few decades. One of the most commonly

used source location methods is to use time of arrival of AE waves to a group of AE sensors, along with a pre-determined wave velocity, to measure the distance between the AE source and each of the sensors. The location of the source can be determined using the method of triangulation. This method is referred to as the Time of Arrival (TOA) method. To obtain a non-trivial solution, two sensors are required for linear source location, three sensors are required for planar source location and at least four sensors are needed for source location in 3 dimensions. The exact geometric locations of the AE sensors and the AE wave velocity must be known in order to use the TOA method. In solid material there exists two types of waves, also referred to as modes. The first one is the primary (longitudinal/dilatational) wave, or p-wave, where the particles move in the same direction of the wave propagation. The second one is the secondary (shear) wave, or s-wave, with particle motion perpendicular to the direction of the wave propagation. While traveling in an infinite elastic solid, p-waves have higher velocities compared to the s-waves. Therefore, p-wave is usually used for arrival time determination since it represents the first and undisturbed arrival of an AE wave. TOA method has been applied by Köppel and Grosse to determine the source location in concrete. They proposed that accurate arrival time picking is the most crucial factor for an accurate determination of the source location. The arrival time is often determined using the first threshold crossing of the AE waveform arrived at a sensor. This determination method is simple to conduct, but not always accurate. Manual determination of arrival times improves the accuracy of the localization results, but is time-consuming and not reasonable for a huge amount of AE data. Therefore they recommend using an energy-based source location algorithm HypoAE developed by Oncescu and Grosse to extract more accurate arrival time information [57].

In 2010, Ince et al. proposed a method using machine learning approach to recognize the p-wave arrival time in the presence of noise. The characteristics of the AE waveforms are used for hierarchical clustering of AE events. Within each cluster of the AEs, several feature extraction methods like wavelet packets, autoregressive parameters and discrete Fourier transform coefficients were used to identify patterns of the p-waves in the frequency domain. By employing machine learning approaches, the accuracy of the AE source location results in noisy environment is further improved [58].

Another source location approach called Time Difference of Arrival (TDOA or Delta-T method) was developed in the past using the differences in arrival times for a correlated signal detected by a set of spatially distributed sensors. TDOA source location is usually solved in an iterative numerical approach. Baxter et al. modified this method to apply on aeronautical composite parts in 2007. They used the difference in time of arrival between two sensors to form a triangle with the impact point, and created a map associated with each sensor pair. These maps are then overlapped and compared to determine a more exact source location [59]. A study conducted by Ho et al. has proposed a method to locate the source by using TDOA in conjunction with frequency difference of arrival. This method uses nuisance

variables to improve the source location estimates. Only several weighted least-squares minimizations are needed without requiring initial solution guesses to obtain a location estimate. It does not have the initialization and local convergence problem as in the Taylor-series iterative method. The accuracy of the source position and the estimated velocity is shown to achieve the Cramér-Rao lower bound for Gaussian TDOA and FDOA noise at moderate noise level before the thresholding effect occurs [60]. Comparing to TOA method, TDOA approach requires less sensors and it can be used in complex geometric structures. However, using TDOA method requires solving a system of nonlinear equations which is computationally complicated and sometimes it gives non-real complex solutions.

Traditional planar source location in plate or wall structure requires at least three AE sensors to be triggered to solve the source location equations. These three sensors are supposed to be placed far apart on the testing structure so that the arrival time to different sensors can be distinguished. Aljets and Chong at University of Glamorgan proposed a different sensor placement compared to the traditional widely spaced sensor placement. The sensors are arranged into a close triangular array with few centimeters away from each other. TDOA method is applied to calculate the source location by using the time difference of arrival to the closely arranged sensors. This sensor placement provides the possibility of using a small and portable device with the small sensor arrays as the probe to conduct source location tests in the field [61]. Another simple and generic source location technique was proposed as the best-matched point search method. This method generates a number of arrays of points with spatial vectors to represent the testing structure. Each point represents a unique combination of the difference in arrival time between two sensors. Those delta-t values can be used to determine the best matching source location point by comparing the measured time difference to the known delta-t value at each point. This method has been proved to be effective for 2-D source location in anisotropic plate and 3-D source location in limestone [62].

In general, source location in anisotropic material is more difficult to be conducted than in isotropic material due to the fact that many assumptions do not hold when the material is anisotropic. More work has been done to extend the application of source location into anisotropic and/or heterogeneous materials. In 2013, Kundu has proposed and compiled several source location methods for anisotropic plates. Beamforming technique, which is commonly used in isotropic plates, was applied to anisotropic structures coupled with Kundu's optimization schemes to allow accurate determination of the impact point location. Kundu further extends this method by proposing a source location technique without requiring the direction dependent velocity profile in the structure and without solving a system of nonlinear equations. This method utilizes six AE sensors installed on the plate and the direction dependent wave velocity profile can be constructed using the arrival time differences among those sensors. Three additional sensors can be introduced to further reduce the prediction error of the location [63, 64].

Time-reversal method, which is a novel approach for source location acquisition in complex structures was then introduced. The brief history, basic physics, advantages and limitations are addressed by Anderson et al. [65] Time-reversal method builds a collection of training data using the signals generated by mechanical impacts on the testing structure to transform the testing system into interactive interfaces. The correlation of the impulse response functions of an actual impact signal and the impulse response functions of the points in the training data set is used to estimate the location of the impact point. This method was examined and validated by the interactive experiment conducted by Ing et al. [66] in 2005. The advantage of the time-reversal method is the independency of the computation process on the shape of the structure and wave velocity model. The accuracy of this method relies upon how accurate the numerical modeling of the structure has been built. Moreover, the time-reversal process becomes computational complex when nonlinear elastic effects take into account.

Many other source locations schemes have been proposed and applied to seismic source location, and some of them can be directly applied to the AE source location because seismic sources have similar attributes compared to AE sources. As suggested by Schumacher et al. in their study of seismic source location, key variability of parameters in source location, i.e., locations of sensors, p-wave velocity and p-wave arrival times are usually not constant, and the variations of these parameters should be accounted for. The errors and uncertainties were represented as probability density functions and the parameters were estimated in a Bayesian probabilistic approach using their full posterior probability distributions. The experimental results have shown that the predictions based on the estimated parameters employing newly observed arrival times can produce acceptable source location results [67]. Work has been done by Dong and Li to improve the accuracy of current source location schemes for microseismic and AE sources. In 2013, Dong and Li proposed an innovative seismic source location method. This method measures the arrival time of p-wave and s-wave separately, and the source location could be solved by nonlinear fitting Self-Organizing Migrating Algorithms (SOMA) method in conjunction with Global Optimization (GO) method without explicitly knowing the wave velocities [68]. In their recent studies conducted in 2014, Dong and Li have simplified the nonlinear location equations for conventional TDOA method to linear equations and developed a unique three-dimensional analytical solution without having square root calculation [69]. This modified TDOA scheme is similar to the source location method proposed in 1972 by the United States Bureau of Mines (USBM). The USBM method was developed to evaluate the rock stability by monitoring the rock noise, which has similar concept compared to AE source location analysis [70].

TDOA, USBM and TOA algorithms are categorized as non-iterative point source location method. Non-iterative method solves a set of linear or non-linear equations without using any numerical approach. This method has the advantage of quick and easy computation processing compared to iterative methods which involve using approximation

and convergence techniques. Most of the non-iterative source location methods are using simplified models, such as constant velocity model for the testing structures. The results obtained using non-iterative source location methods are more prone to errors in the raw data. On the other hand, iterative source location methods provide slower, but more flexible approach to calculate the source locations [71]. Geiger's method, proposed in 1912, is one of the most famous stable and effective iterative source location algorithms [72].

In the following, both non-iterative and iterative source location algorithms are used in this study to calculate locations of the cracks inside the asphalt specimens. Experiments in this study employ 8-channel acoustic emission sensing system to calculate the exact positions of the cracks happened inside the asphalt concrete under the straight wave paths assumption with a constant velocity model.

CHAPTER 3: SOURCE LOCATION METHODOLOGY

AE source location method uses the information of AE signals received at multiple AE sensors to calculate the coordinates of AE sources. The stochastic nature of asphalt concrete makes it difficult to give a precise physical model of the distribution of aggregates and binder in an asphalt specimen. Additionally, the presence of cracks and air voids in the specimen introduces variabilities to the wave velocity profile. Therefore, constant wave velocity and straight wave propagation path assumptions were made to mitigate the effect of heterogeneity inherent in wave velocity and wave propagation paths. The dilatational velocities in asphalt concrete were measured by McGovern et al. at different aging levels using the velocity measurement method proposed by Sachse and Pao [73]. As discussed by McGovern et al. [17], the velocity of the dilatational wave varies as the oxidative aging level of the asphalt specimen increases. In this study, the aging level for the rejuvenated asphalt specimen is not deterministic, so the values of the dilatational wave velocity are approximated by taking the average value of dilatational velocities in asphalt concrete samples aged from 0 to 36 hours. The dilatational velocities for asphalt concrete are plotted with respect to the frequency of the acoustic waves in Figure 3.1, which is extracted from McGovern's study [1].

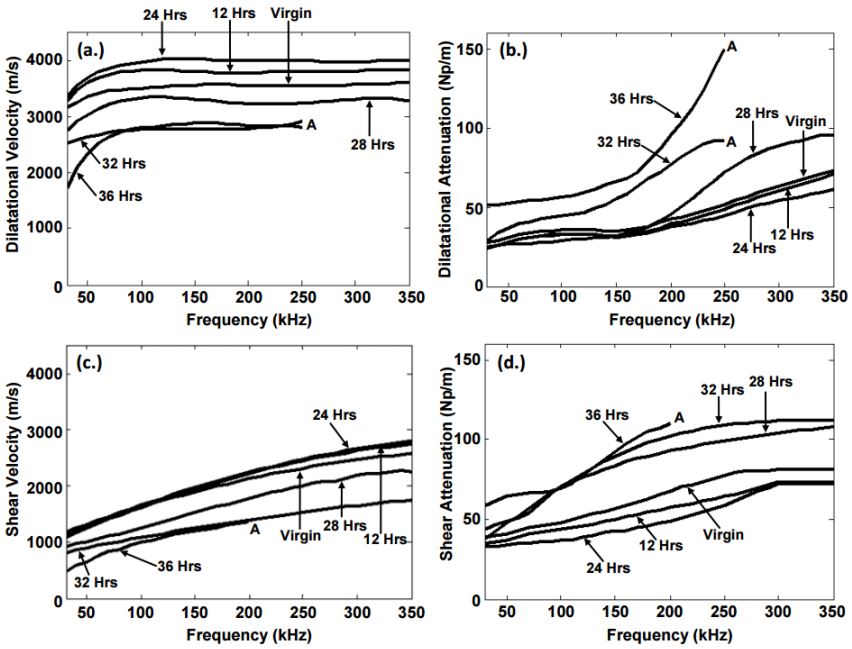

Figure 3.1: Top Row: (a) Dilatational wave velocities and (b) corresponding attenuations for asphalt concrete samples aged from 0 to 36 hours. Bottom Row: (c) Shear velocities and (d) corresponding attenuations for asphalt concrete aged from 0 to 36 hours

[1]Reprinted, with permission, from McGovern, M. E., et al. "Concrete Testing: Characterisation of oxidative ageing in asphalt concrete - Part 1: Ultrasonic velocity and attenuation measurements and acoustic emission response under thermal cooling." Insight-Non-Destructive Testing and Condition Monitoring 55.11 (2013): 596-604.

Using the known wave velocity values, two different types of AE source location methods were used in this study: non-iterative USBM method and iterative Geiger's method. These two methods use different approaches to calculate the coordinates of the AE source and are subjected to different sources of error. Iterative and non-iterative methods may generate different source location results for the same AE event, and these two methods have different computation complexity. Their computation methods and complexity will be analyzed in the following sections.

3.1 Non-iterative Method

3.1.1 Basic Triangulation Method

The basic triangulation method here refers to the widely used time-of-arrival (TOA) scheme. The coordinates of the AE source are calculated algebraically by using the known coordinates of a set of sensors and the arrival time of the AE waves to the sensors.

The coordinates of the eight sensors are : (x_1, y_1, z_1), (x_2, y_2, z_2),(x_3, y_3, z_3),(x_4, y_4, z_4), (x_5, y_5, z_5),(x_6, y_6, z_6), (x_7, y_7, z_7), (x_8, y_8, z_8). The arrival times of the acoustic waves to the sensors are measured, which are: $t_1, t_2, t_3, t_4, t_5, t_6$, t_7, t_8. In order to find the analytical solution of the AE source location coordinates, the AE waveform needs to be received by at least four sensors. A small receiving time means that the crack is located at a region close to the sensor. If the time of arrival at a sensor is larger compared to the time of arrival at other sensors, it may imply that the acoustic wave is traveling for a longer distance in the material, or the acoustic wave bounces back after hitting the material boundary. Either of the two cases could result in a larger percentage error in the source location calculations. Therefore, only the four sensors with the smallest four receiving times are used for the source location calculation.

Using these information, a set of equations could be obtained:

$$(X_s - x_1)^2 + (Y_s - y_1)^2 + (Z_s - z_1)^2 = v^2(t_1 - T_s) \tag{1}$$

$$(X_s - x_2)^2 + (Y_s - y_2)^2 + (Z_s - z_2)^2 = v^2(t_2 - T_s) \tag{2}$$

$$(X_s - x_3)^2 + (Y_s - y_3)^2 + (Z_s - z_3)^2 = v^2(t_3 - T_s) \tag{3}$$

$$(X_s - x_4)^2 + (Y_s - y_4)^2 + (Z_s - z_4)^2 = v^2(t_4 - T_s) \tag{4}$$

Where (X_s, Y_s, Z_s) denote the coordinates of the location of the crack, T_s is the time at which the crack occurs and v is the pre-determined velocity of acoustic waves in asphalt concrete.

There are four unknown variables in equation (1) to (4): X_s, Y_s, Z_s and T_s, and there are four quadratic equations. Solving this set of nonlinear equations could possibly generate two distinct real roots, two identical real roots, or two complex roots. In many cases, solving this set of equation directly gives complex roots which cannot be used for computation of crack locations. Therefore it is necessary to expand and rearrange equation (1) to (4) so that the quadratic terms could be eliminated. The way of expanding these four equations is essentially the USBM source location algorithm, which will be elaborated on next section.

3.1.2 USBM Method

The non-iterative USBM method is commonly used to linearize the non-linear source location equations. The computation of USBM method is faster and easier than the iterative numerical approaches. This method requires at least five AE sensors receiving the AE signals. There is one additional sensor compared to directly solving non-linear source location equations, which only requires four sensors receiving the AE signals.

By assuming that the wave propagation paths from the sources to AE sensors are straight, the distance D_i between the location of the source and the i-th sensor can be computed as:

$$D_i^2 = (X_s - x_i)^2 + (Y_s - y_i)^2 + (Z_s - z_i)^2 = v^2 \times (t_i - T_s) \tag{5}$$

(X_s, Y_s, Z_s) represent the spatial coordinates of the source, (x_i, y_i, z_i) represent the coordinates of the i-th sensor, v is the determined wave velocity, and T_s and t_i are the unknown source event occurring time and the known receiving time by the i-th sensor respectively. The sensor number i ranges from 1 to 5.

D_1^2, which is the square of the distance from the source to the first arriving sensor, is subtracted by D_k^2, where k = 2,3,4,5. It yields:

$$D_k^2 - D_1^2 = [x_k^2 - x_k^2 - 2(x_k - x_1)X_s] + [y_k^2 - y_1^2 - 2(y_k - y_1)Y_s] + [z_k^2 - z_1^2 - 2(z_k - z_1)Z_s] = v^2[t_k^2 - t_1^2 - 2(t_k - t_1)T_s] \tag{6}$$

Equation (6) can be rearranged into:

$$f_(x,k)X_s + f_(y,k)Y_s + f_(z,k)Z_s + f_(t,k)T_s = h_k \tag{7}$$

Where:

$$f_(x,k) = 2(x_1 - x_k)$$

$$f_(y,k) = 2(y_1 - y_k)$$

$$f_(z,k) = 2(z_1 - z_k)$$

$$f_(t,k) = 2(v^2 t_k - v^2 t_1)$$

$$h_k = x_1^2 - x_k^2 + y_1^2 - y_k^2 + z_1^2 - z_k^2 + v^2 t_k^2 - v^2 t_1^2$$

Equation (7) can be represented in matrix form as:

$$H = \Phi\Theta \tag{8}$$

Where:

$$H = \begin{bmatrix} h_2 \\ \vdots \\ h_5 \end{bmatrix} \quad \Phi = \begin{bmatrix} f_{x,2} & f_{y,2} & f_{z,2} & f_{t,2} \\ \vdots & \vdots & \vdots & \vdots \\ f_{x,5} & f_{y,5} & f_{z,5} & f_{t,5} \end{bmatrix} \quad \Theta = \begin{bmatrix} X_s \\ Y_s \\ Z_s \\ T_s \end{bmatrix}$$

The unknown parameter Θ can be computed using least squares estimation:

$$\hat{\Theta} = (\Phi^T \Phi)^{-1} \Phi^T H \tag{9}$$

Equation (9) has a unique solution (X_s, Y_s, Z_s, T_s) if and only if the vector product $\Phi^T \Phi$ is nonsingular. It means that the non-iterative method does not always generate a valid source location solution, and the uniqueness of the solution depends on the coordinates of the sensors and the arrival time received by the sensors. In order to make the matrix Φ consisted of linearly independent columns, collinear or symmetric sensor placement should be avoided.

3.1.3 A Modified Version of USBM Method

When AE testings are conducted on the pavement, sometimes it only allows test operators to install AE sensors on the top surface of the pavement to avoid damaging the pavement for underground sensor installment. The USBM method stated in Section 3.1.2 does not fully function when the sensors are placed on the same plane on the testing sample because of missing parameters in the equations. A modified version of the USBM method is thus proposed here to

compute the source location coordinates if all of the sensors are installed on the same surface.

Given the condition that the AE sensors are all placed on one surface of the testing sample, the y-coordinates of all the sensors are the same, i.e., $y_1 = y_2 = y_3 = y_4 = y_5$. In equation (7), $f(y,k) = 2(y_1 - y_k)$ is then equal to zero. Equation (7) becomes:

$$f_(x,k)X_s + f_(z,k)Z_s + f_(t,k)T_s = h_k \tag{10}$$

Equation (8) becomes:

$$H = \Phi\Theta \tag{11}$$

Where:

$$H = \begin{bmatrix} h_2 \\ \vdots \\ h_5 \end{bmatrix} \quad \Phi = \begin{bmatrix} f_{x,2} & f_{z,2} & f_{t,2} \\ \vdots & \vdots & \vdots \\ f_{x,5} & f_{z,5} & f_{t,5} \end{bmatrix} \quad \Theta = \begin{bmatrix} X_s \\ Z_s \\ T_s \end{bmatrix}$$

Solving equation (11) gives the value of (X_s, Z_s, T_s). The y-coordinate of the AE source remains unknown. An additional step is needed to solve the y-coordinate using the calculated x and z coordinates of the source. Figure 3.2 illustrates this scenario. A black dot on the rectangular testing sample in Figure 3.2 is located on the x-z plane with coordinates of $(X_s, 0, Z_s)$, where X_s and Z_s are the calculated x and z coordinates. This black dot is coplanar with all of the sensors, which are installed on the plane with y-coordinate equal to zero.

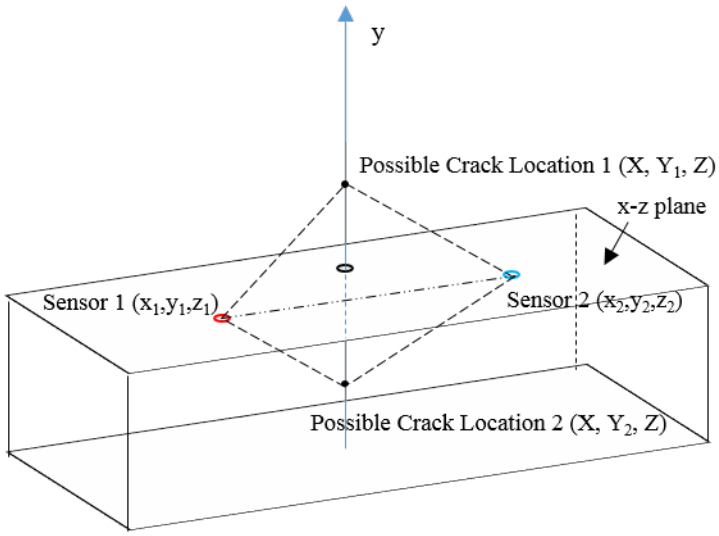

Figure 3.2: Graphical representation of the two possible crack locations

The additional step is essentially a modified time difference of arrival (TDOA) approach. The idea of this step is that the product of wave velocity and the difference in time of arrival to two different sensors equals to the distance

difference from the AE source to these two sensors. Using this relationship, the following equation is obtained:

$$\Delta d_{i,j} = v(t_i - t_j), 1 \leq i < j \leq 5 \tag{12}$$

There are $\binom{5}{2}$=10 possible equations obtained from pairwise comparisons among the 5 sensors. Using sensor 1 and sensor 2, i.e., the red and blue dots in Figure 3.2, as an example, equation (12) becomes:

$$\sqrt{(X_s - x_1)^2 + (Y_s - y_1)^2 + (Z_s - z_1)^2} - \sqrt{(X_s - x_2)^2 + (Y_s - y_2)^2 + (Z_s - z_2)^2} = v \times (t_1 - t_2) \tag{13}$$

where y_1 and y_2 are zeros.

From equation (13), it can be seen that there is only one unknown variable Y_s remaining in the equation. The value of Y_s can be solved from this second order equation directly. Two roots with the same value but opposite signs are obtained: Y_1 and Y_2. These two solutions correspond to the two points on the perpendicular line passing through the black dot on x-z plane in Figure 3.2. The two points have the same distances to sensor 1 and sensor 2, as depicted in the figure. The sensors are all placed on one side of the asphalt sample, so only the positive Y_s value which makes the source locate inside the asphalt should be kept. In this case, we keep the value Y_2 as the actual y-coordinate of the source. As a result, the coordinates of the crack (X_s, Y_s, Z_s) is solved using time difference of arrival between sensor 1 and sensor 2. In order to obtain a more accurate y-coordinate, the TDOA method is used among the four sensors with the earliest arrival time by pairwise comparison and the results are averaged to obtain the final y-coordinate of the AE source.

3.2 Iterative Method

Gauss-Newton's method is a classical algorithm for solving non-linear least squares problems through a numerical search routine. Geiger's method is an application of Gauss-Newton algorithm in the field of seismic location. The algorithm is called recursively for several times, using the outputs from the previous run as the parameter input of the next iteration to obtain fast convergence to the solution of the unknown parameters. Being different from the non-iterative method described above, iterative source location such as Geiger's method only requires information from at least 4 sensors. Geiger's method starts from building the arrival time function of the i-th sensor $f_i(x, y, z, t)$ as:

$$f_i(x, y, z, t) = T_s + \frac{1}{v}\sqrt{(x_i - X_s)^2 + (y_i - Y_s)^2 + (z_i - Z_s)^2)} \tag{14}$$

Equation (14) is further evaluated at a point (x_0, y_0, z_0) near the actual source, and expand this equation using first-degree Taylor polynomial:

$$f_i(x,y,z,t) = f_i(x_0,y_0,z_0,t_0) + \varepsilon_i \tag{15}$$

Where ε_i is the residual term, which is the difference between the calculated arrival time and the observe arrival time with respect to the i-th sensor:

$$\varepsilon_i = \frac{\partial f_i}{\partial x}\delta x + \frac{\partial f_i}{\partial y}\delta y + \frac{\partial f_i}{\partial z}\delta z + \frac{\partial f_i}{\partial t}\delta t \tag{16}$$

The term ε_i is also called the correction vector, which is determined using the first order derivatives of the arrival time function. The goal of Geiger's method is to minimize the residual term ε_i by going through several iterations by equation (15). The results of (x,y,z,t) of the previous iteration will be substituted as (x_0, y_0, z_0, t_0) in the next iteration until ε_i converges to a sufficiently small threshold value. The starting trial location (x_0, y_0, z_0, t_0) is chosen to be the location of the sensor with the smallest observed arrival time among the four sensors because the first arrived sensor should have the closest distance to the AE source. Generally the trial solution $f_i(x,y,z,t)$ converges to the real location of the source within 3-5 iterations, or otherwise the arrival time function diverges to an infinitely large value when the correction term keeps increasing and never meets the terminating criteria. The problem of divergence sometimes is a result of using inaccurate arrival time as the inputs for the iterative search. An AE event will be regarded as an invalid event once divergence is observed in the iterative process.

One extra step was taken during the iteration process to avoid errors induced by surface waves. If the AE source is located near the top or bottom flat surface of the asphalt concrete specimen, the signals received by the sensors attached on those surfaces are most probably consisted of surface waves with much slower propagation speed than the dilatational waves received by sensors on the opposite side of the specimen. Therefore when an initial iterative search locates a source to be near the top or bottom surface, an additional iterative search will be conducted using only the information from the sensors attached on the opposite side of the specimen to update its location. With this extra iteration, the errors caused by surface waves can be minimized.

Iterative source location method provides a linear approximation of the nonlinear source location problem. By using first order Taylor polynomials to characterize the arrival time function, Geiger's method provides an alternative approach to the conventional triangulation-based source location methods. Iterative method is more time consuming compared to the USBM method because each AE event has to go through several iteration processes, but the iteration process gives more tolerance to the errors involved in the measurements because the correction term in each iteration improves the accuracy of the location result.

CHAPTER 4: EXPERIMENTAL PROCEDURES

4.1 Preparation of Test Specimens

Four gyratory compacted asphalt concrete specimens were prepared using the same mixture design under Superpave guidelines [17]. A nominal maximum aggregate size (NMAS) of 19 mm was used for the mixture with asphalt content of 5.9% by weight of the total mixture. The binder Superpave PG 64-22 was used in this mixture, where PG is an acronym for performance grade. The asphalt mixture blend uses aggregates from four stockpiles: 65% of coarse aggregate (CM16), 23% of manufactured sand (FM20), 10.5% of manufactured sand (FM02), and 1.5% of mineral filler (MF). The mass for each kind of aggregate was measured after batching, and those aggregates were put into a foil pan and placed in the oven for 2 hours at 155 $^{\circ}C$ to simulate short-term aging according to AASHTO PP2 protocol. The PG 64-22 asphalt binder and the mixing equipment were also heated in the same oven at 155 $^{\circ}C$. Short-term aging simulates the aging which occurs during plant production of the mixture.

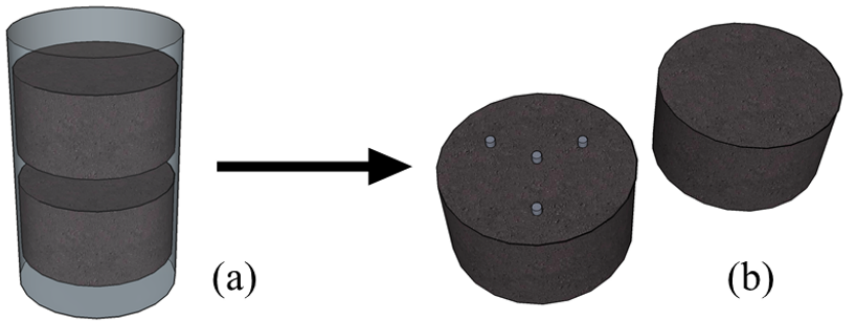

Figure 4.1: Specimen preparation; (a) a 120-mm tall specimen after gyratory compaction was cut into two 5-cm specimens, (b) two 5-cm tall cylindrical specimens were obtained by cutting the specimen on the left into half for AE testing – the left specimen in 1(b) shows the placement of four AE sensors on each side of the specimen

After the short-term aging, the aggregates were mixed with the binder at 155 $^{\circ}C$ in a mixing bucket, and the hot asphalt mixture was divided into four pans. Three pans of the asphalt mixture were then subjected to long-term oven-aging for 36 hours in the oven at 135 $^{\circ}C$. The mixtures were hand-stirred every 12 hours to ensure uniform aging. The asphalt mixture in the last pan does not undergo the 36 hours of aging, and it is described as the virgin specimen. A servo-controlled gyratory compactor, IPC Servopac, was used for compacting the asphalt mixtures into cylindrical specimens with a prescribed level of air voids. For each specimen, 4500 grams of the aged hot asphalt mixtures were heated to 155 $^{\circ}C$, then put into the mold for compaction for at least 100 gyrations at 600 kPa. Once the gyrations were complete, the mold was removed from the compacter. The specimens were then removed from the mold and allowed

to cool to room temperature. Four cylindrical samples with height of 120 mm and diameter of 150 mm were prepared.

The four gyratory compacted cylindrical specimens were cut into halves to obtain eight 5-cm tall cylindrical specimens with a diameter of 150 mm, as shown in Figure 4.2. Six of these specimens were made using the asphalt mixture that was oven-aged for 36 hours and two were made using a short-term aged mixture. During cutting, the ends of the gyratory compacted specimens were trimmed off in order to obtain a smooth surface for sensor placement. Figure 4.1 illustrates how two 5-cm thick cylindrical specimens were cut from one gyratory compacted specimen.

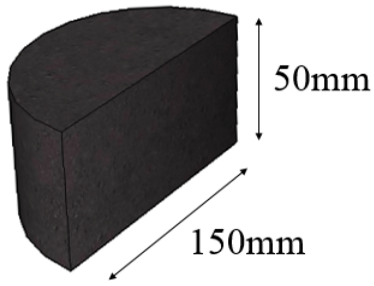

Figure 4.2: Dimensions of an asphalt concrete specimen

Four AE sensors were then coupled on each side of the specimen. Figure 4.3 shows the placement of eight AE sensors on one of the specimens. This sensor placement ensures a large portion of the asphalt concrete is covered within the monitoring range of the eight sensors. The sensors placed at the bottom side of the specimens have 45 $^{\circ}$ offset angle with respect to the sensors coupled on the top surface. The offset angle is to prevent obtaining inaccurate source location results due to symmetric sensor placement.

Figure 4.3: Front and side photograph of a specimen two weeks after being treated with rejuvenator with four acoustic emission sensors coupled to each of the two flat surfaces

4.2 Application of Rejuvenators to Asphalt Specimens

The Reclamite® rejuvenator (donated by The Heritage Group) is an emulsion of petroleum oils and resin. In order to evaluate the restoration and penetration ability of the rejuvenator, AE tests need to be conducted to both rejuvenator treated and untreated specimens for comparison. Out of the eight 5-cm tall asphalt specimens, two long-term-aged specimens (aged for 36 hours) and two short-term aged virgin specimens were used as the control samples for the AE testing. The remaining four specimens made with 36 hours long-term oven-aged mixtures were treated with the rejuvenator on the top flat surface.

The mass of each 5-cm tall specimen was measured using an electronic scale, and 5.9% of the measured sample mass is the mass of the binder. In this study, the amount of the rejuvenator applied on each specimen is 10% of the binder content in the specimen by weight. Rejuvenator with the required weight was measured and spread over the top surface of the specimens, and the rejuvenated specimens were put into pans for a period of dwell time before conducting the AE tests. The dwell time is the time for the rejuvenator to penetrate through the specimen surface and react with the asphalt binders. These specimens were then tested using the same AE-based approach after the dwell time of two, four, six, and eight weeks. The short-term aged virgin control specimens and the 36-hour aged control specimens were also tested using the same acoustic emission procedure for comparison.

Figure 4.3 shows a photograph of the front and side view of a specimen after being treated with rejuvenator for two weeks. Four acoustic emission transducers were coupled to each of the two flat surfaces of the specimen. Before testing on the asphalt sample, the rejuvenator remained on the surface was wiped off to ensure a better coupling of the sensors.

4.3 Acoustic Emission Testing Procedures

To simulate low temperature environment to develop thermal stress within the asphalt concrete, the specimen was put into the cooling chamber and cooled from room temperature to -35 $^{\circ}C$, see Figure 4.4. Figure 4.4 demonstrates the schematic diagram of the cooling chamber (ULP-25 Portable Freezer) with one specimen with four AE sensors coupled to each of the specimen's two flat surfaces. The specimen was placed on a shelf to allow air circulation for consistent cooling and felt pads were put underneath the shelf to minimize vibrations of the cooling chamber which may generate noise. The cooling of the asphalt specimen usually lasts 1 to 1.5 hours until the temperature at the surfaces of the specimen reaches -35 $^{\circ}C$. Sometimes the cooling test is stopped before reaching -35 $^{\circ}C$ when the number of AE events recorded exceeds the maximum AE events recording capacity of the monitoring system.

The temperature at the specimen surface was monitored and recorded using two K-type thermocouples. The two thermocouples were coupled on both the top and bottom flat surfaces of the test specimen using high vacuum grease to give the thermocouples better contact to the asphalt surface and provide insulation to the ambient temperature in the cooling chamber. The temperatures recorded using the two thermocouples were averaged to estimate the overall surface temperature of the specimen. A typical plot of AE testing cooling rate for the specimen from 0 $^{\circ}C$ to -35 $^{\circ}C$ is shown in Figure 4.5.

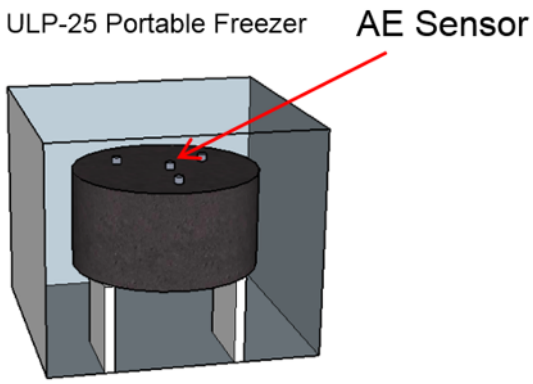

Figure 4.4: Schematic diagram of the cooling chamber (ULP-25 Portable Freezer) and test specimen showing four AE sensors coupled to each of the two flat surfaces and specimen support (specimen and cooling chamber not to scale)

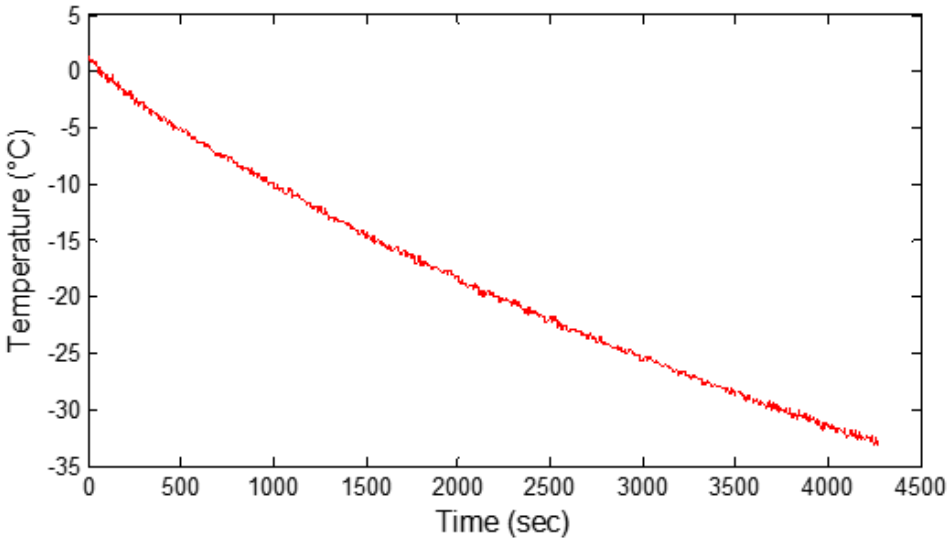

Figure 4.5: Typical cooling temperature versus time curve for the cooling experiment

Eight wideband AE sensors (Digital Wave, Model B1025) with a nominal frequency range of 50 kHz to 1.5 MHz were used to record acoustic emission activities within the sample. The sensors were coupled directly to the surface of the test specimen using high-vacuum grease, four sensors on each flat surface. The top surface of the sample is the side

treated with rejuvenator. Prior to testing, the AE sensors were conditioned in the cooling chamber to eliminate the AE events that arise due to the different rates of thermal expansion of the sensor's materials by keeping the sensors below -50 $^{\circ}C$ for two hours. The signals received by the AE sensors were pre-amplified 20dB using a broad-band pre-amplifier, and further amplified 21 dB and filtered with a 20 kHz high-pass filter. A pre-trigger was used, and the waveforms were digitized using a 16-bit analogue-to-digital converter (ICS 645B-8) using a sampling frequency of 2 MHz with 2048 sampled data points per channel per acquisition trigger. The channels were triggered when the signal crosses the triggering threshold voltage of 0.2 V. Figure 4.6 schematically represents a typical AE testing and data collection setup.

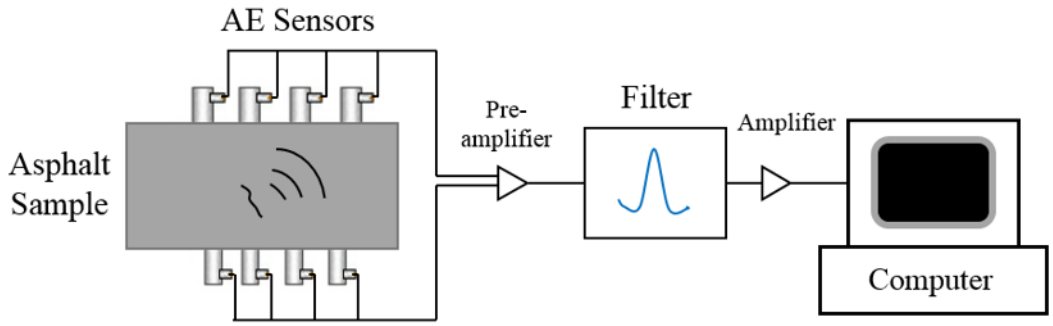

Figure 4.6: Schematic representation of a typical acoustic emission testing setup

Figure 4.7 shows a typical AE event waveform in the time domain and the corresponding spectral content in the frequency domain. To eliminate noise, all signals with an AE energy lower than 4 $V^2 - \mu s$ were filtered out. The AE events were stored in Digital Wave WaveExplorer^{TM} for later AE analysis and source location processing.

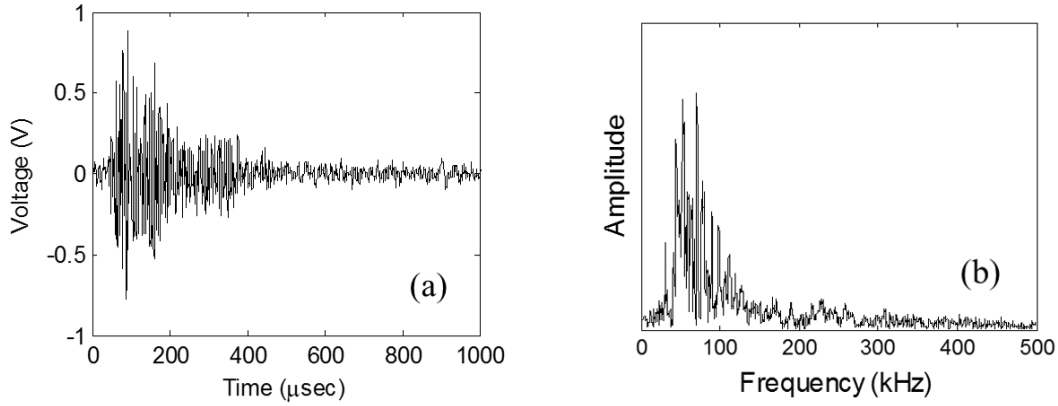

Figure 4.7: Typical acoustic emission: (a) time domain record, and (b) corresponding spectral content

As mentioned above, the computer software first filters the AE events based on their amplitudes and wave energy. AE events without an amplitude of 0.2 V or with energy level smaller or equal to 4 $V^2 - \mu s$ are discarded by the software.

These discarded AE events have similar amplitudes and energy levels as the background noise signals, so they are not used for any further computations.

There are 3 additional filters applied to the AE signals after recorded by the software. The first filter is to filter the AE events based on the number of AE sensors receiving them. As we discussed in Chapter 3, source location techniques used in this study are only applicable when an AE signal is received by at least four AE sensors. Therefore if an AE event is picked up by less or equal to three AE sensors, it is regarded as an invalid AE event for source location. The second filter uses the ratio of the signal duration to the amplitude of wave data to eliminate the reflection wave. This filter is called Duration-Amplitude filter, also known as Swansong II filter [74]. The limit of the ratio of duration to amplitude is set to 500 μs/v, which is determined by a statistical analysis of the reflected wave data in this study. The third filter is similar to the second filter, where this filter is to filter the AE events based on the ratio of the signal rising time to the amplitude of wave. The threshold of this ratio is set to 100 μs/v. Figure 4.8 illustrates the amplitude threshold, duration and the rise time of an example of the acoustic emission waves.

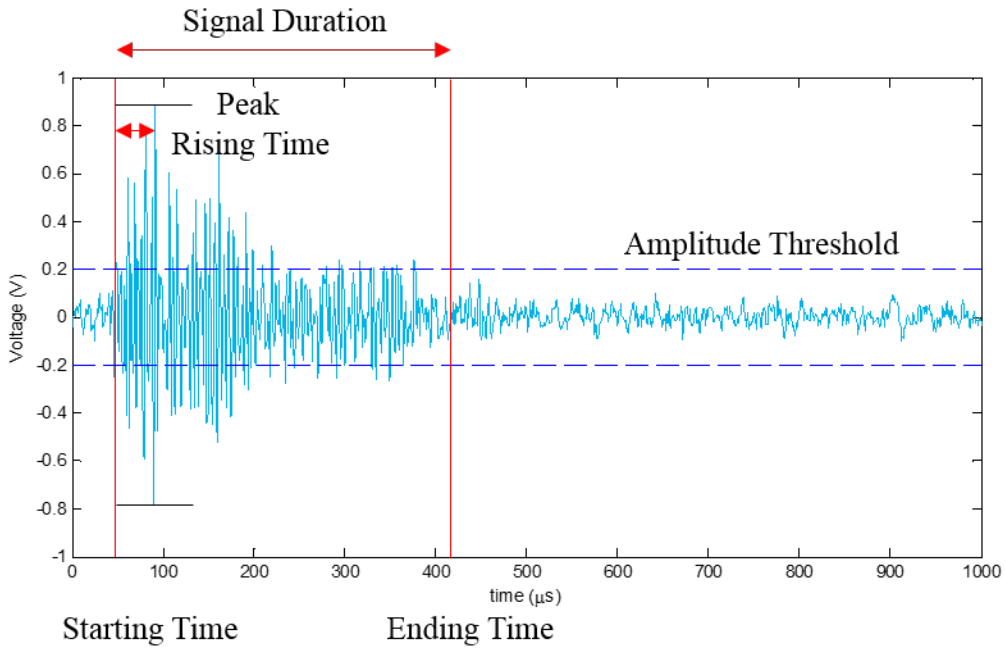

Figure 4.8: Illustration of the amplitude threshold, duration and the rise time of an acoustic emission signal

After implementing these 3 filters, the software iterates through the waveform data obtained by each AE sensor. It looks for the first instance of time when the voltage is higher than the threshold voltage 0.2 V. The occurring time of this instance represents the arrival time of an AE signal to a sensor. The processed data will then be used for the source location calculation using the methods introduced in Chapter 3. Additional information regarding AE-based estimation of embrittlement temperatures of HMA mixtures is provided in the following references [13, 15–18].

CHAPTER 5: AE SOURCE LOCATION EXPERIMENTAL RESULTS

5.1 Source Location Techniques Evaluation Procedures

A rectangular asphalt specimen extracted from the pavement is used for the source location validation experiments. This asphalt sample has the dimensions of 62.8 cm x 15.3 cm x 41.5 cm, as shown in Figure 5.1.

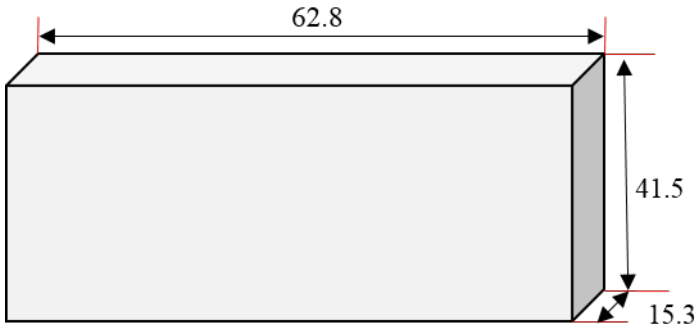

Figure 5.1: The rectangular asphalt sample (unit: cm)

The 8 acoustic emission sensors are placed on the back side of the rectangular asphalt sample. A rectangular-shaped sensor holder was made to be attached to the back surface of the asphalt sample so that the sensors could be placed on the surface securely, see Figure 5.2. Holes are drilled on this plate to place the sensors and they are spaced 5 cm from each other. The sensor placed in the hole at the top left corner has the coordinates of (5 cm, 0 cm, 5 cm).

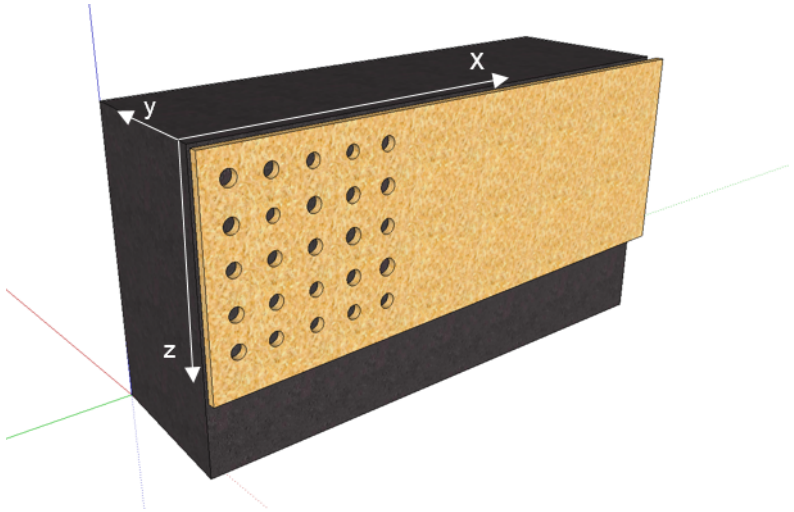

Figure 5.2: Sensor placement on the rectangular asphalt sample

The eight AE sensors are placed in a pattern as shown in Figure 5.3. The coordinates of these eight sensors are: (5, 0, 5), (10, 0, 10), (15, 0, 15), (20, 0, 20), (5, 0, 15), (10, 0, 20), (15, 0, 25), (20, 0, 30) respectively, where the coordinates are in centimeters. The sensors are placed in this manner to avoid involving symmetric sensor coordinates in the calculations. The monitoring range of these sensors are plotted as the gray area in Figure 5.3. If an AE source occurs outside this gray area, the AE wave produced by this source may not be able to be received by at least four sensors due to a longer wave traveling path. Therefore for this sensor placement, the AE sources are simulated only within the region bounded by this gray valid monitoring range.

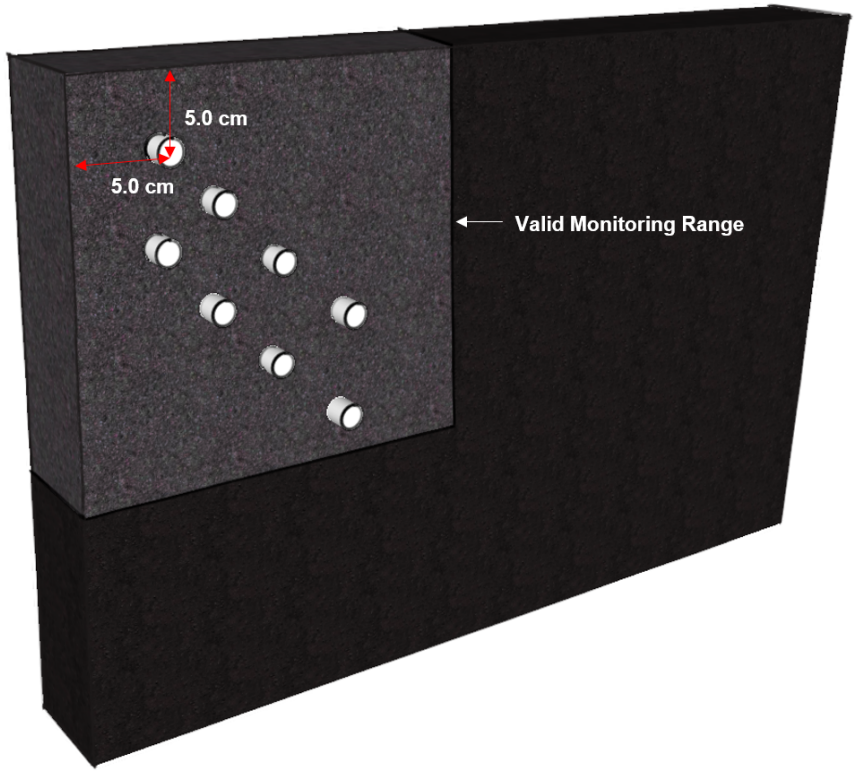

Figure 5.3: First sensor placement on rectangular asphalt sample with the valid monitoring range labeled

The initial gray valid monitoring area is at the left side of the asphalt sample. If the AE events occurred in the right half of the rectangular asphalt sample are of interest, the eight sensors need to be shifted rightward by 30 cm. After shifting these sensors, AE sources can be simulated in the new monitoring range at the right side of the sample. The reason for doing source simulation on both left and right halves of the asphalt sample is that the properties of the left and right halves of the specimen are slightly different. The asphalt binder at the left side of the specimen is softer comparing to the binder at the right side, so there are some large cracks located at the left side of the asphalt concrete. The aggregates and the binder at the right half of the specimen are more rigidly compacted together and there is no major crack observed on the specimen. Therefore two sensor placements at different locations are used on this asphalt

specimen in order to examine whether the rigidity of the material has an impact on the accuracy of source location.

The acoustic emission source used in the experiment is the Hsu-Nielsen source, which is simulated by breaking a pencil lead on the surface of the asphalt [75]. There are three AE sources simulated on the asphalt specimen. The coordinates of these sources are: (5.0, 14.2, 5.0), (15.0, 13.8, 18.5), (40.0, 13.0, 7.0) respectively, where the first two sources are at the left side of the specimen and the third source is located at the right side. Five Hsu-Nielsen sources are simulated at each of these three locations, and the coordinates of these five sources are computed using the non-iterative and iterative source location methods. The results of these source location calculations using different source location methods are presented in the following sections.

5.2 Non-iterative Source Location Results

At each of the three locations, five AE emissions were simulated at the same spot by breaking mechanical pencil leads. The AE waves were received by the AE sensors, and the collected waveforms were then filtered by the filters and processed using the non-iterative USBM source location algorithm. The AE sensors are all placed on the same side of the rectangular asphalt sample, so the modified version of the USBM source location method described in Section 3.1.3 is used to compute the coordinates of the sources.

The results of the crack location coordinates are presented in Table 5.1, and the corresponding source location errors are computed and presented in Table 5.2. The errors listed in Table 5.2 are the absolute distances from the computed source locations to the actual locations of the sources.

Table 5.1: Non-iterative source location results

Source Number	Trial 1			Trial 2			Trial 3			Trial 4			Trial 5		
	x	y	z	x	y	z	x	y	z	x	y	z	x	y	z
Calculated Coordinates (cm)															
1 (5, 14.2, 5)	5.88	13.17	6.64	6.58	12.87	6.65	5.68	14.81	5.68	4.77	13.85	5.68	5.29	13.10	5.78
2 (15, 13.8, 18.5)	13.73	14.20	17.82	13.81	13.01	17.19	14.13	14.26	17.39	13.73	14.20	17.82	14.91	11.08	17.86
3 (40, 13, 7)	40.00	14.18	6.91	39.46	12.34	6.29	39.02	13.42	7.14	39.47	13.77	6.50	39.46	12.34	6.29
Error (cm)															
1	0.88	1.03	1.64	1.58	1.33	1.65	0.68	0.61	0.68	0.23	0.35	0.68	0.29	1.1	0.78
2	1.27	0.4	0.68	1.19	0.79	1.31	0.87	0.46	1.11	1.27	0.4	0.68	0.09	2.72	0.64
3	0	1.18	0.09	0.54	0.66	0.71	0.98	0.42	0.14	0.53	0.77	0.5	0.54	0.66	0.71

Table 5.2: Non-iterative source location errors

Error in absolute distance (cm)						
Source Number	Trial 1	Trial 2	Trial 3	Trial 4	Trial 5	Average
1	2.13	2.64	1.14	0.80	1.38	1.62
2	1.50	1.94	1.48	1.50	2.80	1.84
3	1.18	1.11	1.08	1.06	1.11	1.11

The locations of the sensors, actual location of the cracks and the calculated source locations are displayed in Figure 5.4.

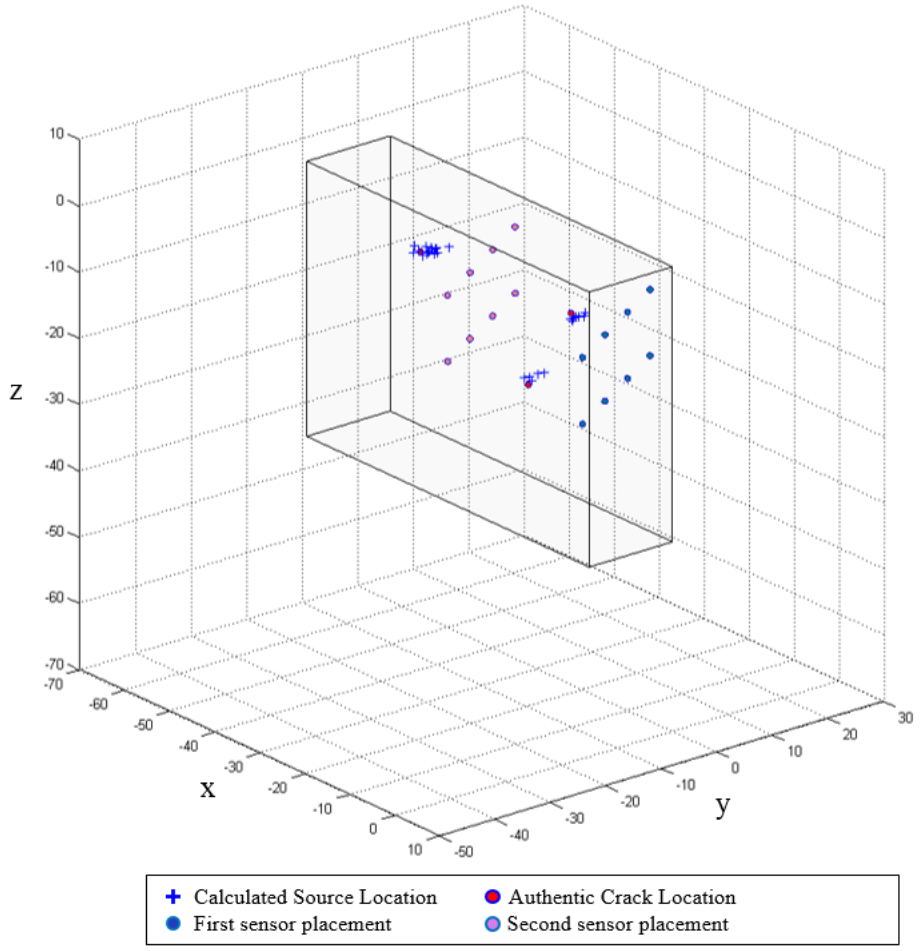

Figure 5.4: Graphical representation of the authentic and calculated source locations using non-iterative source location method (unit: cm)

5.3 Iterative Source Location Results

The same testing procedures described in Section 5.2 are repeated by using the iterative Geiger's source location method. Five AE emissions were simulated at each of the three locations by breaking mechanical pencil leads. The AE waves were received by the AE sensors, and the collected waveforms were then filtered by the filters and then processed using the iterative Geiger's method. Only data collected by the first four sensors receiving the AE signals were used for the computation.

The results of the crack location coordinates calculated using Geiger's method are presented in Table 5.3, and the corresponding source location errors in absolute distance are computed and presented in Table 5.4. The locations of the sensors, actual location of the cracks and the calculated source locations are shown in Figure 5.5.

Table 5.3: Iterative source location results

Source Number	Trial 1			Trial 2			Trial 3			Trial 4			Trial 5		
	x	y	z	x	y	z	x	y	z	x	y	z	x	y	z
Calculated Coordinates (cm)															
1 (5, 14.2, 5)	6.08	15.07	6.08	5.99	14.88	5.99	5.8	14.49	5.8	6.39	13.92	6.39	6.12	13.29	6.13
2 (15, 13.8, 18.5)	12.51	20.94	14.61	12.78	20.25	15.05	15.71	16.29	16.45	16.19	17.27	16.86	17.11	16.21	17.3
3 (40, 13, 7)	39.72	12.59	7.58	39.28	12.87	6.85	39.36	11.94	7.28	39.56	14.46	6.73	38.88	13.47	7.18
Error (cm)															
1	1.08	0.87	1.08	0.99	0.68	0.99	0.8	0.29	0.8	1.39	0.28	1.39	1.12	0.91	1.13
2	2.49	7.14	3.89	2.22	6.45	3.45	0.71	2.49	2.05	1.19	3.47	1.64	2.11	2.41	1.2
3	0.28	0.41	0.58	0.72	0.13	0.15	0.64	1.06	0.28	0.44	1.46	0.27	1.12	0.47	0.18

Table 5.4: Iterative source location errors

Error in absolute distance (cm)						
Source Number	Trial 1	Trial 2	Trial 3	Trial 4	Trial 5	Average
1	1.77	1.56	1.17	1.99	1.84	1.666
2	8.75	7.88	3.64	4.25	3.63	5.63
3	0.759	0.74	1.26	1.55	1.23	1.1078

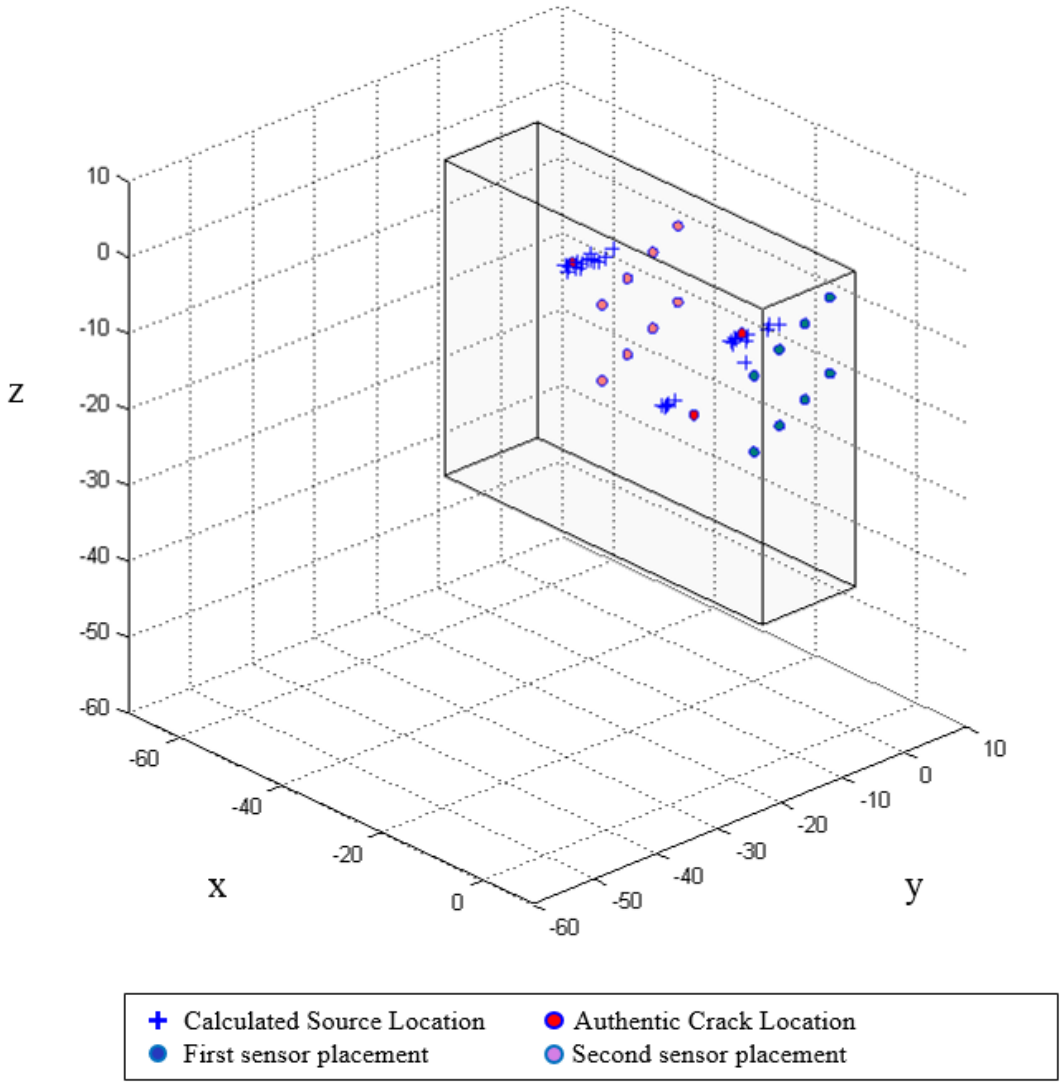

Figure 5.5: Graphical representation of the real and calculated source locations using iterative source location method (unit: cm)

5.4 Discussion on Source Location Results

The two source location algorithms used in this study are both based on the assumption that the velocity of AE wave travelling inside asphalt is constant. Figure 3.1 shows the dilatational (longitudinal/primary) wave velocities, shear (secondary) wave velocities and corresponding attenuations for asphalt concrete samples aged from 0 to 36 hours. As discussed by McGovern et al [17], the velocity of the faster dilatational wave varies as the oxidative aging level of the asphalt specimen increases. In this chapter, the aging level for the rectangular asphalt sample is assumed to be virgin, and the velocity for the dilatational wave used in the computation is taken as the average value of 3200 m/s for virgin

asphalt specimens with wave frequencies ranging from 30 to 150 kHz in Figure 3.1(a).

Due to the stochastic nature of the asphalt concrete, the velocities and attenuations do not have a deterministic value. A sensitivity analysis is performed to determine the influence of the variation of the velocities on the accuracy of the source location computations. With reference to Figure 3.1(a), the range of variation for the dilatational velocity in virgin asphalt specimen is observed to be limited within 15% with respect to its average value of 3200 m/s. For the sensitivity analysis, dilatational velocities with variations of 2.5%, 5%, 10% and 15% are used to compute the source location respectively. The lower and upper bound for the velocities with different levels of variation are listed in Table 5.5.

Table 5.5: Dilatational velocity varying ranges

Percentage error in velocity (%)	Velocity value (ms^{-1})	
	Lower Bound	Upper Bound
0	3200	3200
2.5	3120	3280
5	3040	3360
10	2880	3520
15	2720	3680

The locations of the sources are computed using non-iterative source location method with the velocity values in Table 5.5, and the errors of the computed source location results are presented in Appendix A. These errors are calculated using the average of the distance differences between the actual crack location and the calculated source location using lower and upper bound values of velocities at each percentage variation of the wave velocity.

With reference to Figure A.1 - A.3, the X and Z coordinates calculated using the non-iterative method are not affected significantly even with a variation of 15% in velocity value. The Y coordinate calculated using the TDOA approach is more prone to the errors in velocity values. With 15% variation in velocity, the error in Y coordinate increases from less than 1.0 cm to 2.5 cm. Figure A.4 shows that the absolute distance error increases from around 1.5 cm with 0% variation in wave velocity to around 3.0 cm when wave velocity varies by 15%.

By comparing the real crack location coordinates to the calculated source location, the average error in absolute distance ranges from 1.0 cm to 2.0 cm based on the values presented in Table 5.2 and Table 5.4. The only exception is the computed source location results in location 2 using the iterative source location method. Source location results at this spot using the iterative method have an average error of 5.63 cm. This large error might be a result of experimental or human errors, i.e., the pencil lead might not be cracked at the exact location at (15, 13.8 18.5) during the AE source simulation experiment. Asphalt material has a heterogeneous nature due to the presence of aggregates with various sizes. Acoustic wave velocities traveling through asphalt binder and those aggregates are different. In addition, the paths traveled by the acoustic waves may not be straight lines. These factors make it very difficult to obtain a source location result with 100% accuracy. The largest aggregate present in the asphalt specimen has a diameter around 1.0 cm, so it can be concluded that the errors ranging from 1.0 cm to 2.0 cm are still within acceptable tolerance range in this experiment.

Figure 5.6: The presence of the large cracks in the asphalt concrete

Another factor affecting the source location is the presence of cracks in the asphalt concrete. The left side of the asphalt specimen has several major cracks as depicted in Figure 5.6, and the width of the largest crack is 0.7 cm. The impedance of the air in the gap is so large that the AE wave cannot travel through the gap. Therefore it is suggested that AE crack sources should not be simulated near the crack to avoid losing AE signals due to extremely high attenuation. In the experiment described above, source location 1 and 2 are located near the large cracks on the left side of the asphalt concrete, and source location 3 is located at the right side of the asphalt where there is no major cracks observed. The comparison among the source location results at location 1, 2 and 3 in Table 5.2 and 5.4 shows that the presence of cracks near the AE source also increases the errors in source location.

CHAPTER 6: AE-BASED EVALUATION OF REJUVENATOR PERFORMANCE RESULTS

The stochastic nature of asphalt concrete with two distinct phases, i.e., mastic and aggregates, where each phase has different acoustic properties, leads to energy scattering and mode conversion. This effect increases with frequency. The presence of multiple scatters makes it possible to have multiple mode conversions and multiple paths of the (primary and scattered) wave fields from the source location to the observation point. As a result, both the bulk dilatational and shear velocities and the corresponding attenuations depend upon the frequency and the level of aging. McGovern et al [17, 18] provide a very good discussion of the difficulties in estimating velocities and corresponding attenuations in asphalt concrete. Both the short-term aged specimens and the specimens oven-aged for 36 hours had uniform properties through their thickness. However, in the case of the oven-aged specimens for 36 hours exposed to rejuvenator on the top surface, the material properties of the specimens became graded through their thickness as the rejuvenator acted upon the aged binder throughout the thickness of the specimen. As a result, the longitudinal and shear velocities and the corresponding attenuations also became graded throughout the specimen's thickness.

For asphalt concrete mixtures without the presence of rejuvenator, the AE-based embrittlement temperature is determined as the temperature at which an event with an energy equal or above a prescribed value occurs. The prescribed energy value is determined using a mixture of known value for its embrittlement temperature. For these cases, the specimen volume is irrelevant, provided it is large enough to provide constraints to the binder contraction during thermal cooling. This occurs when the specimen size is about four-to-five times the size of the larger aggregate [13,15,17].

For asphalt concrete mixtures in the presence of rejuvenator, the specimens became graded structures whose gradation is a function of time. The penetration of the rejuvenator into the specimen depends upon the porosity distribution and the corresponding tortuosity, which is typically not uniform within the volume of the specimens. As a result, at a given time there are pockets of asphalt concrete within the test specimens where the rejuvenating effect did not yet occur. Therefore, these pockets of asphalt concrete have warmer embrittlement temperatures than the material that has already been rejuvenated. During thermal cooling these pockets of warmer embrittlement temperatures produce sporadic energetic AE events, which makes the evaluation of the specimen material embrittlement temperature more difficult. To avoid this difficulty, i.e., the influence of these sporadic energetic events, a rate criterion was developed where the embrittlement temperature is defined as the temperature when a prescribed event rate occurs where the events have an energy equal of above a prescribed value. The prescribed event energy and the event rate need however

to be calibrated, which in this study is done by testing two mixtures with known embrittlement temperatures, i.e., the short-term aged (virgin) mixture and the oven-aged mixture for 36 hours, which have embrittlement temperatures of -25 $^{\circ}C$ and -15 $^{\circ}C$, respectively. Because a larger volume produces corresponding more emissions, care must also be taken during the calibration process. In this study all the specimens have the same volume.

6.1 Quantitative Evaluation of Rejuvenators Using AE Event Rate

In this section, the temperature corresponding to an event-rate equal or above five events per second (of events having an energy equal or above 4 $V^2 - \mu s$) is termed the mixture's embrittlement temperature. Note that occasionally a test will produce a few isolated AE events above 4 $V^2 - \mu s$ early on in the test at warmer temperatures. Because these events are isolated, i.e., AE events do not occur at a regular rate after such an event as the specimen continues to cool, they are neglected and not considered to estimate the mixture embrittlement temperatures.

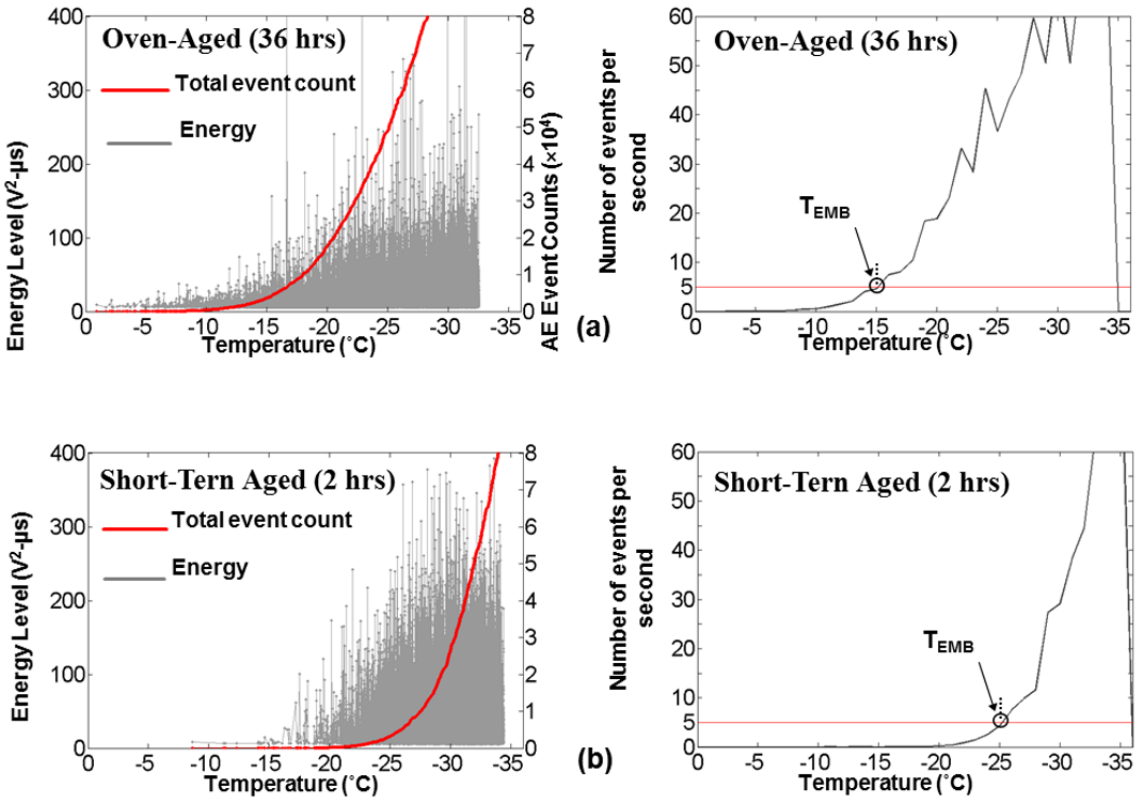

Figure 6.1: The first and second row represent AE tests results for asphalt concrete samples oven-aged for 36-hours and for 2-hours, respectively. Left column represents AE event energy levels and AE total event counts versus temperature for asphalt samples observed during cooling. Right column represents the average event count rate versus cooling temperature, and shows the corresponding embrittlement temperatures.

Figure 6.1 shows the acoustic emission response of a sample oven-aged for 36 hours and of a sample aged for 2-

hours, i.e., short-term aging, respectively, when cooled from room temperature to -35 $^{\circ}C$. Following our definition of embrittlement temperature, the right column of Figure 6.1 shows the embrittlement temperatures of the oven-aged specimen for 36 hours and for the short-term aged specimen to be around -15 $^{\circ}C$ and -25 $^{\circ}C$, respectively. Figure 6.1 shows that the aging of the binder results in a sample with warmer embrittlement temperature of -15 $^{\circ}C$ rather than -25 $^{\circ}C$. Figure 6.1 also shows that the virgin sample, while having less AE events, also has events that are more energetic and occur at cooler temperatures than the AE events associated with the 36 hours oven-aged specimen. This difference in acoustic emission response is consistent with the observation that the binder of the specimen aged for 36 hours is stiffer and has lower adhesive properties than the virgin binder, i.e., binder with short-term aging. Because of the ovenaged process, in addition to the binder becoming stiffer, micro-flaw populations also develop between the binder and the aggregates and between the binder and the mastic because of lower adhesive properties of the binder. This also explains why the embrittlement temperature of the specimen oven-aged for 36 hours is warmer than the embrittlement temperature of the specimen for short-term aging. During cooling the developed thermal stresses reach the binder fracture strength at warmer temperatures (because of the presence of the micro-flaw populations) as compared to the short-term aged specimen.

Figures in Appendix B show the acoustic emission responses of the four test samples exposed to rejuvenators on the top surface after the dwell times of two, four, six, and eight weeks, respectively. Figure B.1-B.4 represent the average acoustic emission response of the four sensors coupled to the asphalt surface not exposed to rejuvenator, i.e., bottom surface. Figures B.5-B.6 represent the average acoustic emission response of the four sensors coupled to the asphalt surface exposed to rejuvenator, i.e., the surface where the rejuvenator was applied or the top surface. The rejuvenator penetrates the specimen via gravity and capillary action. Once the rejuvenator contacts the binder, it acts on the binder, making it more viscoelastic as compared to the oven-aged binder for 36 hours. It can be observed from figures in Appendix B that after only two weeks of dwell time the surface exposed to rejuvenator has significant less acoustic emission activity than the bottom surface, i.e., the surface not exposed to the rejuvenator, which is similar to the AE response of the specimen aged for 36 hours without rejuvenator, see Figure 6.1. As the dwell time increases and the rejuvenator has the time to reach the bottom of the specimen and act upon the binder, similar emission activities are observed by the sensors coupled to both the specimens' top and bottom flat surfaces.

To estimate the effect of rejuvenator upon the embrittlement temperatures, figures in Appendix C display the number of events per second versus the cooling temperature. Figures C.1-C.4 represent the average of AE activities collected by the four sensors coupled to asphalt surface not exposed to rejuvenator, i.e., bottom surface, and Figures C.5-C.8 represent the average AE activities received by the four sensors coupled to asphalt surface exposed to rejuvenator, i.e., top surface. Figures in Appendix C show that as the dwell time increases, and the rejuvenator has time to act on

the oven-aged binder, the embrittlement temperatures of the specimens become cooler, i.e., improve. It can also be observed that just after four weeks of dwell time, the embrittlement temperatures quantitatively evaluated from data provided by AE sensors coupled to both surfaces reached the embrittlement temperatures of the virgin specimen, i.e., the original embrittlement temperatures were recuperated. These figures also show that as the dwell time increases, the embrittlement temperatures of the specimens become cooler than the embrittlement temperature associated with the short-term aged specimen. Please note that, while much care was exercised during the manufacturing of the test specimens, the variability observed in figures in Appendix B and Appendix C is due to the inherent variability of material properties in the specimens such as porosity, aggregate distribution, level of compaction, etc.

6.2 Quantitative Evaluation of Rejuvenator Performance Using AE Source Location

After the embrittlement temperature has been reached, asphalt concrete changes from a quasi-brittle material to a brittle material which has lower resistance to thermal damages. Large amount of AE events are then collected by the AE sensors. Past studies have proposed many different definitions of the asphalt embrittlement temperature. The most common definition of embrittlement temperature is the temperature corresponding to the first high energy level event occurred during cooling. Figure 6.2 depicts a plot of the AE energy and AE event count obtained by one of the eight sensors installed on a 36-hour aged asphalt specimen. The temperature corresponding to the event with the first high energy level above 100 $V^2 - \mu s$ is -15.51 $^\circ C$. This embrittlement temperature is close to the embrittlement temperature of -15 $^\circ C$ obtained in the previous section, where the embrittlement temperature of the asphalt concrete is defined by the rate of increase in the number of AE events.

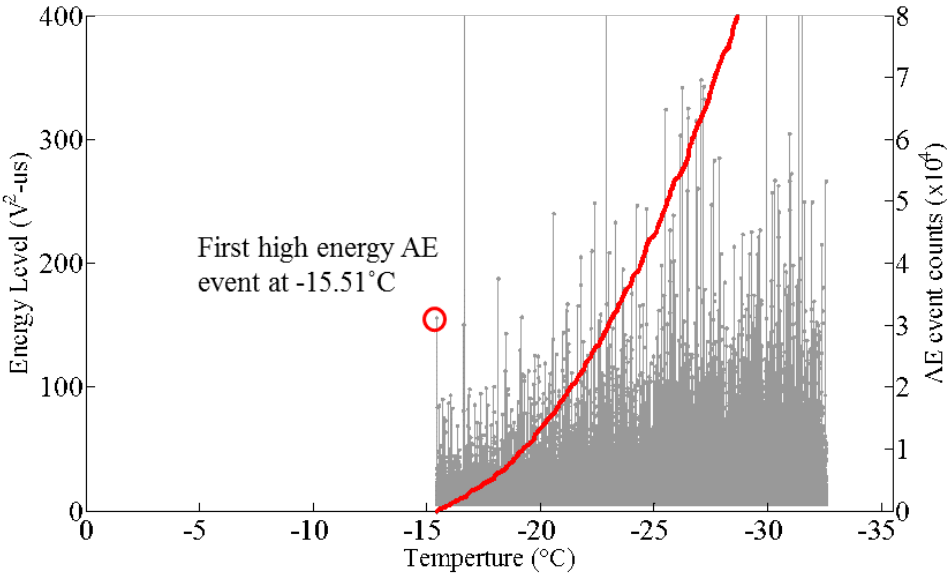

Figure 6.2: AE event energies and AE event count versus temperature received by one sensor for a typical 36-hour aged specimen

These definitions of the embrittlement temperature focus on the globally monitoring of the number of AE events. When the penetration ability of the rejuvenator is of interest, the information about the embrittlement temperatures obtained in the past studies are not sufficient to draw reasonable conclusions regarding to the penetration depth. Therefore AE source location techniques are relevant here to compute the coordinates of each AE source produced during cooling and then determine the embrittlement temperature at different heights within the asphalt specimens using the source location results.

In this section, AE events received by at least 4 sensors were used for iterative source location computation, and AE event received by at least 5 sensors were used for non-iterative source location method. The coordinates of every AE event were first calculated using Geiger's method, then calculated using non-iterative source location method. Only the valid results were kept. Valid result means that the location of the source should be within the asphalt specimen, and the calculated occurring time of the event should be always earlier than the observed arrival time on each sensor.

6.2.1 Source Location Results Using Iterative Method

The valid locations of all AE sources for a typical 36-hour aged asphalt specimen are displayed as blue dots in Figure 6.3. It can be observed from this figure that most of the AE sources are clustered in the center region of the cylindrical asphalt specimen, which can be clearly observed from the side views shown in Figure 6.4. The size of the inner clustering area is not deterministic. In this part of the study, the radius of the inner clustering area is chosen to be 4 cm, but this size can be relaxed to 5 cm as shown in Figure 6.4. This inner clustering area was defined to be the valid monitoring region.

The red inner cylinder with a diameter of 8 cm represents the valid monitoring region for the AE sources with the sensor placement shown in Figure 6.5. An AE source located within this inner cylinder has closer distances to all of the eight sensors, so the acoustic waves produced by sources in this region are more likely to be picked up by at least four sensors compared to AE sources located outside the inner cylinder. In contrast, the locations of many AE sources outside the inner cylinder were more difficult to be calculated, because of the insufficient number of available receiving sensors. In addition, errors caused by reflections are likely to occur when those outside AE sources are located near the surrounding boundary of the specimen. Acoustic waves will be partially reflected back after hitting the asphalt-air boundary. The reflected waves could be picked up by the sensors, causing false measurements of the receiving time and resulting in less accurate source location calculations due to these errors. The errors caused by the reflections at the boundary can be mitigated by retaining only the AE sources within the red cylinder for the source location analysis. Discarding the AE sources near the boundary does not affect the analysis results, because only

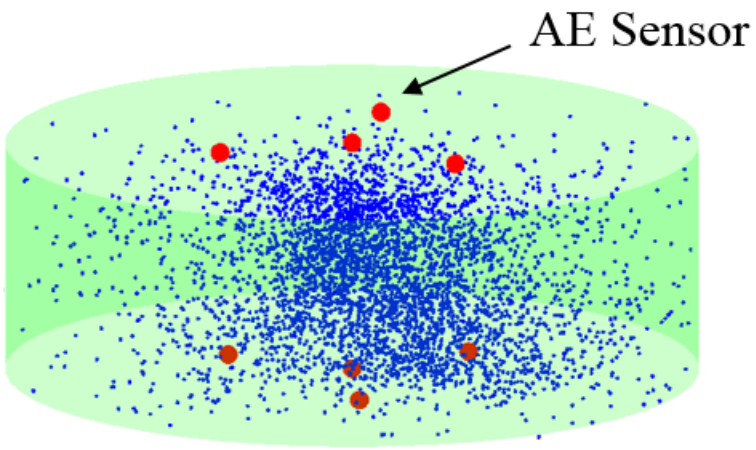

Figure 6.3: Valid AE source location distribution for a typical 36-hour aged specimen

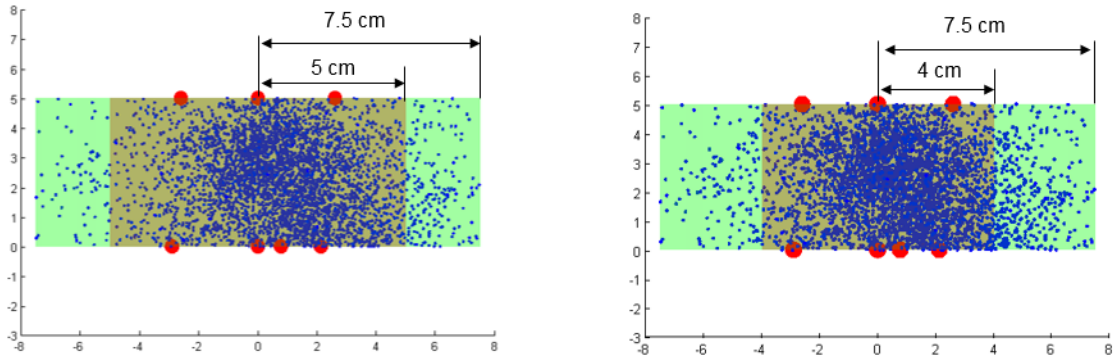

Figure 6.4: Side view of the valid AE source location distribution for a typical 36-hour aged specimen

the depth of each AE source is of interest for the evaluation of the penetration ability of rejuvenators. AE sources located within the valid monitoring region are sufficient enough to demonstrate the relationship between the AE event occurring temperature and the depth of the AE sources.

The coordinates of the AE sources are then computed using the iterative Geiger's method described in Section 3.2. Only the height, i.e., the z-coordinates of the AE sources are used for the evaluation of the penetration depth of the rejuvenators. For the 36-hour aged specimen, the relationship between the height of the specimen at where each AE source occurs and the occurring temperature of the AE sources is shown in Figure 6.6.

Figure 6.6 shows that after the specimen was cooled to -12$^{\circ}C$, AE events started to populate at various heights in the specimen. Those early AE events occurred at the pre-cracking region, or the early transition region. At this stage, the

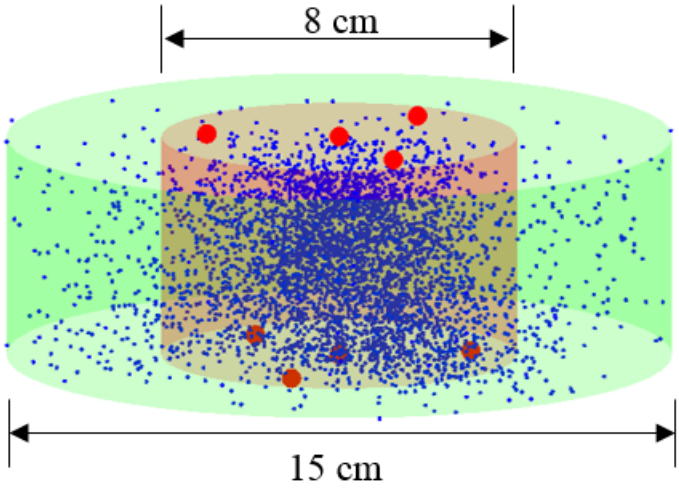

Figure 6.5: AE sources are clustered in the red inner cylinder with a diameter of 8 cm

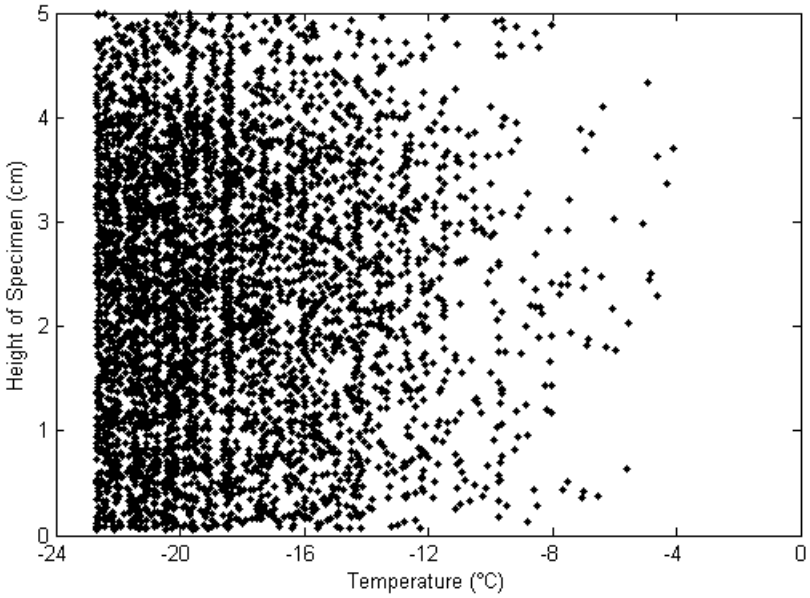

Figure 6.6: Height at which the AE sources locate along the cooling temperature for the 36-hour aged specimen

AE events having very small energies are randomly distributed within the specimen. They are likely to be produced by the freezing of the moisture content or the early formation of the thermal microcracks as the asphalt material gradually changes from a quasi-brittle to a brittle state. As the temperature drops lower, the fracture resistance of the asphalt decreases and massive damages occur within the asphalt concrete. This stage is called the stable cracking region, where a rapid increase in the number of AE events is observed. The embrittlement temperature is the temperature at which this stage begins. As supported by the experiments conducted in past studies, the embrittlement temperature

for a 36-hour aged specimen should be at around -15 $^{\circ}C$. In Figure 6.6, a rapid increase in the number of AE events is observed after -15 $^{\circ}C$.

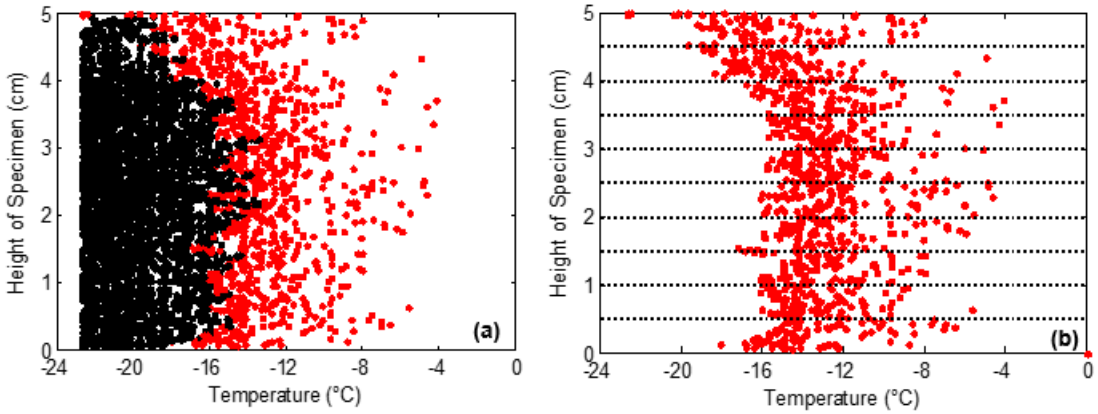

Figure 6.7: (a) Red dots are AE events happened in the pre-cracking region or early transition region. (b) The height of the specimen is divided into 10 intervals, and the red dots are the first 100 events occurred within each interval.

In Figure 6.6, it is hard to define a clear starting point of the stable cracking region. A very intuitive approach of defining this starting point is to discard a certain number of early AE events happened at each height interval of the specimen, and the remaining AE sources are categorized to be happened after the stable cracking region has begun. Figure 6.7 illustrates an example of this approach. The 5 cm tall specimen is divided into 10 intervals, with each interval having a height of 0.5 cm. The division of the intervals is demonstrated in Figure 6.7(b). The first 100 AE events occurred at each interval are characterized as the early AE events happened within the pre-cracking region and the early transition region. These early AE events are represented as red dots in Figure 6.7(b). The 100-th AE events occurred at each height interval signals the start of the stable cracking region. In Figure 6.7(a), AE sources occurred in the pre-cracking region and the early transition region are colored in red, and the AE events happened in the stable cracking region are colored in black. It can be observed that the black dots region initiates around -16 $^{\circ}C$, which is pretty close to the embrittlement temperature of a typical 36-hour aged specimen.

However, this intuitive approach is not very accurate in defining the embrittlement temperature for asphalt concrete. There is no guarantee that the embrittlement temperature obtained in this approach is accurate, as the first 100 AE events are arbitrarily regarded as early AE events. Changing this arbitrary number 100 will largely alter the obtained embrittlement temperature. This method is also subject to the variability of those early events happened in the pre-cracking region. AE events happened at the beginning of cooling are possibly caused by the freezing of the moisture content in the asphalt specimen. If a certain portion of the specimen has higher amount of moisture content, this portion will have a much higher embrittlement temperature obtained using this approach compared to other parts of

the specimen.

A new method is proposed to estimate the embrittlement temperature from the source location results. This method is inspired by the event-rate method described in Section 6.1. Instead of looking at the temperature at which each AE source occurred, the occurring time of each AE event is of interest. Using the occurring time of AE events, the increasing rate of AE events at each height interval of the asphalt specimen can be found and utilized to estimate the embrittlement temperatures at different heights. In order to accomplish that, the height of each AE source is plotted against the cooling time as shown in Figure 6.8.

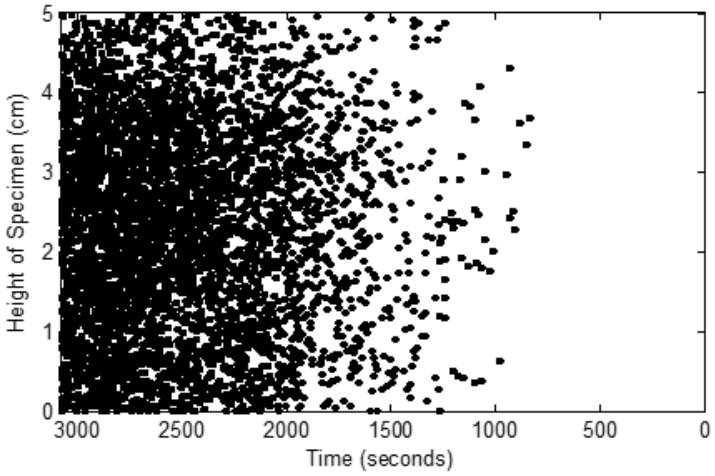

Figure 6.8: Height at which the AE sources locate along the cooling time for the 36-hour aged specimen

In Figure 6.8, a rapid increase in the number of AE events is observed after a cooling time of 2000 seconds. A more precisely defined time corresponding to a rapid increase of AE events could be found by looking at the rate of increase of the AE events.

Using the same height interval partition approach described in Figure 6.7(b), the number of the AE events occurred per minute is evaluated per 0.5 cm height interval of the specimen.The process of finding the increasing rate of AE events is like moving a 0.5 cm tall and 60 seconds wide rectangular box from the starting time to the left until the rectangular box encloses a certain number of AE sources. This process is repeated 45 times, each time the box is moved downwards by 0.1 cm.

A threshold AE event increasing rate is required to define "a rapid increase of AE events." In this part, the threshold increasing rate per 0.5 cm interval is set to be 10 events per 1 minute. It implies that the box (0.5 cm vs. 1 min) is moved to the left until it encloses 10 emissions. The AE sources enclosed by the boxes at each level of height during this process are plotted as red dots in Figure 6.9. In this figure, AE events displayed as the red dots indicate

the beginning of the stable cracking region for each height interval. The increasing rate 10 emission per 1 minute per 0.5 cm was chosen because this threshold rate could accurately define a region where the number of AE events starts to increase rapidly, as shown in Figure 6.9. The occurring temperature of these red dots could also give an accurate characterization of the embrittlement temperature at each height of the specimen.

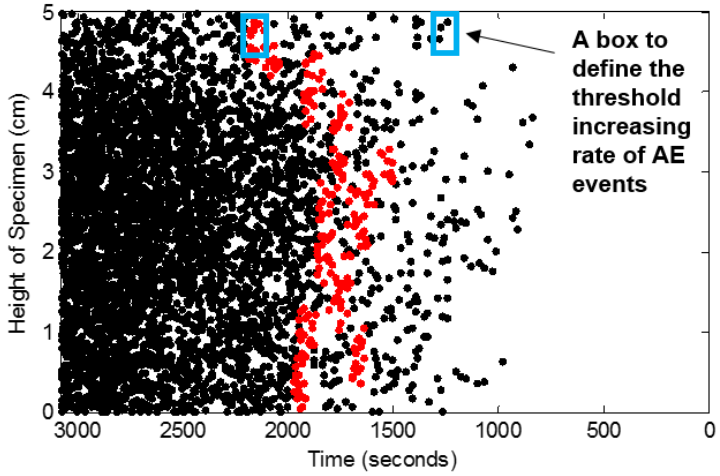

Figure 6.9: The box (0.5 cm vs. 1 min) is moved to the left until it encloses 10 emissions, which defines the embrittlement temperature at the centroid of the box.

This process is repeated on the virgin specimen, and the results are presented in Figure 6.10. The 36-hour aged asphalt specimen is expected to have a much warmer (worse) embrittlement temperature than the virgin specimen based on the experiment results in Section 6.1 and previous studies. Figure 6.10 also demonstrates that the stable cracking region of 36-hour aged specimen happens around 500 seconds earlier than the virgin specimen. The occurring temperatures of these red colored AE events are transposed and calculated from the cooling time using the temperature-time cooling curves, and the average occurring temperature of the red AE events in each interval is calculated. These average occurring temperatures of the AE events are regarded as good representatives of the embrittlement temperature at each height interval of the specimen. Figure 6.11 graphically displays the average temperatures of the red AE events at each height interval, with the average embrittlement temperatures of the whole 36-hour aged specimen and the virgin specimen plotted as red and blue dashed lines in the figure.

Please note that changing the threshold increasing rate will result in different embrittlement temperature results. A comparison among the embrittlement temperature results using different threshold increasing rates is conducted in Appendix D. The key idea here is to choose an appropriate threshold rate so that the embrittlement temperatures for 36-hour aged specimen and virgin specimen found using source location results match with the known embrittlement temperatures found in previous studies.

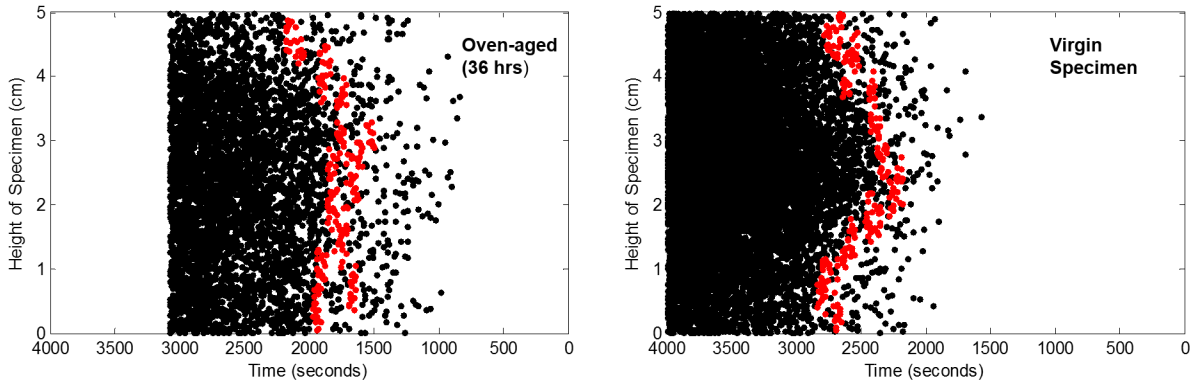

Figure 6.10: The beginning of the stable crack region for 36-hour aged specimen and virgin specimen

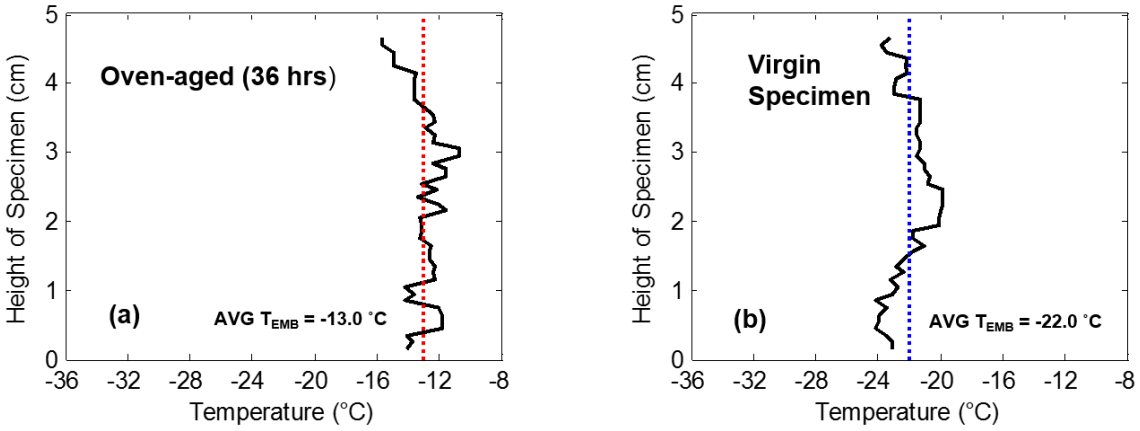

Figure 6.11: (a) Average embrittlement temperature at each height interval of asphalt concrete samples oven-aged for 36-hours, (b) Average embrittlement temperature at each height interval of the virgin asphalt specimens

Figure 6.11 shows the average embrittlement temperature across the height of the 36-hour aged specimen is -13.0 $^{\circ}C$, while the average embrittlement temperature for the virgin specimen is -22.0 $^{\circ}C$. The embrittlement temperature values for these two specimens are consistent with the embrittlement temperatures determined by the binder's rheological properties [10–12] and other acoustic emission techniques [17, 18, 54]. During the oven-aging process, the asphalt binder becomes stiffer and microcracks are developed between the binder and the aggregates due to the loss of adhesion. Thus the binder of the 36-hour aged specimen is stiffer and has lower adhesive properties compared to the binder in virgin specimen. This explains the observed warmer embrittlement temperature of the 36-hour aged specimen compared to the embrittlement temperature of the virgin specimen. Strain energy within the mastic accumulates as the temperature drops, and thermal stresses developed in the 36-hour aged specimen reach the mastic fracture strength at a temperature 9 $^{\circ}C$ warmer than in the virgin specimen.

The same AE testing is repeated for the four 36 hours aged specimens treated by the rejuvenator on the top surface

after dwell times of two, four, six and eight weeks. During the dwell period, the rejuvenator applied on the top surface penetrates the specimen via gravity and capillary action and acts on the binder to make it more viscoelastic. Figure 6.12 shows the relationship between embrittlement temperatures and the height of AE sources for the four rejuvenated specimens after dwell times of two, four, six and eight weeks. In Figure 6.12, the y-axis represents the distance away from the bottom surface of the specimens. The top surface, i.e., the surface where the rejuvenator was applied, has a height of 5 cm.

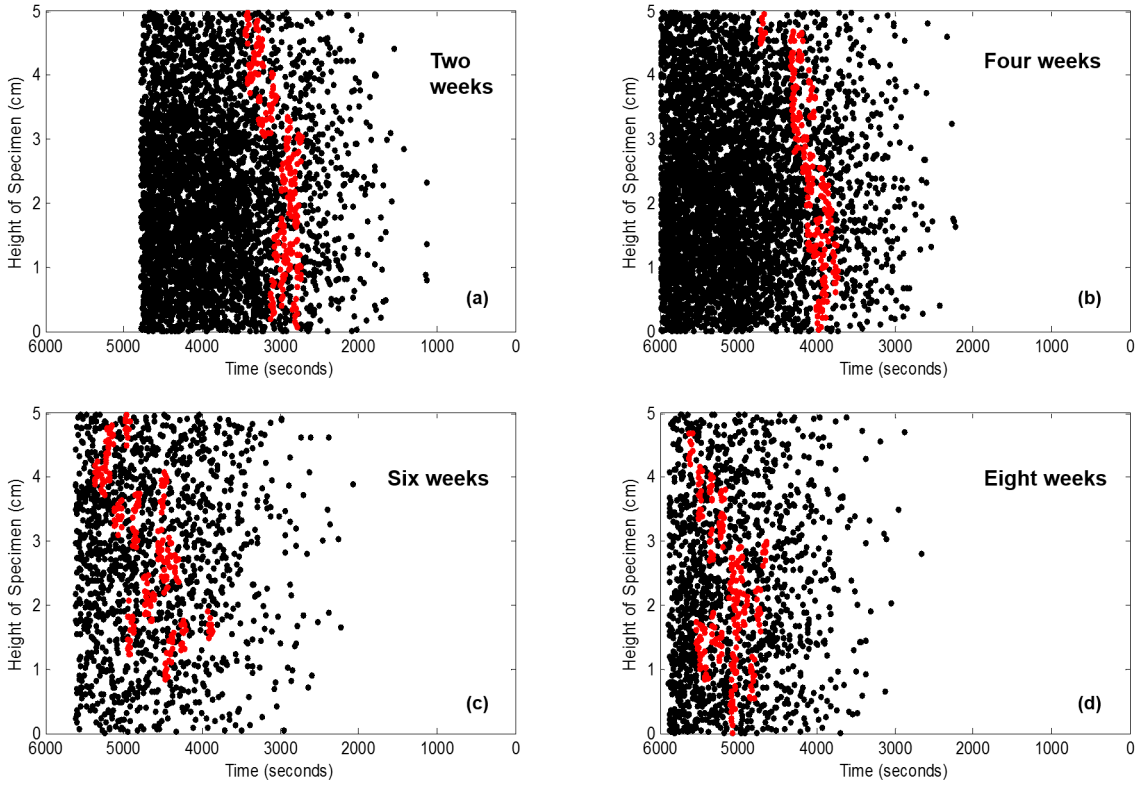

Figure 6.12: The beginning of the stable crack region for 36-hour aged specimens exposed to rejuvenator with a dwell time of (a) two weeks, (b) four weeks, (c) six weeks and (d) eight weeks

It can be observed from Figure 6.12 that as the dwell time increases, the average embrittlement temperature across the height of the specimen becomes cooler. It shows that the rejuvenator takes time to react with the oven-aged binder, making the binder more viscoelastic, i.e., improving asphalt's resistance to thermal damages. Figure 6.12 shows that after 2 and 4 weeks of dwell time, the embrittlement temperatures of the rejuvenated specimens have already been recuperated to the embrittlement temperature of the virgin specimen, i.e., around -22 $^{\circ}C$. As the dwell time increases to 6 and 8 weeks, the embrittlement temperature continues to drop. At the end of the eighth week, the average embrittlement temperature across the height of the rejuvenated specimen reaches -31.7 $^{\circ}C$, which is around one to two grades cooler than the embrittlement temperature corresponding to the virgin specimen, where one grade refers to 6

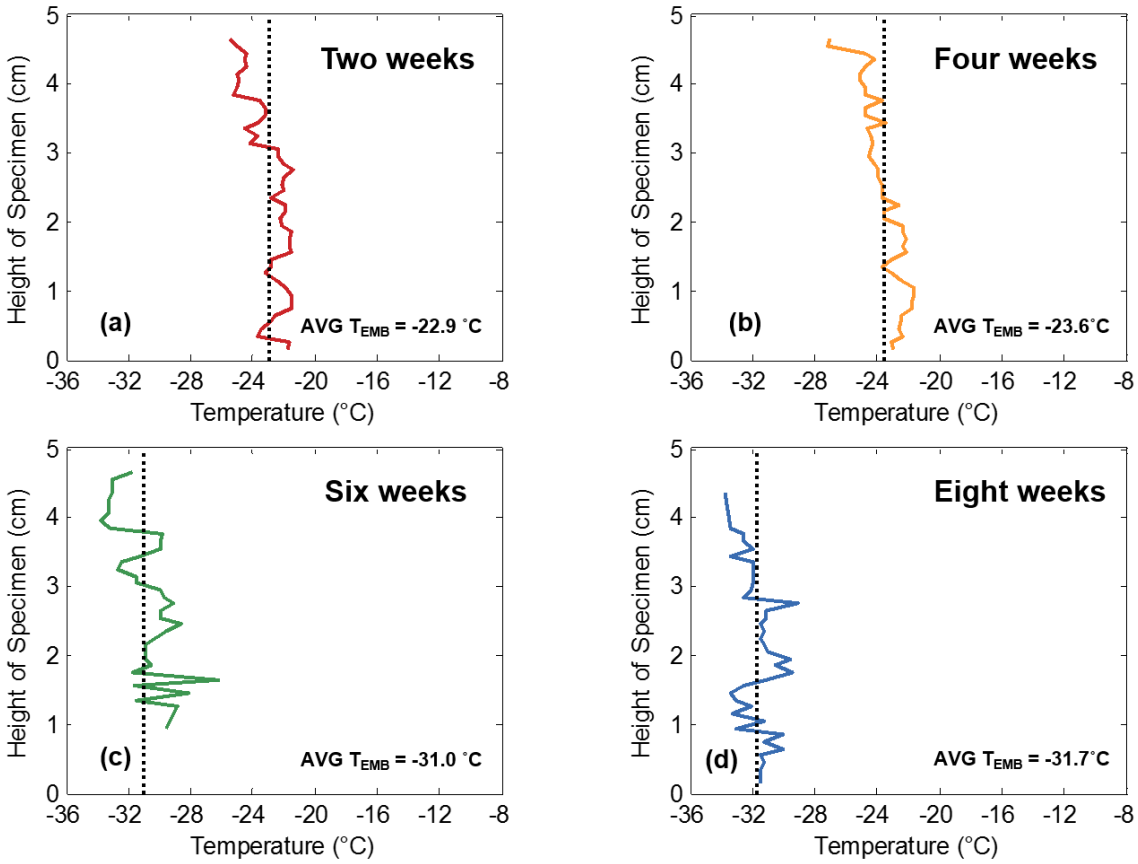

Figure 6.13: Embrittlement temperature at each height interval of asphalt samples oven-aged for 36 hours and exposed to rejuvenator with a dwell time of (a) two weeks, (b) four weeks, (c) six weeks and (d) eight weeks. Height of 5 centimeters represents the top surface, i.e., surface where the rejuvenator was applied.

$^{\circ}C$ as specified by the Superpave asphalt binder performance grading system. Please note that in Figure 6.12(c), the embrittlement temperatures at the bottom layer of the specimen are not shown in the figure, because the number of AE events at that height is not sufficient enough to meet the threshold value of 10 events per 1 minute. The same applies to the top layer of the specimen shown in Figure 6.12(d). The potential reason is that the embrittlement temperature at that region is lower than the lowest cooling temperature during the test, which is -35 $^{\circ}C$. Another possible explanation is that the threshold increasing rate of 10 events per one minute per 0.5 cm interval is a slightly overestimated criteria to estimate the beginning of stable crack region. As discussed in Appendix D.1, a high threshold increasing rate could result in an insufficient number of AE events to display a valid beginning of the stable crack region. Comparing to the other threshold increasing rate values in Appendix D, 10 events per 1 minute per 0.5 cm interval is still considered as a reasonable threshold increasing rate, although this threshold rate could be further tuned.

The four plots in Figure 6.13 are combined in Figure 6.14 to demonstrate the trend of how the embrittlement temperature shifts with the increase in dwell time. Comparing to the average embrittlement temperature of 36 hours oven-aged

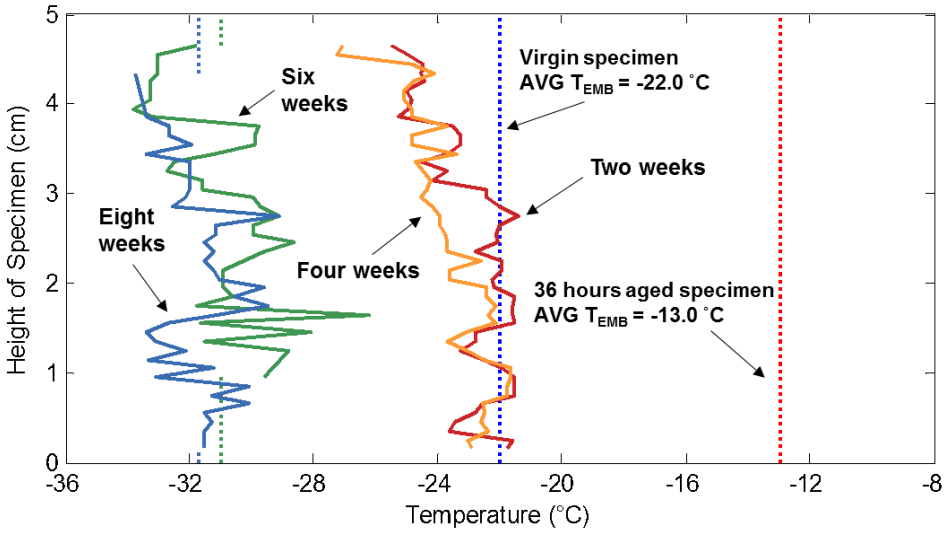

Figure 6.14: Combined embrittlement temperature results for asphalt specimens based on Geiger's iterative source location method

asphalt concrete at -13.0 °*C*, the average embrittlement temperature has been lowered by around 10 degrees after two and four weeks of dwell time. A trend is observed in Figure 6.14, showing that by the end of a dwell time of two and four weeks, the top half portion of the specimens has lower embrittlement temperatures compared to the lower half portion of the specimens. The possible reason is that as the rejuvenator penetrates the specimens from the top surface by gravity and capillary action, the top half of the specimen has more exposure time to the rejuvenator, which results in having more viscoelastic binder and higher resistance to thermal damages, hence lower embrittlement temperature. It can be observed that after the sixth week of rejuvenator treatment, the specimens have homogeneous embrittlement temperatures in the upper and lower portion. This trend suggests that the rejuvenator has already effectively lower the embrittlement temperature of the whole specimen instead of just the top portion near the treatment surface.

6.2.2 Source Location Results Using Non-Iterative Method

The same testing and processing procedures described in Section 6.2.1 are repeated for the asphalt specimens in this section. The only difference is that non-iterative USBM method is used to calculate the source locations instead of the iterative Geiger's method. Only the AE sources located within the valid monitoring region are used to demonstrate the relationship between the cracking temperature and the depths of the AE sources.

The source location results computed using the non-iterative method are different from the source location results obtained in Section 6.2.1. Therefore, a different threshold increasing rate is used to estimate the beginning of the stable crack region and the embrittlement temperature. After comparing several threshold increasing rates, 5 AE

events per 1 minute per 0.5 cm interval was found to be a reasonable threshold increasing rate of AE events, because the embrittlement temperatures for 36-hour aged and virgin specimen found using this rate are close to the values obtained using other standard methods.

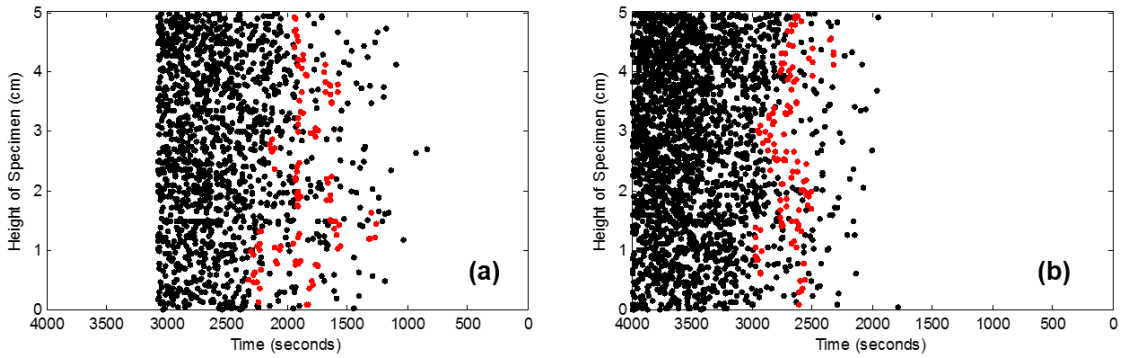

Figure 6.15: The beginning of the stable crack region for (a) 36-hour aged specimen and (b) virgin specimen estimated using non-iterative source location method

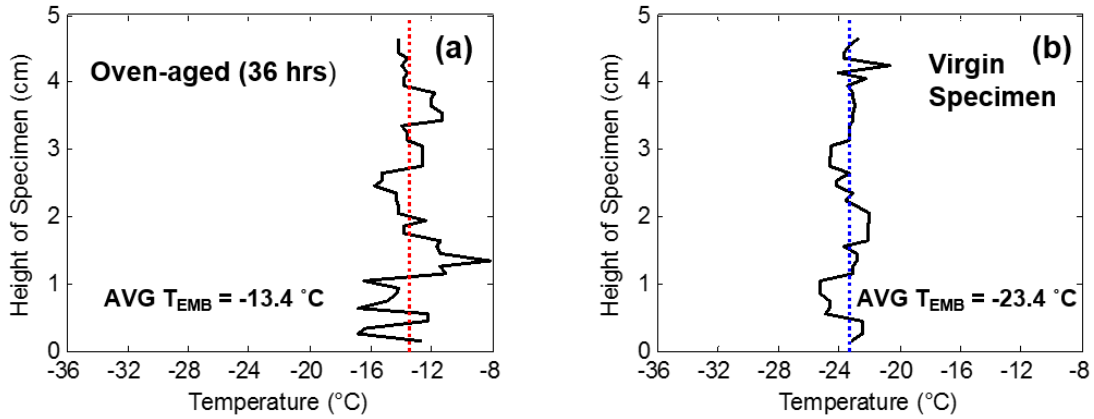

Figure 6.16: Non-iterative source location results: (a) average embrittlement temperature at each height interval of asphalt concrete samples oven-aged for 36-hours, (b) average embrittlement temperature at each height interval of the virgin asphalt specimens

The beginning of the stable crack region for 36-hour aged specimen and virgin specimen is demonstrated in Figure 6.15, and Figure 6.16 shows the average embrittlement temperature results obtained using the non-iterative source location method for 36-hour aged and virgin specimen. It can be observed from these two figures that the embrittlement temperatures estimated using 5 events per 1 minute per 0.5 cm interval as the threshold increasing rate are consistent with the results obtained in Figure 6.11, with -13.4 $^{\circ}C$ for 36-hour aged specimen and -23.4 $^{\circ}C$ for virgin specimen. Therefore, the same estimation procedures can be applied to the four rejuvenated specimens using this new threshold increasing rate, as shown in Figure 6.17.

Figure 6.16 and Figure 6.17 are then combined in Figure 6.18. As shown in Figure 6.18, the shapes of the embrittlement temperature plots for the rejuvenated specimens suggest that the variance in the embrittlement temperatures

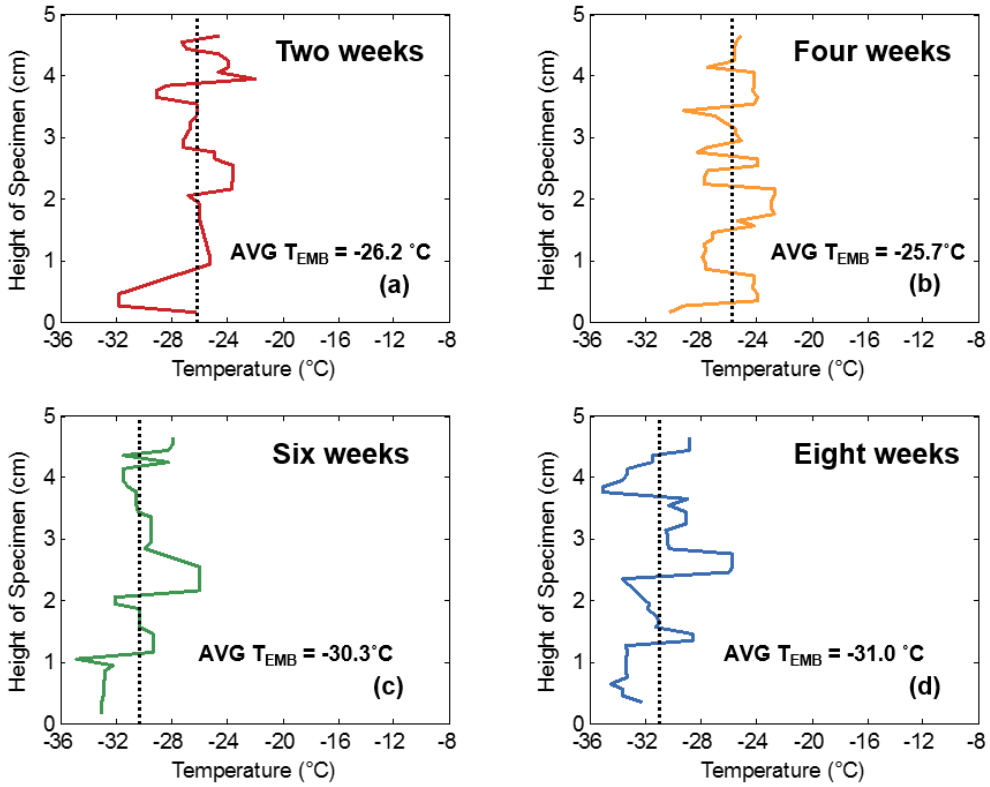

Figure 6.17: Non-iterative source location results: embrittlement temperature at each height interval of asphalt samples oven-aged for 36 hours and exposed to rejuvenator with a dwell time of (a) two weeks, (b) four weeks, (c) six weeks and (d) eight weeks

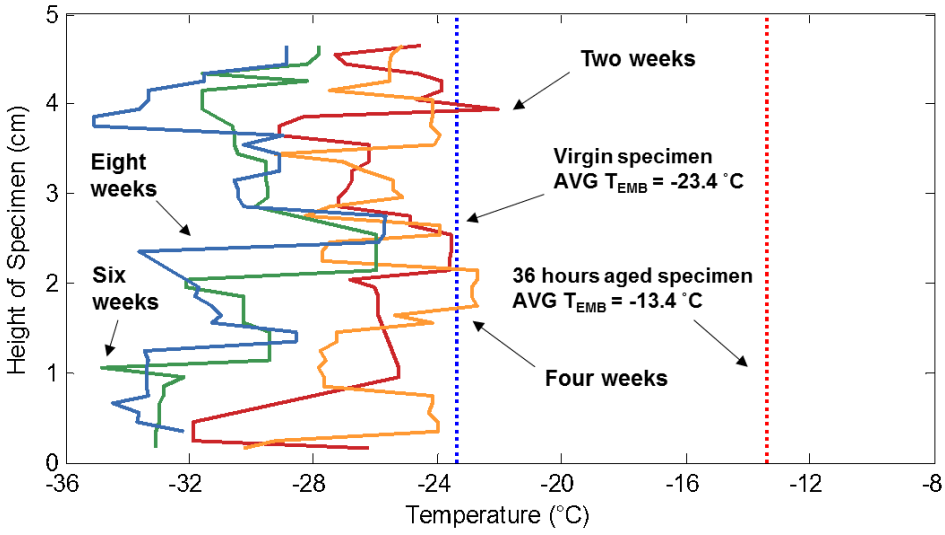

Figure 6.18: Combined embrittlement temperature results for asphalt specimens based on non-iterative source location method

at different heights in the same specimen is significantly large. Non-iterative methods have more demanding requirements on the acquired AE data. Each acoustic wave emitted by an AE source must be received by at least 5 sensors,

i.e., waves emitted by an AE source must be received by sensors attached on both sides of the specimens. Similar arrival times on multiple sensors may result in getting trivial solutions to equation (9). In addition, there is no room for improvement to the source location result by mitigating errors through iterative numerical approaches. It was also observed that non-iterative methods generated much less valid source location solutions as compared to using Geiger's method, i.e., only a small portion of the collected AE data contributed to the analysis of embrittlement temperatures. As compared to the iterative source location method, the stricter requirements for the AE signals may hinder the accuracy of the source location results. The reduced number of available AE data is also one of the factors causing the large variance in the embrittlement temperatures.

CHAPTER 7: AE SOURCE LOCATION RESULTS USING SENSORS MOUNTED ON ONE PLANE

The AE-based evaluation methods proposed in this study have been proved to work well when the sensors are attached on both top and bottom surfaces of the asphalt specimens. In reality, installing sensors on the the bottom surface of the asphalt pavements might not always be feasible. Exploring a method to conduct AE evaluation using sensors mounted on only one side, usually the top surface, of the pavements is necessary. A modified version of the non-iterative USBM method has been proposed in Section 3.1.3 to calculate the coordinates of the AE sources when the eight AE sensors are mounted on one side of the rectangular asphalt specimen. This method was proved to produce accurate source location results in Section 5.2. The iterative Geiger's method mentioned in Section 3.2 could also be applied to calculate source location using sensors mounted on only one side of the specimen. Accurate source location results obtained by Geiger's method are presented in Section 5.3.

In this chapter, one virgin asphalt specimen was prepared and eight sensors are mounted on one surface of this specimen as specified in Section 7.1. This specimen was cooled in the cooling chamber from room temperature to -35 $^{\circ}C$, and the AE signals produced by the microcracks formed in the specimen were collected by eight sensors. The AE signals were then processed using the non-iterative method and the iterative method discussed previously in Section 3.1.3 and Section 3.2. The source location results for this virgin specimen are given in Section 7.2 below, followed by a discussion in Section 7.3.

7.1 Sensor Placement

The asphalt specimen used in this experiment has the same preparation process and dimensions as the specimens described in Section 4.1. The specimen used in this experiment was not prepared from the same batch as the specimens used in Section 4.1, so this specimen might have slightly different properties, such as embrittlement temperature, compared to the results obtained in previous chapters.

Instead of placing four sensors on the top surface and four sensors on the bottom surface with 45° offset angle with respect to the sensors on the top surface, all of the eight sensors are installed on the bottom surface of the asphalt specimen in this experiment. The placement of the eight sensors are depicted in Figure 7.1. The eight sensors are placed in an irregular pattern in order to avoid symmetric sensor placement, which might induce computation errors

in source location calculations.

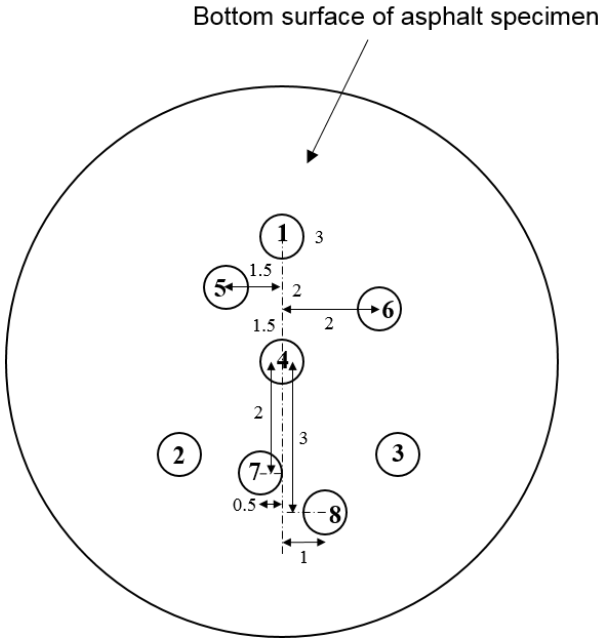

Figure 7.1: Sensor placement on the bottom surface of the asphalt specimen (unit: cm)

7.2 Experiment Results

The virgin asphalt specimen was put into the cooling chamber and cooled from room temperature to -35 $^{\circ}C$ as described in Section 4.3. The AE signals were collected by the eight sensors and the locations of the AE sources were computed using the iterative Geiger's method. The z-coordinates of the AE sources are plotted against the cooling time in Figure 7.2. The sensors are installed on the plane with a height of 0 cm.

The red dots displayed in Figure 7.2 indicate the estimated beginning of the stable crack region. This estimation method was described in Section 6.2.1 and Figure 6.9. A threshold increasing rate of 10 events per 1 minute per 0.5 cm interval was used for the estimation. The average occurring temperatures of the red AE events at each height interval were computed and plotted in Figure 7.3.

The locations of the AE sources were then computed using non-iterative modified USBM method described in Section 3.1.3. The z-coordinates of the AE sources are plotted against the cooling time, and the estimated beginning of the stable crack region are represented by the red dots in Figure 7.4. The average occurring temperatures of the red AE events at each height interval were computed and plotted in Figure 7.5.

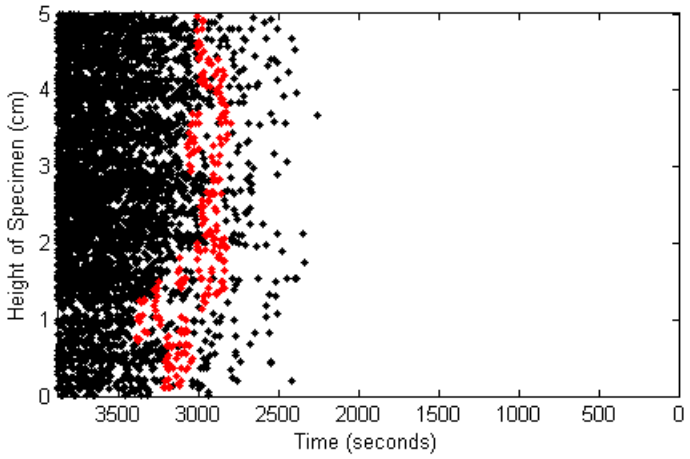

Figure 7.2: The relationship between the cooling time and the height of the AE source calculated using iterative source location method. The estimated beginning of the stable cracking region for the virgin specimen is colored in red.

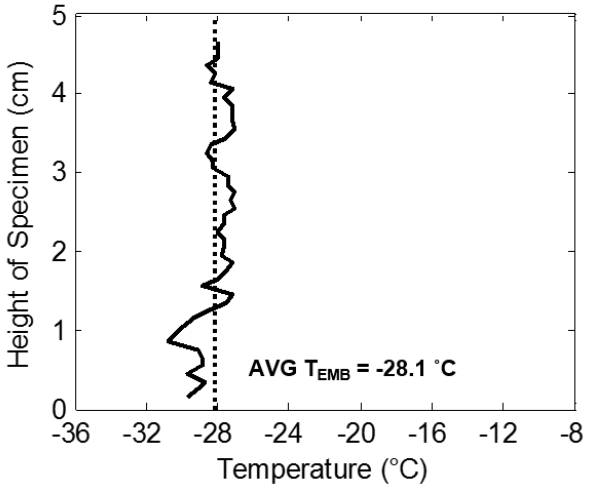

Figure 7.3: Average embrittlement temperature at each height interval of the virgin asphalt specimen

7.3 Discussion

From Figure 7.3 it is seen that the average embrittlement temperature for the virgin specimen obtained using the iterative Geiger's method is -28.1 $^{\circ}C$, which is about 3 $^{\circ}C$ lower than the standard -25 $^{\circ}C$ embrittlement temperature for virgin specimen. In contrast, Figure 7.5 shows that the average embrittlement temperature computed using the modified non-iterative USBM method is -25.7 $^{\circ}C$, which is close to the standard embrittlement temperature for virgin asphalt specimen. This observation implies that both non-iterative and iterative source location method can be used to compute embrittlement temperatures for asphalt specimens when the sensors are only installed on one surface of the specimens, although the results generated by the two methods are not consistent.

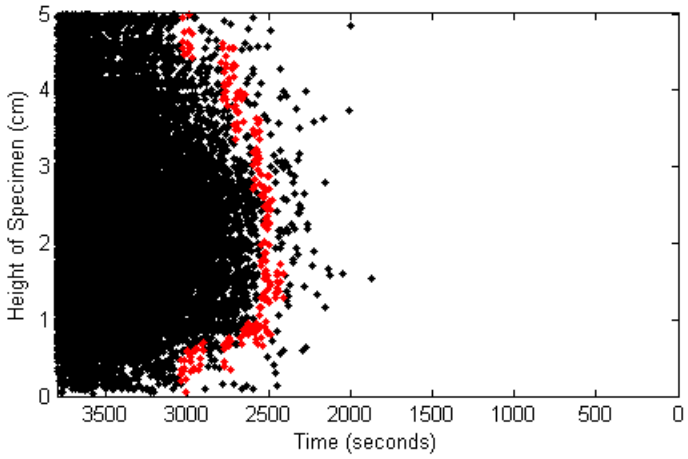

Figure 7.4: The relationship between the cooling time and the height of the AE source calculated using non-iterative source location method. The estimated beginning of the stable cracking region for the virgin specimen is colored in red.

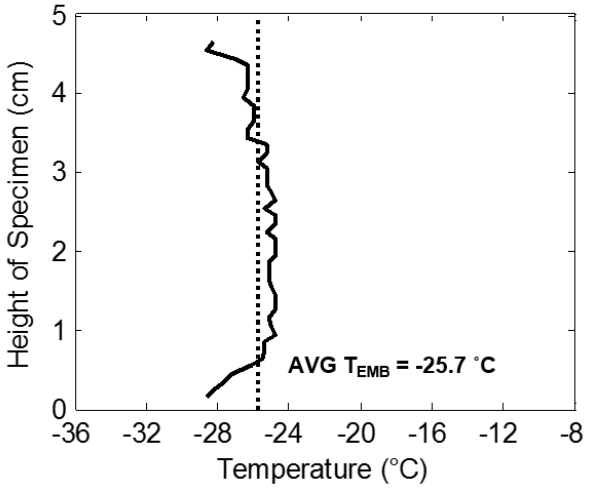

Figure 7.5: Average embrittlement temperature at each height interval of the virgin asphalt specimens using non-iterative source location method

The Geiger's method uses the AE signals received by only 4 sensors to compute the source location. On the other hand, the modified non-iterative USBM method employs the information from 5 sensors in the source location calculation. Although Geiger's method has a more tolerant requirement on the minimum number of the available sensors, the source location results generated by this algorithm might not be as accurate as the results obtained using the modified USBM method. When the sensors are all installed on one plane, iterative Geiger's method is shown to have lower accuracy than the modified USBM method by comparing the source location results presented in Section 5.2 and 5.3, especially for the height of the AE sources. Moreover, figures in Appendix A demonstrate that the heights of the AE sources are more susceptible to variations in the wave velocity. It was observed that a large portion of the source location results computed by the iterative Geiger's method have the z-coordinates much larger than the total

thickness of the asphalt specimen, and these results were then discarded as invalid source locations. This explains why Geiger's method produces fewer valid source locations displayed in Figure 7.2 compared to Figure 7.4. As a result, the embrittlement temperature estimated using source location results obtained by Geiger's method might be underestimated.

This underestimation of embrittlement temperature can be mitigated by lowering the threshold increasing rate to estimate the embrittlement temperature. Figure 7.6 and 7.7 demonstrates the estimation of embrittlement temperature for virgin specimen using a threshold AE event increasing rate of 3 events per 1 minute per 0.5 cm interval. By using a lower threshold increasing rate, it can be observed that the estimated average embrittlement temperature for the virgin specimen has been raised from -28.1 $^{\circ}C$ in Figure 7.3 to -25.9 $^{\circ}C$ in Figure 7.7, which is closer to the standard embrittlement temperature for virgin specimens.

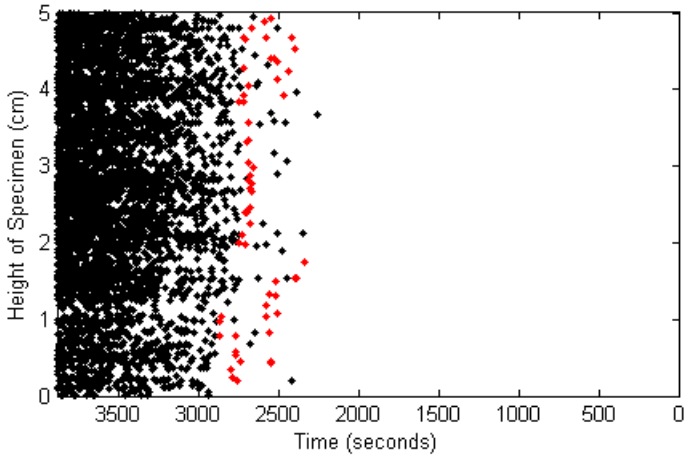

Figure 7.6: The relationship between the cooling time and the height of the AE source. The estimated beginning of the stable cracking region for the virgin specimen using a threshold increasing rate of 3 events per 1 minute per 0.5 cm interval is colored in red.

However, it is not recommended to lower the threshold AE event increasing rate to a significantly low value such as 3 events per 1 minute per 0.5 cm interval. As shown in Figure 7.6, a low threshold increasing rate will make the stable crack region begin at a very early stage. In this case, stable crack region begins as soon as the locations of some AE sources are computed, and could not even be differentiated from the pre-cracking region and the early transition region. At the early crack developing stage, there are many noise signals received by the sensors which may cause false positives in the source location results, and the estimation of embrittlement temperatures are very prune to these errors induced in the source location computations. Consequently, the AE sources colored in red in Figure 7.6 may not reliably reflect the true distribution of the embrittlement temperatures.

As for the modified non-iterative USBM method, the z-coordinate of the AE sources are calculated in a more robust

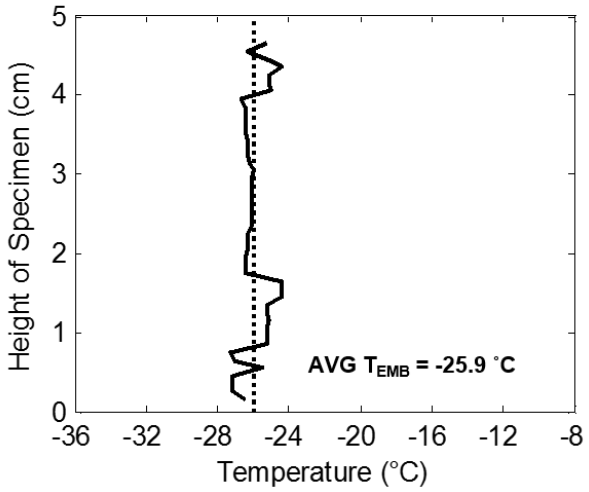

Figure 7.7: Average embrittlement temperature at each height interval of the virgin asphalt specimens using threshold increasing rate of 3 events per 1 minute per 0.5 cm interval

way. The x and y coordinates of an AE source are calculated using the USBM method first. The z-coordinate is then calculated using the x and y coordinates obtained previously, together with the arrival time difference among the first arrived four sensors. This approach is shown to yield more accurate source location results in Section 5.2, because the average value for the z-coordinates obtained by each pair of the sensors is used in the TDOA computation step. Z-coordinates of the sources computed using this approach have higher tendency to be bounded inside the specimen.

Therefore, compared to using the iterative Geiger's method, the source location results obtained using the modified USBM method are more accurate and reliable when the sensors are only installed on one surface of the asphalt specimen. If Geiger's method is used for the computation, a lower threshold AE events increasing rate should be used to estimate the embrittlement temperatures.

It was noted that the embrittlement temperatures for AE sources with a height less than 1.0 cm in Figure 7.3 and Figure 7.5 are four to five degrees lower compared to AE sources with a height larger than 1.0 cm. AE sources with a height less than 1.0 cm are located near the plane where the sensors are installed. By the time AE signals produced by these AE sources reach the sensors, the AE waves are likely to be a mixed wave of surface waves and longitudinal waves. This mixed wave has undetermined velocity, and the calculated source location results based on this unknown wave velocity are likely to be inaccurate. In addition, the z-coordinates of the AE sources near the bottom surface are possible to be located below the bottom surface due to the errors induced in the source location computation. As a result, the number of valid source location results near the bottom surface is significantly smaller compared to other regions. The embrittlement temperatures in this region estimated using the AE events increasing rate also tends to be lower due to the smaller number of valid results.

In Figure 7.4, it can be observed that the region with a height between 4.0 cm and 5.0 cm has a lower embrittlement temperature compared to the center region of the specimen. AE sources in this region are located four to five centimeters away from the AE sensors, so the AE waves produced by these sensors are highly attenuated before they are received by the sensors. It is unlikely for these attenuated AE waves to be received by at least five sensors for the source location computation. Therefore, the embrittlement temperatures at regions more than 4.0 cm away from the bottom surface are likely to be lower than the center region. The two observations above suggest that when the sensors are installed on only one surface of the specimen, the AE sources located within 1.0 cm to sensors plane and more than 4.0 cm away from the sensors plane are less likely to be computed by the source location methods, and thus the embrittlement temperatures obtained at these regions tend to be underestimated. To avoid drawing inaccurate conclusions from these underestimated embrittlement temperatures, source location results with z-coordinates less than 1.0 cm or more than 4.0 cm from the sensor installment plane should be considered to be discarded in the AE data processing stage.

When this AE-based analysis is applied to the real pavement, the sensors can be installed on the top surface of the pavement or underground depending on the experiment design requirements. When the sensors are all installed on the top surface of the pavement, the computed source location results near the top pavement surface are likely to be less accurate. If the AE sensors are installed inside the pavement and beneath the top pavement surface, the sensors should not be installed more than 5.0 cm below the top surface of the pavement to ensure a better monitoring coverage. It should be also noted that if the sensors are installed inside the pavement, the AE signals received by the sensors are likely to come from regions above and below the sensor installment plane. The valid monitoring range of the installed sensors in this case is from 4.0 cm above the sensors to 4.0 cm below the sensors.

CHAPTER 8: CONCLUSIONS

An approach to evaluate the low temperature cracking behavior of the asphalt concrete using acoustic emission source location techniques was developed in this study. This study was divided into three main parts. Part 1 examined the embrittlement temperatures of asphalt concrete mixtures by monitoring the acoustic emission response of the test specimens during cooling. Part 2 uses both iterative Geiger's method and non-iterative USBM method to compute the locations of the AE sources produced in the asphalt specimens in a low temperature environment. A method to determine the embrittlement temperatures using acoustic emission source location results was also discussed. Part 3 tested a virgin asphalt specimen to examine its embrittlement temperature by installing AE sensors on only one surface of the asphalt specimen. The primary purpose of this test is to evaluate the feasibility of applying the evaluation method introduced in Part 2 to the real pavement, where the sensors are only able to be installed on one plane. The effect of asphalt rejuvenators on the aged asphalt concrete specimens was investigated in this study using the methods proposed in Part 1 and Part 2.

8.1 Summary of Part 1: Examine Embrittlement Temperatures by Monitoring the Acoustic Emission Response

In this part of the study, an acoustic emission approach has been developed to quantitatively evaluate the embrittlement temperatures of asphalt concrete mixtures by monitoring the acoustic emission response of the test specimens during cooling. Acoustic emission tests were performed on short-term aged asphalt concrete samples as well as asphalt concrete samples oven-aged for 36 hours at 135 $^{\circ}C$. The temperature corresponding to a rapid increase in the number of AE events produced in an asphalt specimen is termed as the embrittlement temperature. It was observed that the embrittlement temperatures of the short-term aged specimens and specimens oven-aged for 36 hours were -25 $^{\circ}C$ and -15 $^{\circ}C$, respectively. Four 36-hour oven-aged specimens were then treated with rejuvenator (10% by binder weight) by spreading the rejuvenator on the specimens' top surface. Using the same acoustic emission approach, the embrittlement temperatures of the rejuvenated specimens were also evaluated after two, four, six, and eight weeks of rejuvenation application (or dwell time, i.e., time to allow rejuvenator to diffuse into the specimen and act upon the binder) on the asphalt concrete samples oven-aged for 36 hours. It was observed that during the cooling process, the short-term aged specimens have a smaller number of acoustic emission events and less energetic events than the specimens oven-aged for 36 hours. This observation is consistent with previous observations that as the binder

ages it becomes stiffer, with reduced adhesive properties. It was also observed that after four weeks of dwell time, the rejuvenator-treated samples have recuperated the original embrittlement temperatures. In addition, it was also observed that the rejuvenator kept acting upon the binder after four weeks of dwell time; after eight weeks of dwell time, the specimens had an embrittlement temperature about one grade cooler than the embrittlement temperature corresponding to the short-term aged specimen, where one grade cooler denotes 6 $^{\circ}C$ cooler. Based on this experiment, it appears that the proposed acoustic emission approach provides a method to evaluate the efficiency of rejuvenators to recuperate the embrittlement temperatures caused by oxidative aging of asphalt concrete mixtures.

8.2 Summary of Part 2: Examine Embrittlement Temperatures by Acoustic Emission Source Location Techniques

This part of the study aimed at developing an approach to evaluate the low temperature cracking behavior of the asphalt concrete using acoustic emission source location techniques. AE tests were conducted on lab compacted asphalt specimens and the emission data were collected from eight AE sensors. After the collected data were amplified and pre-processed, both iterative Geiger's method and non-iterative USBM method were used to compute the locations of the AE sources produced in the asphalt specimens in a low temperature environment. A method to determine the embrittlement temperature using the acoustic emission source location results was discussed in this part. It was observed that the embrittlement temperature of an asphalt specimen is directly related to its aging level. An asphalt specimen which was oven-aged for 36 hours has the embrittlement temperature of -13 $^{\circ}C$, which is 9 $^{\circ}C$ warmer than the embrittlement temperature for a virgin specimen that did not undergo the long-term aging process. This was an expected observation based on previous studies where the embrittlement temperatures were quantitatively determined using other standardized testing methods. The oven-aged specimens are shown to have lower resistance to the thermal damages, because the oxidative hardening during the aging process decreases the ductility and resilience of asphalt binder, results in higher asphalt stiffness level and lower adhesive bonding between binder and aggregates.

The ability of rejuvenators to restore the embrittlement temperatures of asphalt concrete was examined in this part using two different source location methods. Rejuvenator with a weight of 10% of the binder content was applied on the top surfaces of four 36-hour aged asphalt specimens. These four specimens were then tested using the same AE approach after dwell times of two, four, six and eight weeks. After four weeks of dwell time, the source location results show that the embrittlement temperature of the asphalt specimen has been restored to -23.6 $^{\circ}C$, which is close to the embrittlement temperature for a specimen in virgin condition. Furthermore, after six and eight weeks of dwell time, the embrittlement temperatures were further improved to -31 $^{\circ}C$ and -31.7 $^{\circ}C$ respectively. Source location results

obtained using Geiger's method also show that after 4 weeks of dwell time, the top half portion of the rejuvenated asphalt specimen has a lower embrittlement temperature than the bottom half portion. At the end of the sixth week, the embrittlement temperature was observed to be homogeneous across the height of the asphalt specimen. These evidences suggest that the rejuvenator takes at least 6 weeks to effectively restore the embrittlement temperature of a 36-hour oven-aged asphalt concrete with 5 cm thickness by around 18 $^{\circ}C$, which is about 2-3 grades cooler than the embrittlement temperature for asphalt concretes in 36-hour oven-aged condition and 1-2 grades cooler than the embrittlement temperature for asphalt concretes in virgin condition.

It is necessary to point out that the inherent variability of the asphalt concrete induced during the process of manufacturing gives the observed trend unavoidable variability over different asphalt specimens. The porosity, distribution of aggregates, moisture content and height for asphalt concrete specimens are different even if they were made in the same batch. The randomness of the distribution of aggregates also allows variability in physical properties within the same specimen. For example, the embrittlement temperature distributions for 36 hours oven-aged and virgin specimens are supposed to be homogeneous at each height, but the embrittlement temperature plot in Figure 6.11 is skewed, which suggests that the material properties vary at different parts of the specimen. In addition, the rejuvenator softens the asphalt binder and makes the asphalt specimen have graded material properties, i.e., the wave attenuation and dilatational speed might not be constant in the asphalt concrete mixtures. These uncertainties associated with the AE measurements and source location techniques are the main sources of the computation errors induced in source location calculations.

8.3 Summary of Part 3: Examine Embrittlement Temperatures Using Acoustic Emission Source Location by Installing Sensors on One Side of Asphalt Concretes

In Part 3 of the study, a method to conduct AE evaluation using sensors installed on only one plane, usually the top surface, of the asphalt concrete is evaluated. A virgin asphalt specimen was prepared using the same procedures described in Part 1 and Part 2. All of the eight AE sensors are installed on one surface of the specimen. This specimen was placed in the cooling chamber and cooled from room temperature to -35 $^{\circ}C$. The locations of the AE sources are computed using both iterative Geiger's method and the modified non-iterative USBM method. The experiment results demonstrated that the source location results obtained using the modified non-iterative method are more accurate compared to Geiger's method. Using the same threshold AE event increasing rate, the embrittlement temperatures estimated using Geiger's method are lower compared to the embrittlement temperatures estimated by the modified USBM method. The AE source location distribution shows some indication that the number of valid AE sources

located less than 1.0 cm or more than 4.0 cm from the sensor installment plane are smaller compared to the number of valid AE sources located in other regions. The embrittlement temperatures of regions very close to or very far away from the sensor installation plane are found to be underestimated. Therefore, it implies that when this AE-based embrittlement temperature evaluation approach is applied in the field, it is recommended to discard source location results with a height less than 1.0 cm and more than 4.0 cm from the sensors when the sensors are only installed on the top surface of the pavement. It does not apply to the situation when the sensors are installed underground, since AE signals can come from both above and below the sensors in this case.

8.4 Recommendations and Final Remarks

In Part 1 and Part 2 of this study, only one set of experiments were conducted to evaluate the performance of rejuvenators. Additional testing is suggested to be conducted to consolidate the research findings in this study. For example, the rejuvenators could be applied on multiple sets of asphalt specimens. For each dwell time of the rejuvenator, more reliable conclusions could be drawn if the AE analysis is done on several sets of asphalt specimens. Ideally, the experiment results would be consistent if these sets of asphalt specimens were produced from the same batch using the same preparation process.

During the specimen preparation process, the amount of rejuvenators used in this study is 10% of the binder content in the specimen by weight. The same testing techniques could be repeated on these samples by applying a different amount of rejuvenators on the asphalt specimens. A study investigating the relationship between the rejuvenating effect of the rejuvenators and the amount of applied rejuvenator could be conducted. Through this recommended study, an optimal amount of the applied rejuvenator could be found to maximize its rejuvenating effect.

The problem of source location has been addressed in various fields because it is a crucial problem for many material evaluation applications. One of the most critical aspects of source location is the method to distinguish arriving AE waves from the background noise. In this study the background noise is filtered out only based on the amplitude, duration-amplitude ratio and rising time-amplitude ratio of the signals. There are some recent literatures proposing more advanced filtering techniques for the source location results. One of those approaches is to recognize the P-wave arrivals in the presence of noise through machine learning approach [58]. This approach explores various feature extraction methods to look for patterns of real P-wave signals so that the noise signals could be filtered out based on these patterns. When the AE approach described in this study is applied to the pavement, the level of background noise will become much more significant compared to the laboratory experiment setting. Therefore, the accuracy of the source location results described in Part 2 of the study could be further improved if techniques such as machine

learning can be applied to precisely distinguish AE signals from the noise signals.

In conclusion, this study explores several AE-based evaluation approaches to examine the embrittlement temperatures of asphalt concrete mixtures. AE source location techniques were used to calculate the locations for the AE sources produced when asphalt concrete is cooled in a low temperature environment. Several experiments were conducted to verify the accuracy of the source location results. The performance of asphalt rejuvenator, especially its ability of restoring asphalt's resistance to thermal cracking was quantitatively evaluated in this study. In order to fully investigate the optimal amount of asphalt rejuvenator, further testings using more asphalt samples and different amount of rejuvenators are recommended. Overall, the results presented in this study demonstrate that asphalt rejuvenators are capable to recuperate the embrittlement temperatures caused by oxidative aging of asphalt concrete mixtures.

REFERENCES

[1] M. W. Mirza and M. Witczak, "Development of a global aging system for short and long term aging of asphalt cements (with discussion)," *Journal of the Association of Asphalt Paving Technologists*, vol. 64, 1995.

[2] F. L. Roberts, L. N. Mohammad, and L. Wang, "History of hot mix asphalt mixture design in the United States," *Journal of materials in civil engineering*, vol. 14, no. 4, pp. 279–293, 2002.

[3] S. Islam and W. Buttlar, "Effect of pavement roughness on user costs," *Transportation Research Record: Journal of the Transportation Research Board*, no. 2285, pp. 47–55, 2012.

[4] E. V. Dave, G. H. Paulino, and W. G. Buttlar, "Asphalt pavement aging and temperature dependent properties through a functionally graded viscoelastic model, part-i: Development, implementation and verification," in *Materials Science Forum*, vol. 631. Trans Tech Publ, 2010, pp. 47–52.

[5] F. Roberts and N. A. P. Association, *Hot Mix Asphalt Materials, Mixture Design, and Construction*. NAPA Educational Foundation, 1991.

[6] O.-K. Kim, "Development of laboratory oxidative aging procedures for asphalt cements and asphalt mixtures," Ph.D. dissertation, Oregon State University, 1986.

[7] J. Shen, S. Amirkhanian, and J. Aune Miller, "Effects of rejuvenating agents on superpave mixtures containing reclaimed asphalt pavement," *Journal of Materials in Civil Engineering*, vol. 19, no. 5, pp. 376–384, 2007.

[8] l. Garca, E. Schlangen, and M. Van de Ven, "Properties of capsules containing rejuvenators for their use in asphalt concrete," *Fuel*, vol. 90, no. 2, pp. 583–591, 2011.

[9] E. R. Brown, "Preventative maintenance of asphalt concrete pavements," *Transportation Research Record (TRR)*, vol. 1, pp. 6–1, 1988.

[10] *Standard specification for determining low-temperature performance grade of asphalt binders*, American Association of State Highway and Transportation Officials, AASHTO MP1A, Washington, D.C., 2001.

[11] *Standard specification for performance-graded asphalt binder*, American Association of State Highway and Transportation Officials, AASHTO MP1, Washington, D.C., 1998.

[12] *Standard specification for determining the flexural creep stiffness of asphalt binder using the bending beam rheometer (BBR)*, American Association of State Highway and Transportation Officials, AASHTO TP1, Washington, D.C., 1999.

[13] A. Apeagyei, W. Buttlar, and H. Reis, "Assessment of low-temperature embrittlement of asphalt binders using an acoustic emission approach," *Insight-Non-Destructive Testing and Condition Monitoring*, vol. 51, no. 3, pp. 129–136, 2009.

[14] B. Behnia, W. G. Buttlar, and H. Reis, "Cooling cycle effects on low temperature cracking characteristics of asphalt concrete mixture," *Materials and Structures*, vol. 47, no. 8, pp. 1359–1371, 2014.

[15] W. G. Buttlar, B. Behnia, and H. M. Reis, "An acoustic emission-based test to determine asphalt binder and mixture embrittlement temperature," Transportation Research Board, NCHRP IDEA Project 144, 2011.

[16] E. V. Dave, B. Behnia, S. Ahmed, W. G. Buttlar, and H. Reis, "Low temperature fracture evaluation of asphalt mixtures using mechanical testing and acoustic emissions techniques," *Journal of the Association of Asphalt Paving Technologists*, vol. 80, 2011.

[17] M. McGovern, B. Behnia, W. Buttlar, and H. Reis, "Concrete testing: Characterisation of oxidative ageing in asphalt concrete - part 1: Ultrasonic velocity and attenuation measurements and acoustic emission response under thermal cooling," *Insight-Non-Destructive Testing and Condition Monitoring*, vol. 55, no. 11, pp. 596–604, 2013.

[18] M. McGovern, B. Behnia, W. G. Buttlar, and H. Reis, "Concrete testing: Characterisation of oxidative ageing in asphalt concrete - part 2: Estimation of complex moduli," *Insight-Non-Destructive Testing and Condition Monitoring*, vol. 55, no. 11, pp. 605–609, 2013.

[19] R. B. Long, "Concept of asphaltenes," *Am. Chem. Soc., Div. Pet. Chem., Prepr; (United States)*, vol. 24, no. 4, 1979.

[20] R. E. Boyer and P. S. D. Engineer, "Asphalt rejuvenators fact, or fable," *Transportation systems*, 2000.

[21] E. Buenrostro-Gonzalez, H. Groenzin, C. Lira-Galeana, and O. C. Mullins, "The overriding chemical principles that define asphaltenes," *Energy & Fuels*, vol. 15, no. 4, pp. 972–978, 2001.

[22] R. Karlsson and U. Isacsson, "Material-related aspects of asphalt recycling - state-of-the-art," *Journal of Materials in Civil Engineering*, 2006.

[23] S. Nahar, A. Schmets, E. Schlangen, M. Shirazi, M. van de Ven, G. Schitter, and A. Scarpas, "Turning back time: rheological and microstructural assessment of rejuvenated bitumen," in *93rd Annual Meeting Transportation Research Board, Washington, USA, 12-16 January 2014; Authors version*. TRB, 2014.

[24] D. Oldham, E. H. Fini, and T. Abu-Lebdeh, "Investigating the rejuvenating effect of bio-binder on recycled asphalt shingles," in *Transportation Research Board 93rd Annual Meeting*, no. 14-3775, 2014.

[25] J. W. Oliver, "Diffusion of oils in asphalts," *Industrial & Engineering Chemistry Product Research and Development*, vol. 13, no. 1, pp. 65–70, 1974.

[26] F. Rostler and R. White, "Rejuvenation of asphalt pavements." DTIC Document, Tech. Rep., 1970.

[27] L. Scofield and T. Wolfe, "Product evaluation: Bituminous pavement rejuvenator. Final report," Arizona Transportation Research Center, Tech. Rep., 1986.

[28] J. Lin, P. Guo, L. Wan, and S. Wu, "Laboratory investigation of rejuvenator seal materials on performances of asphalt mixtures," *Construction and Building Materials*, vol. 37, pp. 41–45, 2012.

[29] M. A. Elseifi, S. Salari, L. N. Mohammad, M. Hassan, W. H. Daly, and S. Dessouky, "New approach to recycling asphalt shingles in hot-mix asphalt," *Journal of Materials in Civil Engineering*, vol. 24, no. 11, pp. 1403–1411, 2012.

[30] A. Crawley, "Innovative hot in-place recycling of hot-mix asphalt pavement in Mississippi," *Transportation Research Record: Journal of the Transportation Research Board*, no. 1654, pp. 36–41, 1999.

[31] J. E. Shoenberger and T. W. Vollor, "Hot in-place recycling of asphalt pavements," DTIC Document, Tech. Rep., 1990.

[32] J. Button, C. Estakhri, and D. Little, "Overview of hot in-place recycling of bituminous pavements," *Transportation Research Record: Journal of the Transportation Research Board*, no. 1684, pp. 178–185, 1999.

[33] A. C. Beach, "Characterization and micromechanical investigation of recycled asphalt shingle binder blends," Ph.D. dissertation, University of Illinois at Urbana-Champaign, 2013.

[34] N. H. Tran, A. Taylor, and R. Willis, "Effect of rejuvenator on performance properties of HMA mixtures with high RAP and RAS contents," *Auburn, AL: National Center for Asphalt Technology*, 2012.

[35] *Standard Test Method for Determining Fracture Energy of Asphalt-Aggregate Mixtures Using the Disk-Shaped Compact Tension Geometry*, ASTM International, ASTM D7313-13, West Conshohocken, PA, 2013.

[36] N. A. Farace, "Effects of asphalt rejuvenator on thermal and mechanical properties of oxidized hot mixed asphalt," Master's thesis, University of Illinois at Urbana-Champaign, 2015.

[37] C. Hellier, *Handbook of Nondestructive Evaluation*. Mcgraw-hill, 2001.

[38] C. B. Scruby, "An introduction to acoustic emission," *Journal of Physics E - Scientific Instruments (ISSN 0022-3735)*, vol. 20, pp. 945–953, 1987.

[39] A. Beattie, "Acoustic emission, principles and instrumentation," *Journal of acoustic emission*, vol. 2, no. 12, pp. 95–128, 1983.

[40] M. A. Hamstad, "A review: acoustic emission, a tool for composite-materials studies," *Experimental Mechanics*, vol. 26, no. 1, pp. 7–13, 1986.

[41] D. Charentenay, "Delamination of glass fiber reinforced polyester, an acoustic emission study," in *Mechanical Behaviour of Materials*, K. Miller and R. Smith, Eds. Pergamon Press, Oxford, England and Elmsford, NY, 1980, pp. 241–251.

[42] C. Old and J. Charlesworth, "The breaking strain of Nb3Sn in a multifilamentary superconductor," *Cryogenics*, vol. 16, no. 8, pp. 469–472, 1976.

[43] G. Sims, G. Dean, B. Read, and B. Western, "Assessment of damage in GRP laminates by stress wave emission and dynamic mechanical measurements," *Journal of Materials Science*, vol. 12, no. 11, pp. 2329–2342, 1977.

[44] B. Harris, F. Guild, and C. Brown, "Accumulation of damage in GRP laminates," *Journal of Physics D: Applied Physics*, vol. 12, no. 8, p. 1385, 1979.

[45] R. Williams and K. Reifsnider, "Real time nondestructive evaluation of composite materials during fatigue loading," in *ASM, SME, and ASNT, Western Metal and Tool Exposition and Conference, Los Angeles, Calif*, 1975, p. 1975.

[46] M. Phillips and B. Harris, "Acoustic emission study of the development of damage in GRP and GRP structures," in *Advances in Composite Materials*, A. Bunsell, C. Bethias, A. Martrenchar, D. Menkes, and G. Vercher, Eds. Pergamon Press, Oxford, England and Elmsford, NY, 1980, pp. 998–1014.

[47] M. Ohtsu, M. Shigeishi, H. Iwase, and W. Koyanagit, "Determination of crack location, type and orientation in concrete structures by acoustic emission," *Magazine of Concrete Research*, vol. 43, no. 155, pp. 127–134, 1991.

[48] C. Grosse, H. Reinhardt, and T. Dahm, "Localization and classification of fracture types in concrete with quantitative acoustic emission measurement techniques," *NDT & E International*, vol. 30, no. 4, pp. 223–230, 1997.

[49] H. Shimada, K. Sakai, and G. G. Litvan, "Acoustic emissions of mortar subjected to freezing and thawing," *ACI Special Publication*, vol. 126, 1991.

[50] Y. Seo and Y. R. Kim, "Using acoustic emission to monitor fatigue damage and healing in asphalt concrete," *KSCE Journal of Civil Engineering*, vol. 12, no. 4, pp. 237–243, 2008.

[51] J. W. Arnold, B. Behnia, M. E. McGovern, B. Hill, W. G. Buttlar, and H. Reis, "Quantitative evaluation of low-temperature performance of sustainable asphalt pavements containing recycled asphalt shingles (RAS)," *Construction and Building Materials*, vol. 58, pp. 1–8, 2014.

[52] M. McGovern, B. Behnia, B. Hill, W. G. Buttlar, and H. Reis, "Characterization of oxidative aging in asphalt concrete pavements using its complex moduli," in *SPIE Smart Structures and Materials+ Nondestructive Evaluation and Health Monitoring*, vol. 90641Q. International Society for Optics and Photonics (SPIE), 2014, Conference Proceedings.

[53] E. Nesvijski and M. Marasteanu, "Spectral analysis of acoustic emission of cold cracking asphalt," *Journal: The e-Journal of Nondestructive Testing & Ultrasonics*, vol. 11, no. 10, 2006.

[54] B. Behnia, W. G. Buttlar, A. Apeagyei, and H. Reis, "Determining the embrittlement temperature of asphalt binders using an acoustic emission approach," *NDE/NDT for Highways and Bridges: Structural Materials Technology (SMT), New York*, 2010.

[55] M. Wevers, "Listening to the sound of materials: Acoustic emission for the analysis of material behaviour," *NDT & E International*, vol. 30, no. 2, pp. 99–106, 1997.

[56] C. U. Grosse, "Acoustic emission (AE) evaluation of reinforced concrete structures," in *Non-Destructive Evaluation of Reinforced Concrete Structures*, C. Maierhofer, H.-W. Reinhardt, and G. Dobmann, Eds. Woodhead Publishing, 2010, vol. 2, pp. 185–214.

[57] S. Kppel and C. Grosse, "Advanced acoustic emission techniques for failure analysis in concrete," *WCNDT Proceedings*, Oct 2000, (CD-Rom).

[58] N. F. Ince, C.-S. Kao, M. Kaveh, A. Tewfik, and J. F. Labuz, "A machine learning approach for locating acoustic emission," *EURASIP Journal on Advances in Signal Processing*, vol. 2010, p. 15, 2010.

[59] M. G. Baxter, R. Pullin, K. M. Holford, and S. L. Evans, "Delta T source location for acoustic emission," *Mechanical systems and signal processing*, vol. 21, no. 3, pp. 1512–1520, 2007.

[60] K. Ho and W. Xu, "An accurate algebraic solution for moving source location using TDOA and FDOA measurements," *Signal Processing, IEEE Transactions on*, vol. 52, no. 9, pp. 2453–2463, 2004.

[61] D. Aljets, A. Chong, S. Wilcox, and K. Holford, "Acoustic emission source location in plate-like structures using a closely arranged triangular sensor array," *Journal of Acoustic Emission*, vol. 28, pp. 85–98, 2010.

[62] J. J. Scholey, P. D. Wilcox, M. R. Wisnom, M. I. Friswell, M. Pavier, and M. R. Aliha, "A generic technique for acoustic emission source location," *J Acoust Emis*, vol. 27, pp. 291–298, 2009.

[63] T. Kundu, S. Das, and K. V. Jata, "Detection of the point of impact on a stiffened plate by the acoustic emission technique," *Smart Materials and Structures*, vol. 18, no. 3, p. 035006, 2009.

[64] T. Kundu, "Acoustic source localization," *Ultrasonics*, vol. 54, no. 1, pp. 25–38, 2014.

[65] B. E. Anderson, M. Griffa, C. Larmat, T. J. Ulrich, and P. A. Johnson, "Time reversal," *Acoustics Today*, vol. 4, no. 1, pp. 5–16, 2008.

[66] R. K. Ing, N. Quieffin, S. Catheline, and M. Fink, "In solid localization of finger impacts using acoustic time-reversal process," *Applied Physics Letters*, vol. 87, no. 20, p. 204104, 2005.

[67] T. Schumacher, D. Straub, and C. Higgins, "Toward a probabilistic acoustic emission source location algorithm: A bayesian approach," *Journal of Sound and Vibration*, vol. 331, no. 19, pp. 4233–4245, 2012.

[68] L. j. DONG and X. b. LI, "Three-dimensional analytical solution of acoustic emission or microseismic source location under cube monitoring network," *Transactions of Nonferrous Metals Society of China*, vol. 22, no. 12, pp. 3087–3094, 2012.

[69] L. Dong, X. Li, and G. Xie, "An analytical solution for acoustic emission source location for known P wave velocity system," *Mathematical Problems in Engineering*, 2014, vol. 2014, Article ID 290686, 6 pages.

[70] F. Leighton and W. I. Duvall, "Least squares method for improving rock noise source location techniques," Bureau of Mines, Washington, DC (USA), Report, 1972.

[71] M. Ge, "Analysis of source location algorithms part ii: iterative methods," *Journal of Acoustic Emission*, vol. 21, no. 1, pp. 29–51, 2003.

[72] L. Geiger, "Probability method for the determination of earthquake epicenters from the arrival time only," *Bull.St.Louis.Univ*, vol. 8, pp. 60–71, 1912.

[73] W. Sachse and Y. Pao, "On the determination of phase and group velocities of dispersive waves in solids," *Journal of Applied Physics*, vol. 49, no. 8, pp. 4320–4327, 1978.

[74] B. A. Zárate, J. M. Caicedo, and P. Ziehl, "Uncertainty quantification of acoustic emission filtering techniques," in *SPIE Smart Structures and Materials+ Nondestructive Evaluation and Health Monitoring*. International Society for Optics and Photonics (SPIE), 2012, pp. 83 410L–83 410L.

[75] *Standard Guide for Determining the Reproducibility of Acoustic Emission Sensor Response*, ASTM International, ASTM E976-15, West Conshohocken, PA, 2015.

APPENDIX A: SOURCE LOCATION SENSITIVITY PLOTS

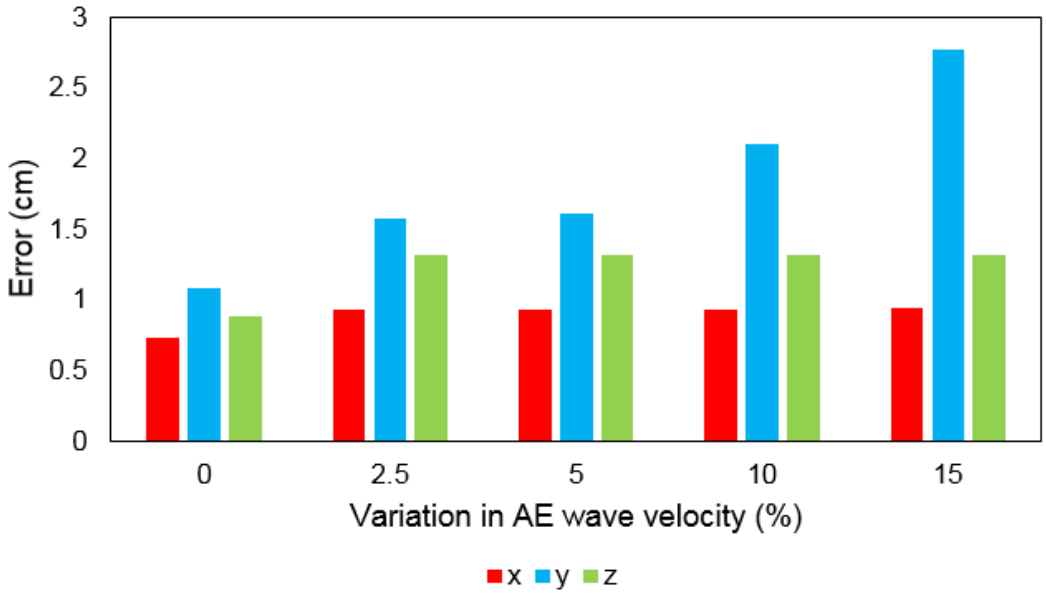

Figure A.1: Sensitivity of source location with different variations in wave velocity at location 1

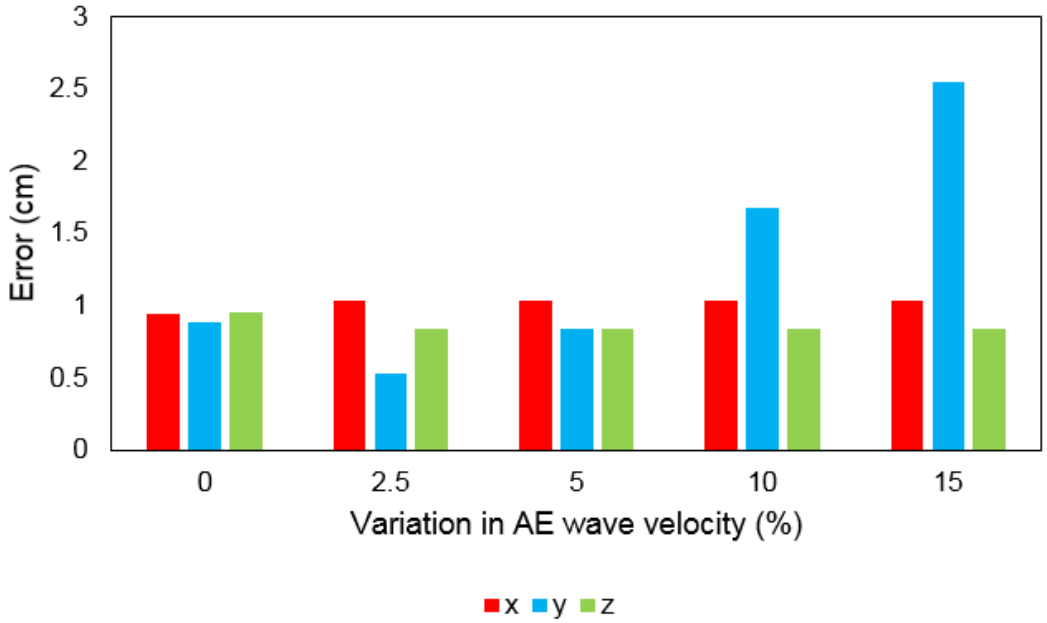

Figure A.2: Sensitivity of source location with different variations in wave velocity at location 2

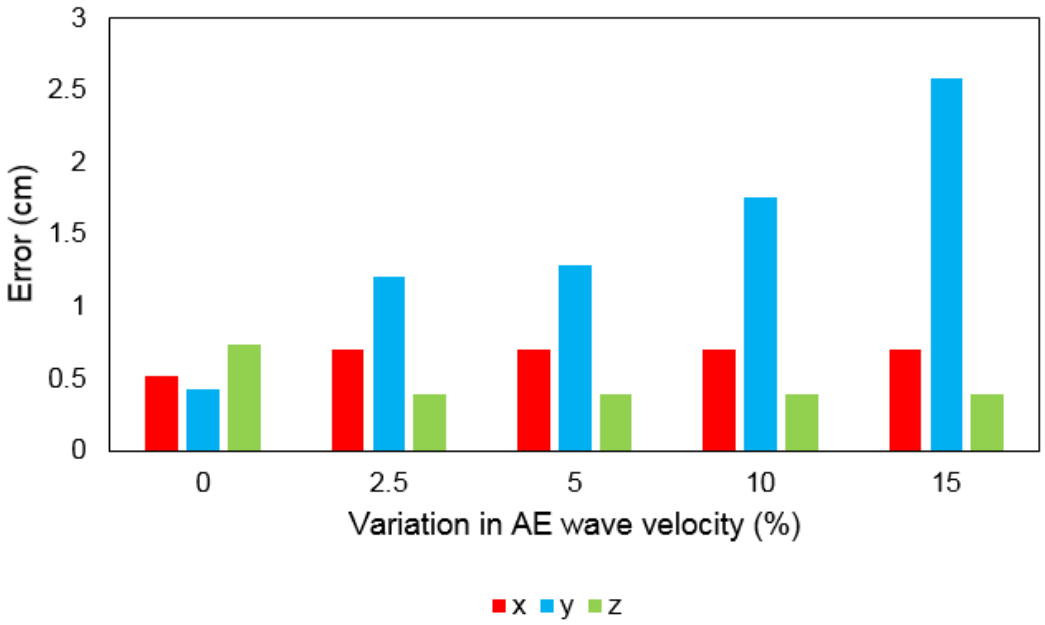

Figure A.3: Sensitivity of source location with different variations in wave velocity at location 3

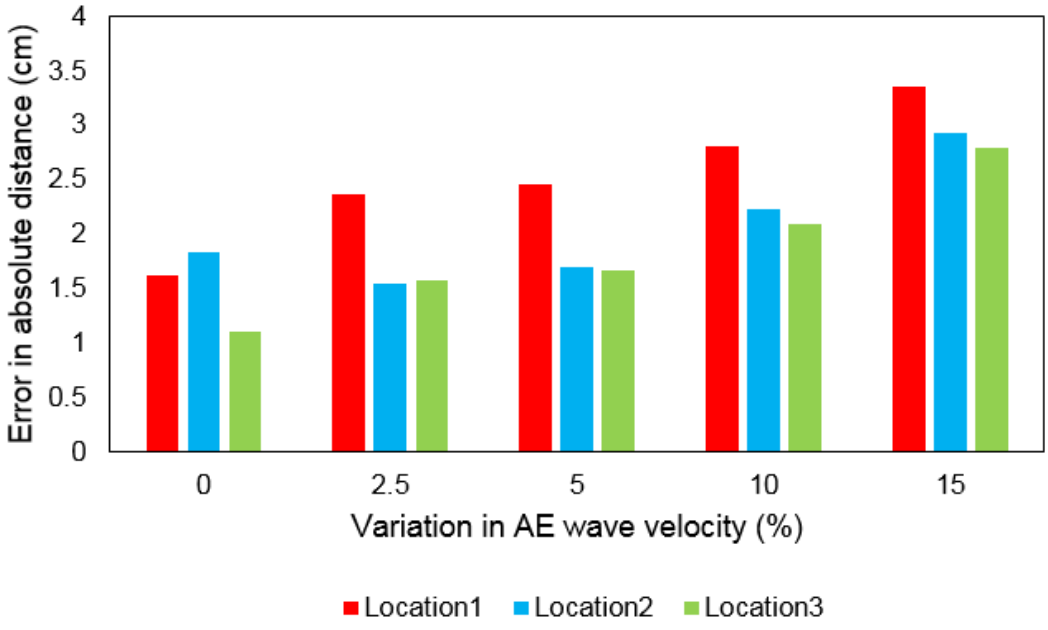

Figure A.4: Sensitivity of source location in absolute distance with different variations in wave velocity

APPENDIX B: AE EVENT COUNTS AND ENERGY PLOTS

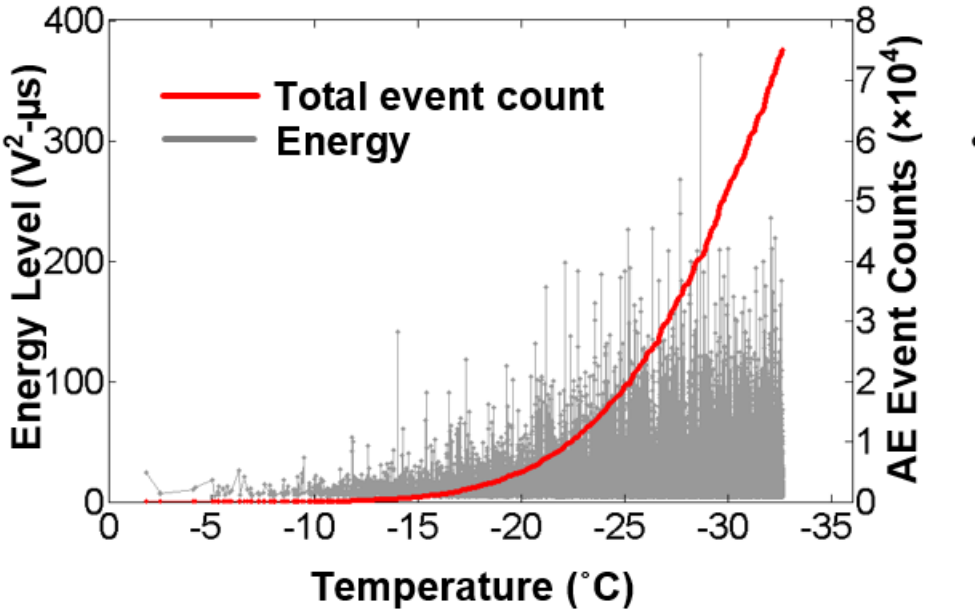

Figure B.1: AE event counts and AE event energy versus temperature for the non-rejuvenated side of asphalt samples oven-aged for 36 hours and exposed to rejuvenator with a dwell time of two weeks

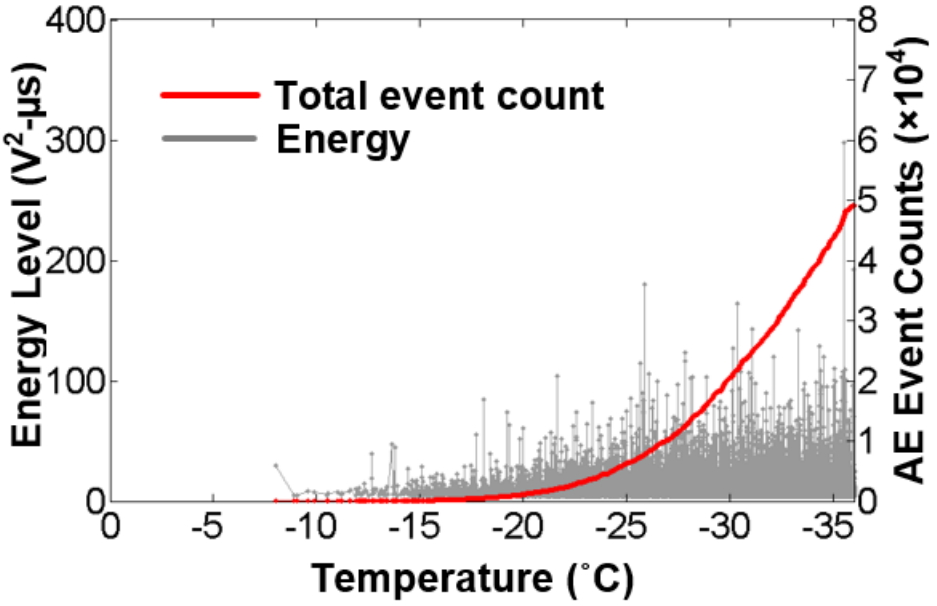

Figure B.2: AE event counts and AE event energy versus temperature for the non-rejuvenated side of asphalt samples oven-aged for 36 hours and exposed to rejuvenator with a dwell time of four weeks

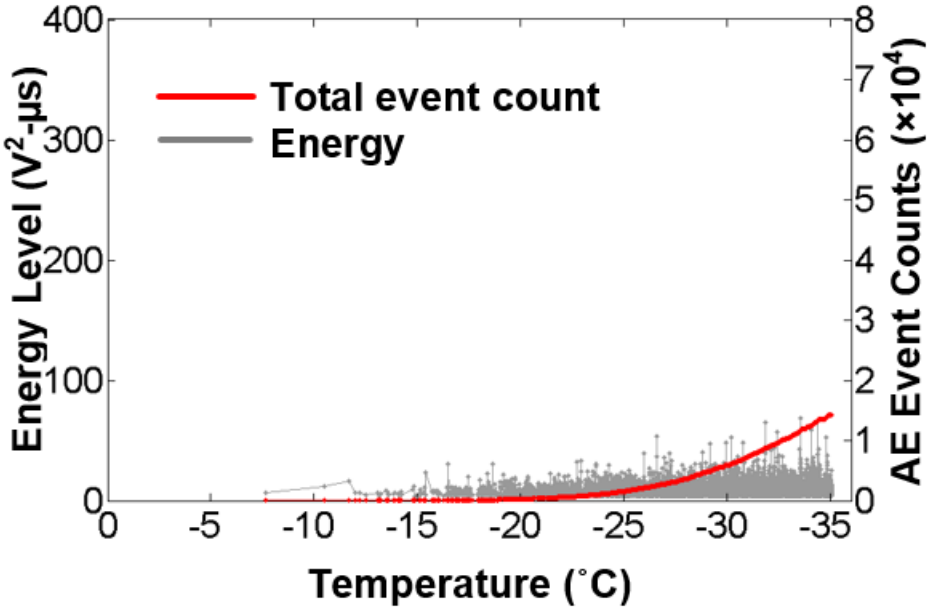

Figure B.3: AE event counts and AE event energy versus temperature for the non-rejuvenated side of asphalt samples oven-aged for 36 hours and exposed to rejuvenator with a dwell time of six weeks

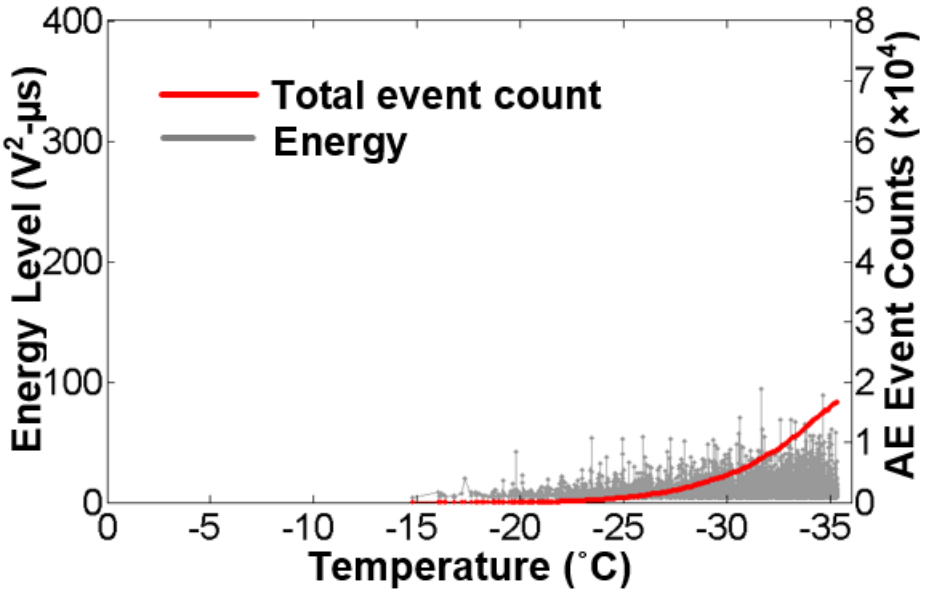

Figure B.4: AE event counts and AE event energy versus temperature for the non-rejuvenated side of asphalt samples oven-aged for 36 hours and exposed to rejuvenator with a dwell time of eight weeks

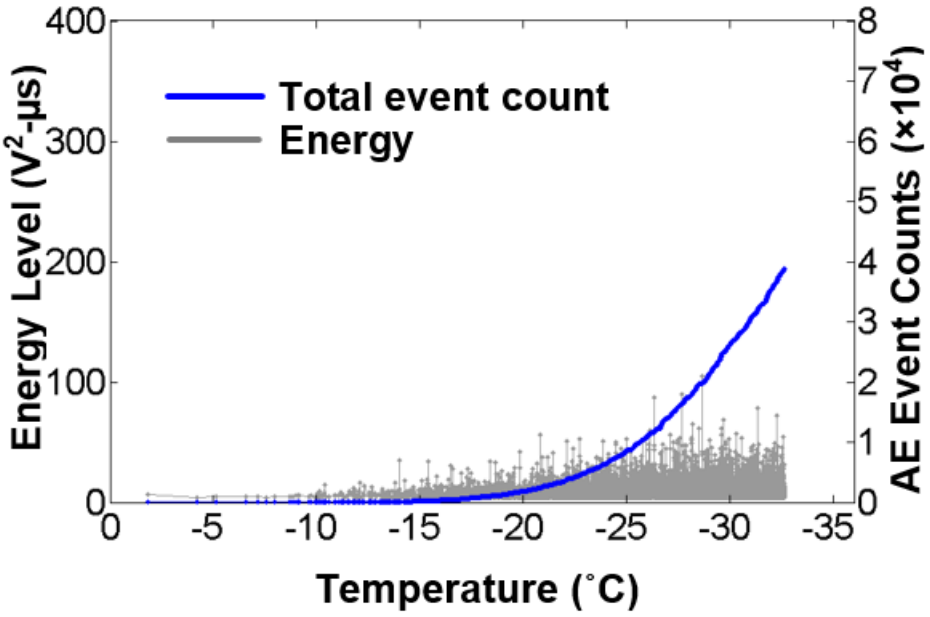

Figure B.5: AE event counts and AE event energy versus temperature for the rejuvenated side of asphalt samples oven-aged for 36 hours and exposed to rejuvenator with a dwell time of two weeks

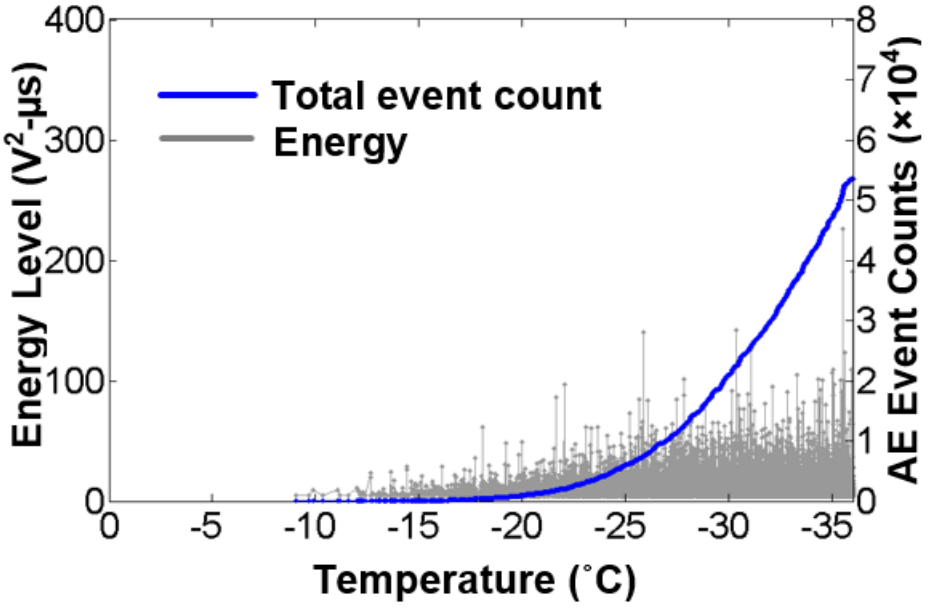

Figure B.6: AE event counts and AE event energy versus temperature for the rejuvenated side of asphalt samples oven-aged for 36 hours and exposed to rejuvenator with a dwell time of four weeks

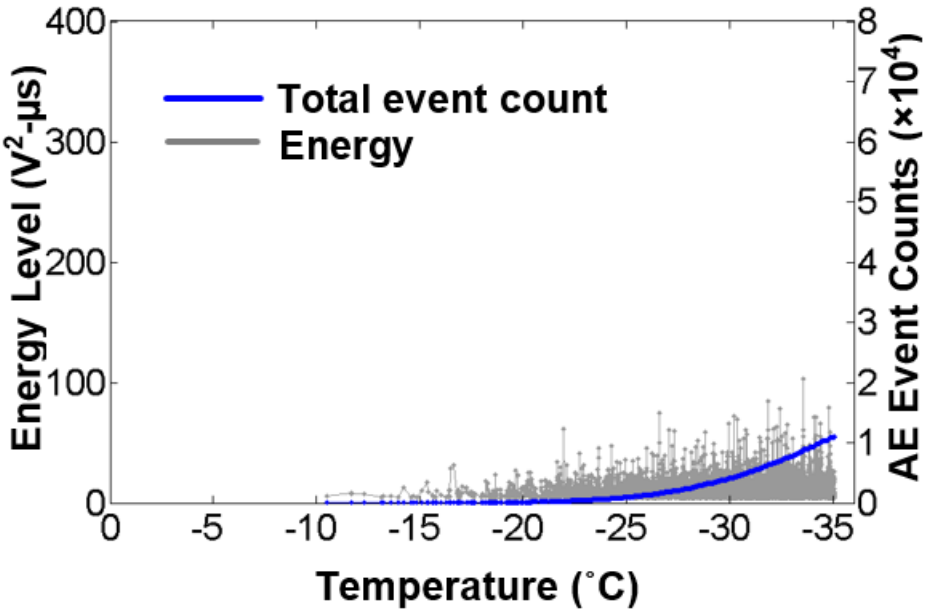

Figure B.7: AE event counts and AE event energy versus temperature for the rejuvenated side of asphalt samples oven-aged for 36 hours and exposed to rejuvenator with a dwell time of six weeks

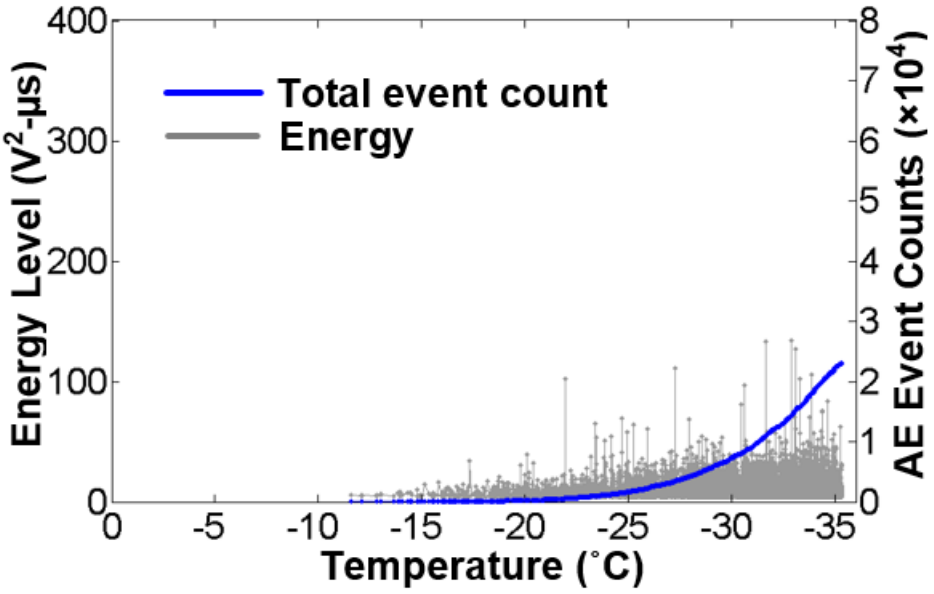

Figure B.8: AE event counts and AE event energy versus temperature for the rejuvenated side of asphalt samples oven-aged for 36 hours and exposed to rejuvenator with a dwell time of eight weeks

APPENDIX C: AE EVENT RATE AND ENERGY PLOTS

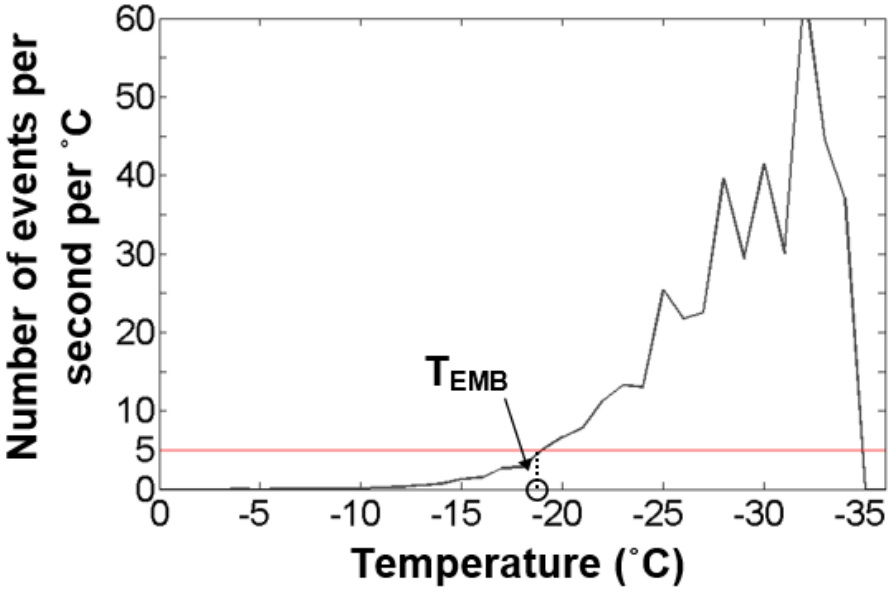

Figure C.1: Average rate of increase in AE event counts versus cooling temperature on the non-rejuvenated side of asphalt concrete samples oven-aged for 36 hours and exposed to rejuvenator with a dwell time of two weeks, and the corresponding embrittlement temperatures

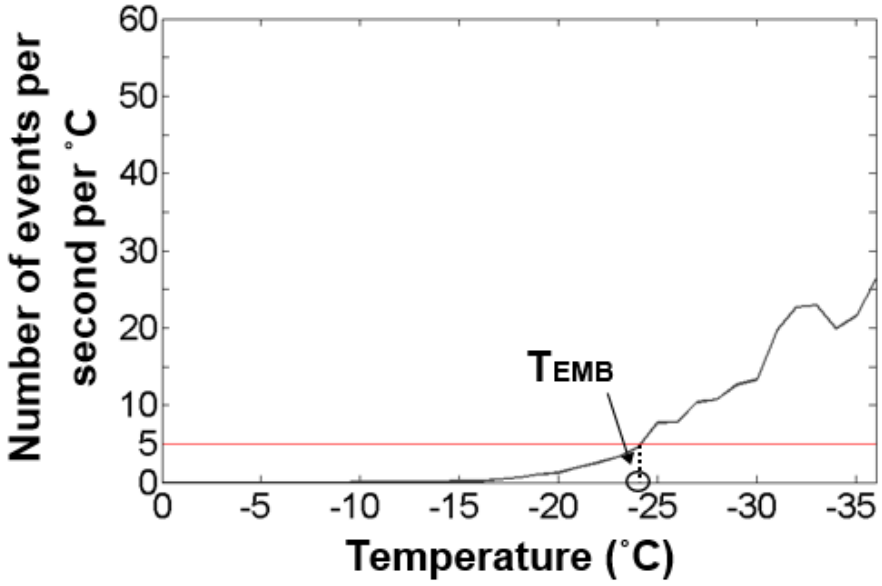

Figure C.2: Average rate of increase in AE event counts versus cooling temperature on the non-rejuvenated side of asphalt concrete samples oven-aged for 36 hours and exposed to rejuvenator with a dwell time of four weeks, and the corresponding embrittlement temperatures

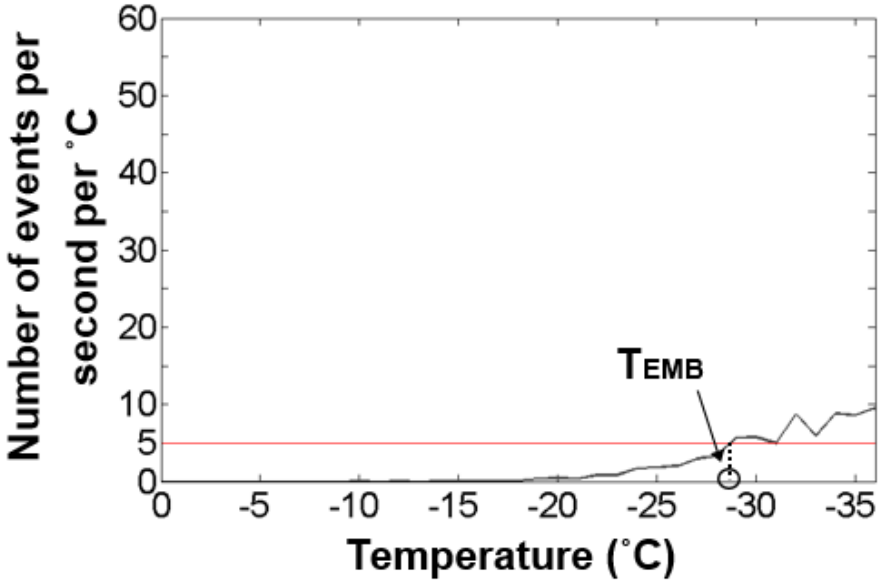

Figure C.3: Average rate of increase in AE event counts versus cooling temperature on the non-rejuvenated side of asphalt concrete samples oven-aged for 36 hours and exposed to rejuvenator with a dwell time of six weeks, and the corresponding embrittlement temperatures

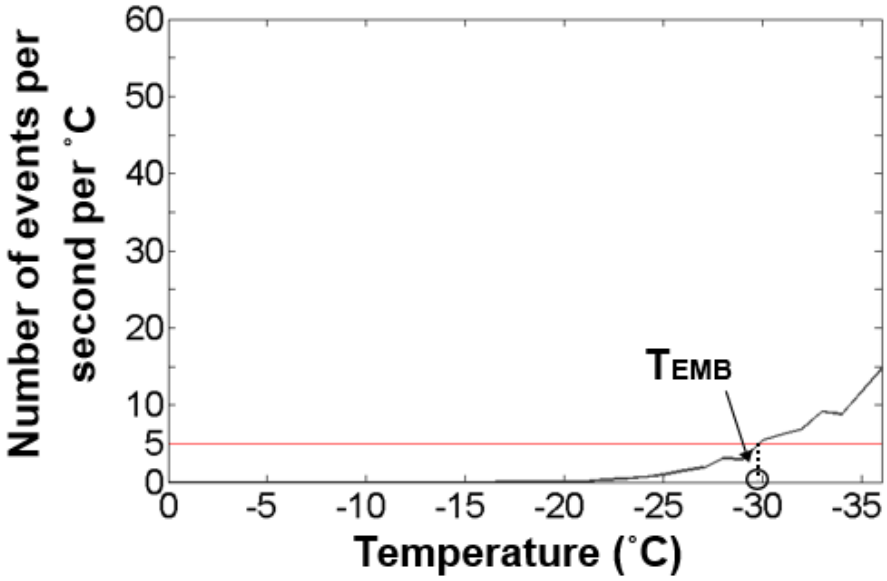

Figure C.4: Average rate of increase in AE event counts versus cooling temperature on the non-rejuvenated side of asphalt concrete samples oven-aged for 36 hours and exposed to rejuvenator with a dwell time of eight weeks, and the corresponding embrittlement temperatures

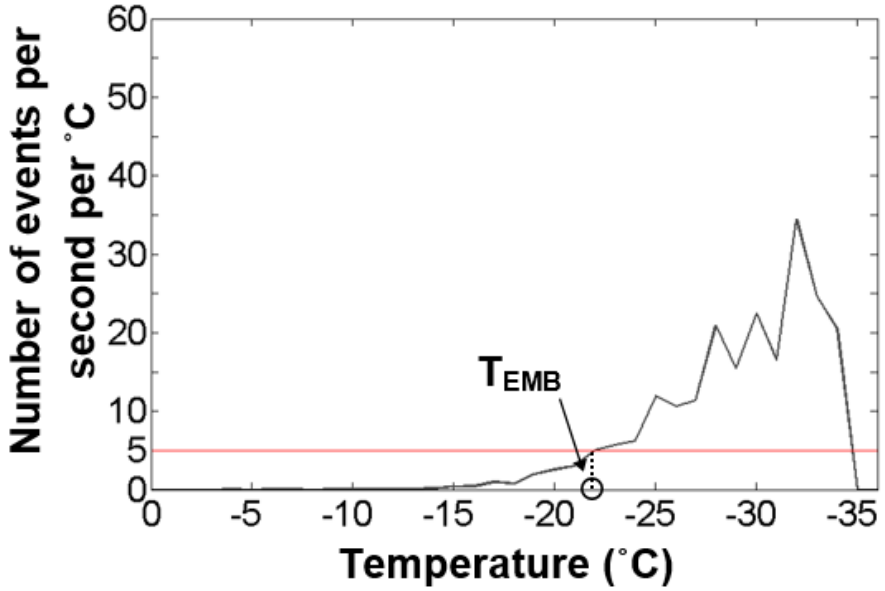

Figure C.5: Average rate of increase in AE event counts versus cooling temperature on the rejuvenated side of asphalt concrete samples oven-aged for 36 hours and exposed to rejuvenator with a dwell time of two weeks, and the corresponding embrittlement temperatures

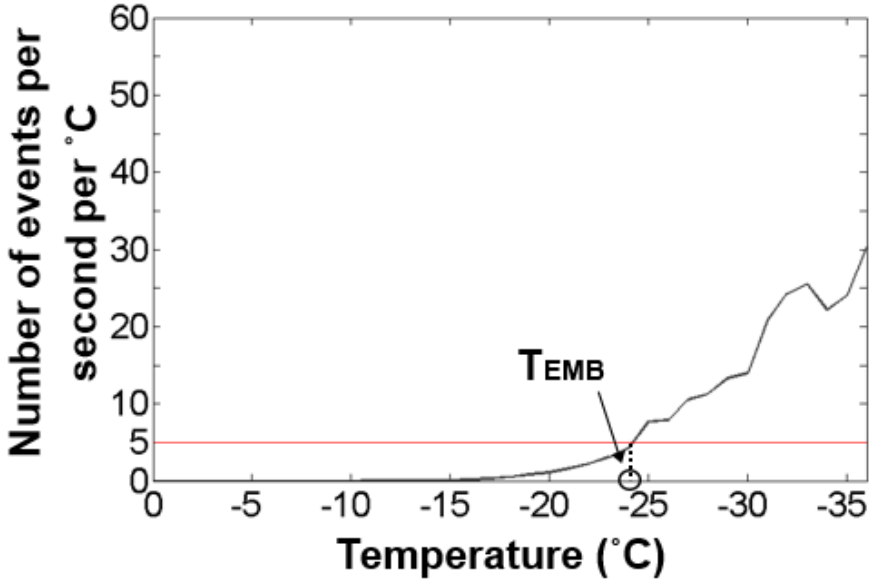

Figure C.6: Average rate of increase in AE event counts versus cooling temperature on the rejuvenated side of asphalt concrete samples oven-aged for 36 hours and exposed to rejuvenator with a dwell time of four weeks, and the corresponding embrittlement temperatures

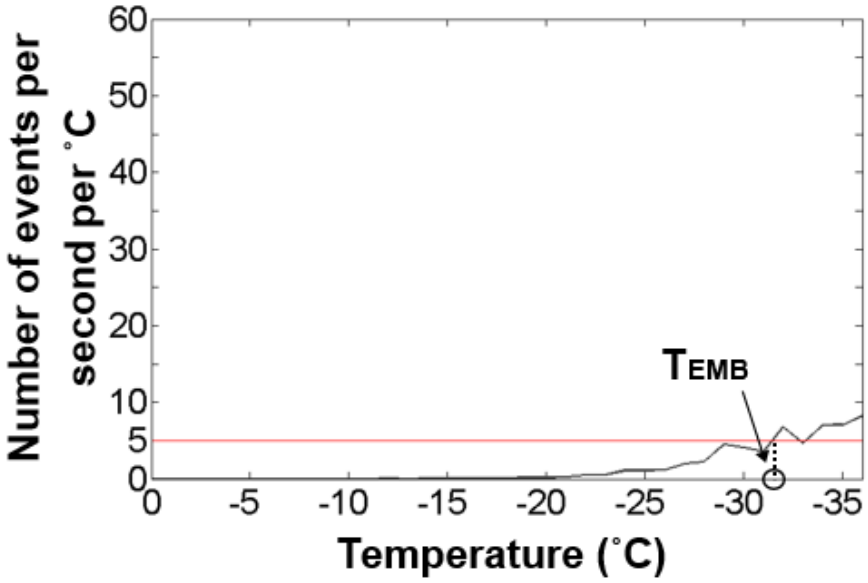

Figure C.7: Average rate of increase in AE event counts versus cooling temperature on the rejuvenated side of asphalt concrete samples oven-aged for 36 hours and exposed to rejuvenator with a dwell time of six weeks, and the corresponding embrittlement temperatures

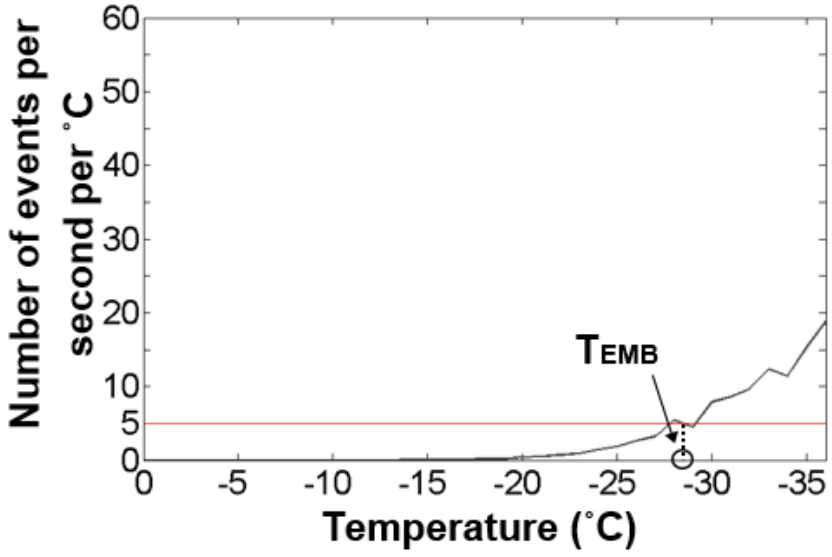

Figure C.8: Average rate of increase in AE event counts versus cooling temperature on the rejuvenated side of asphalt concrete samples oven-aged for 36 hours and exposed to rejuvenator with a dwell time of eight weeks, and the corresponding embrittlement temperatures

APPENDIX D: EMBRITTLEMENT TEMPERATURES FOUND USING DIFFERENT THRESHOLD INCREASING RATES

This appendix aims to evaluate the effect of different threshold AE event increasing rates on embrittlement temperature estimation results using the iterative Geiger's method on the 36-hour aged, virgin and rejuvenated asphalt specimens. In Section 6.2.1, embrittlement temperature of the asphalt concrete was estimated based on the average occurring temperature of the AE events when the event increasing rate reaches a threshold value of 10 events per 1 minute per 0.5 cm interval. Changing this threshold value will alter the average embrittlement temperatures. The idea is to choose an appropriate threshold rate so that the embrittlement temperatures found using source location results for 36-hour aged specimen and virgin specimen match with the known embrittlement temperatures found in previous studies. Embrittlement temperature estimation results obtained using different threshold increasing rates are presented here. The results are presented graphically, with the average embrittlement temperature across the height of each specimen labeled.

D.1 Threshold Increasing Rate: 30 Emissions Per 3 Minutes Per 0.5 cm

In Section 6.2.1, the process of finding the starting point of the stable crack region is described as moving a box (5mm vs. 1 min) to the left until it encloses 10 emissions, which defines the embrittlement temperature at the centroid of the box. This process is demonstrated in Figure D.1(a).

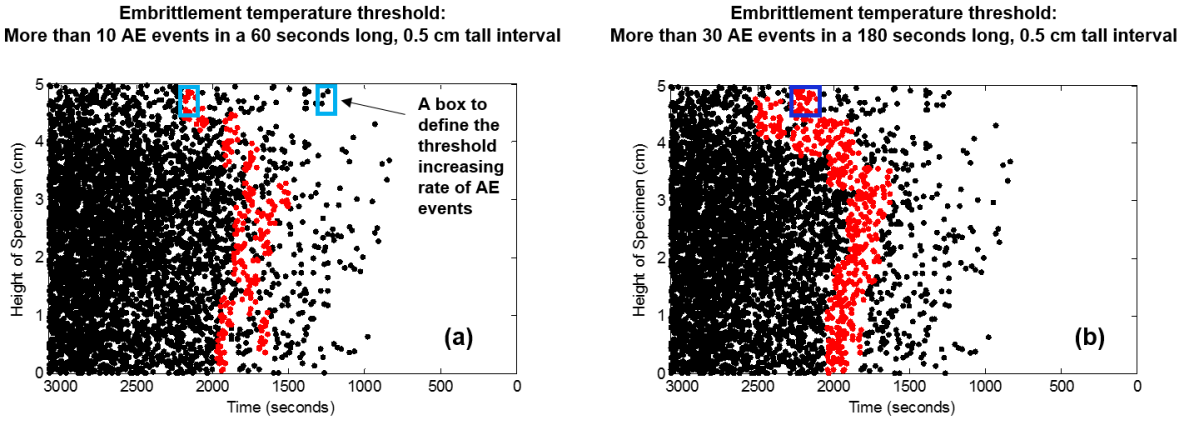

Figure D.1: The process of finding the beginning of the stable crack region using the threshold increasing rate of (a) 10 emission per 1 minute per 0.5 cm and (b) 30 emissions per 3 minutes per 0.5 cm.

An increasing rate of 30 emissions per 3 minutes is physically equivalent to 10 emissions per minute, but it makes a difference when this rate is used to determine the embrittlement temperature using source location results. If the time interval used to calculate the increasing rate of AE events is increased, the size of the box indicated in Figure D.1(a) actually is increased to the size of the box in Figure D.1(b). This change could affect the embrittlement temperatures estimated by using the average occurring temperature of all the events enclosed within the box. It can be observed from the comparison between the results shown in Figure 6.11 and Figure D.3 that using 30 emissions per 3 minutes as the threshold increasing rate will obtain a lower embrittlement temperature for both 36-hour aged and virgin specimen. For 36-hour aged specimen, the average embrittlement temperature changes from -13 $^{\circ}C$ to -14 $^{\circ}C$. For virgin specimen, the embrittlement temperature changes from -22 $^{\circ}C$ to -22.5 $^{\circ}C$.

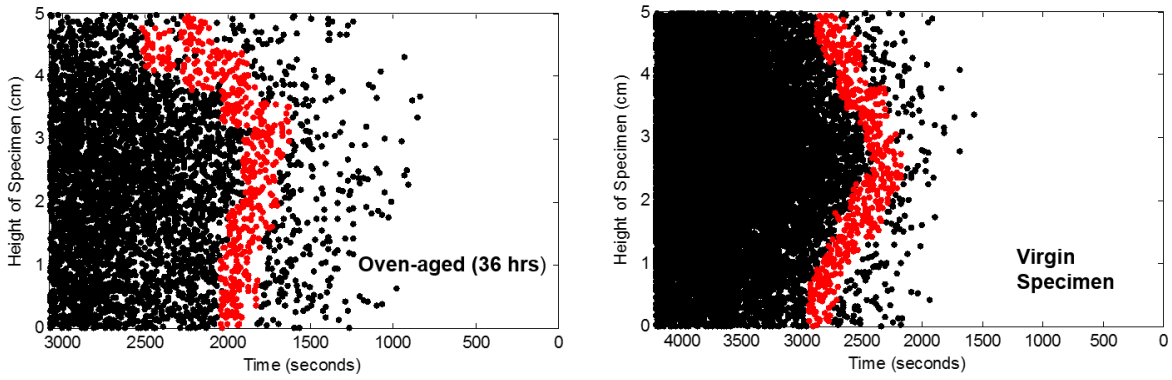

Figure D.2: The beginning of the stable crack region for 36-hour aged and virgin specimen using 30 emissions per 3 minutes per 0.5 cm as the threshold increasing rate

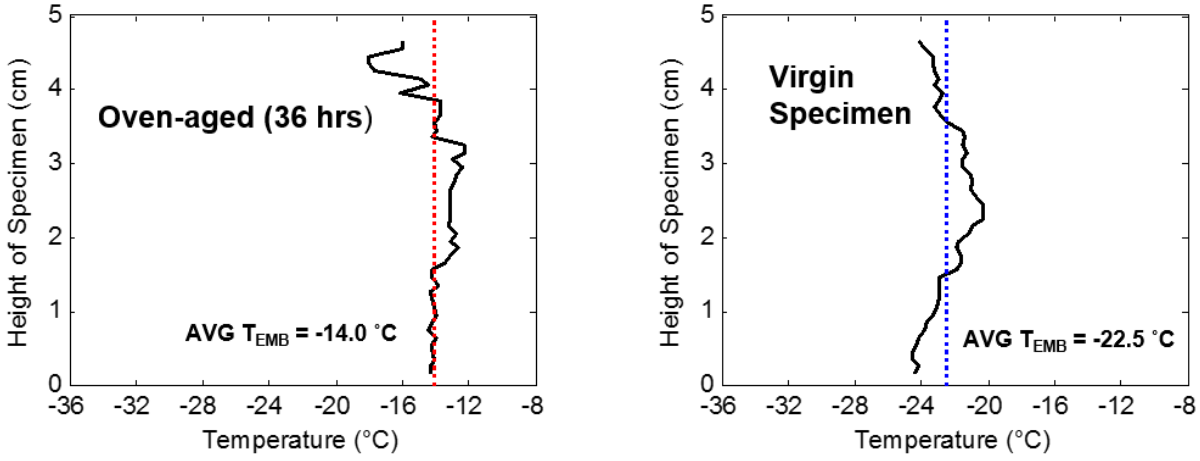

Figure D.3: The estimation of embrittlement temperature using 30 emissions per 3 minutes per 0.5 cm as the threshold increasing rate: (a) average embrittlement temperature at each height interval of asphalt concrete samples oven-aged for 36-hours, (b) average embrittlement temperature at each height interval of the virgin asphalt specimens.

Figure D.4 shows the beginning of stable crack region for the four rejuvenated specimens after exposed to rejuvenator

with the dwell times of two, four, six and eight weeks, obtained using 30 emissions per 3 minutes as the threshold increasing rate. Figure D.5 shows the relationship between embrittlement temperatures and the height of AE sources for the four rejuvenated specimens. An interesting observation can be made from Figure D.4(c), Figure D.4(d), Figure D.5(c) and Figure D.5d. For the 6-week and 8-week specimens, the distribution of AE events across their heights is more sparse compared to the 2-week and 4-week specimens. When the size of the box is changed from 0.5 cm vs. 1 minute to 0.5 cm vs. 3 minutes, the box does not necessarily enclose three times of AE events at the same cooling time. As a result, the embrittlement temperatures at different heights cannot be entirely captured for the 6-week specimen and 8-week specimen as shown in Figure D.4(c) and Figure D.4(d). Assuming the cooling continues below -35 $^{\circ}C$, the estimated embrittlement temperatures for 6-week and 8-week specimens would become much lower than -35 $^{\circ}C$. The embrittlement temperatures across the height of the specimen would become very inconsistent. Hence, the results will make more sense if the threshold increasing rate is computed in a smaller time interval. In this case, using 10 emissions per 1 minute as the threshold increasing rate is preferred.

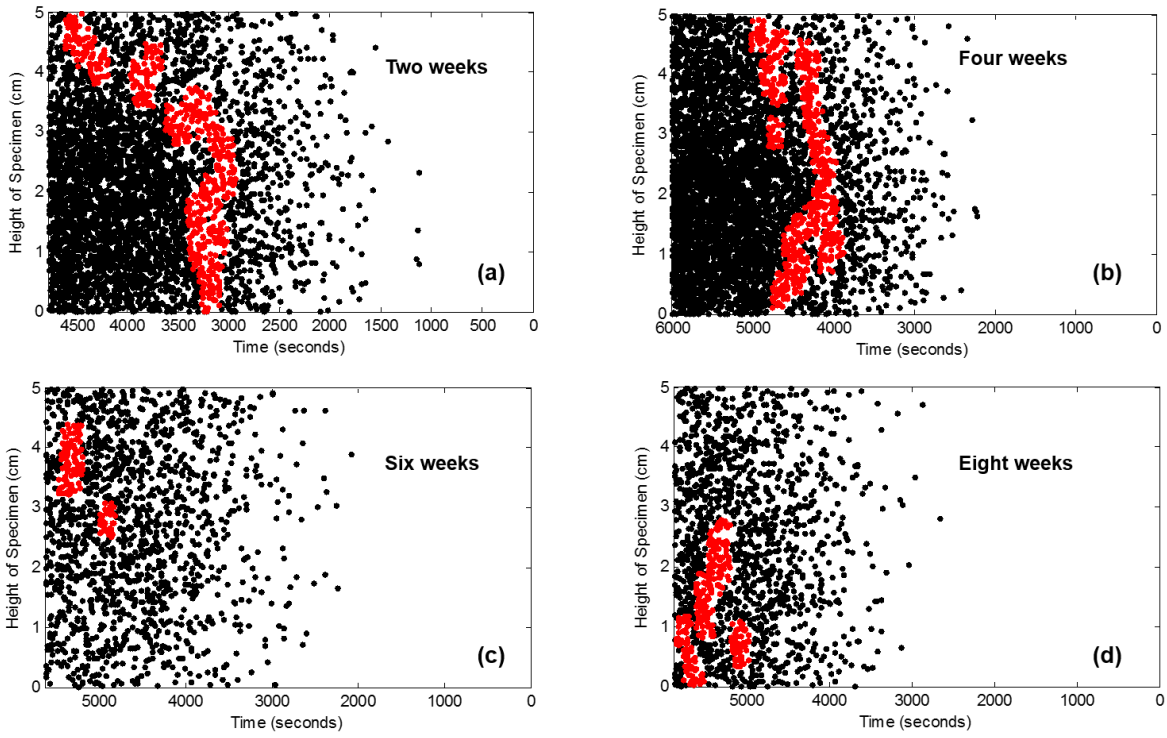

Figure D.4: The beginning of the stable crack region for for 36-hour aged specimens exposed to rejuvenator with a dwell time of (a) two weeks, (b) four weeks, (c) six weeks and (d) eight weeks using 30 emissions per 3 minutes per 0.5 cm as the threshold increasing rate

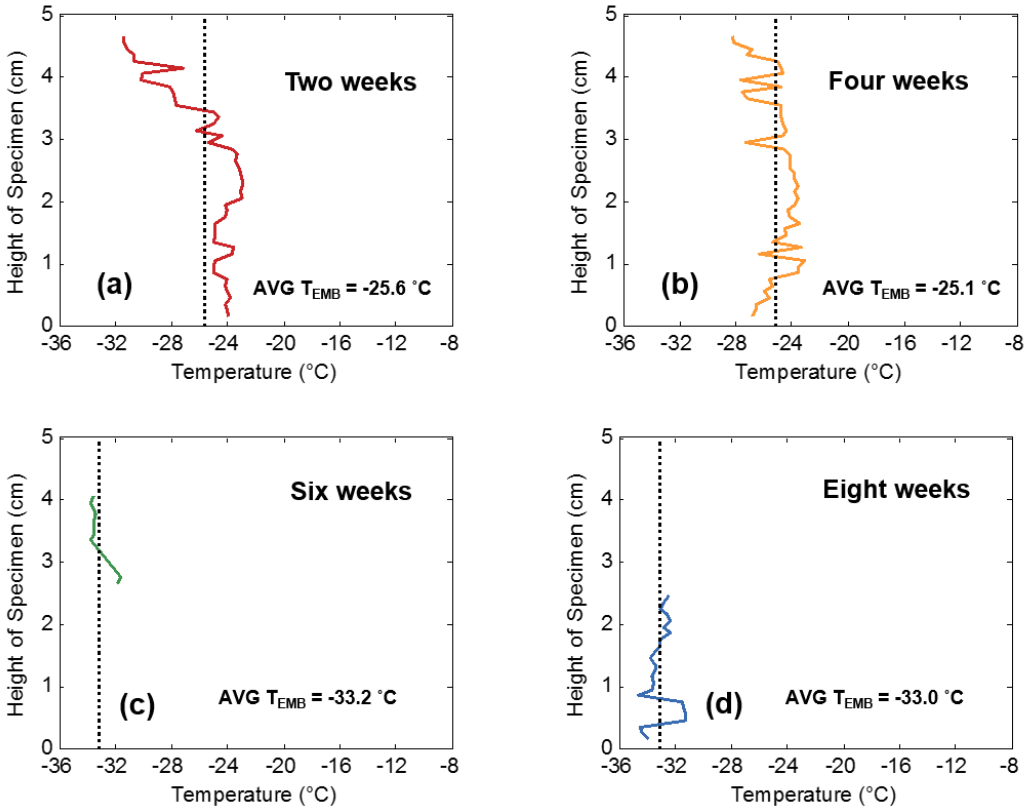

Figure D.5: Embrittlement temperature at each height interval of asphalt samples oven-aged for 36 hours and exposed to rejuvenator with a dwell time of (a) two weeks, (b) four weeks, (c) six weeks and (d) eight weeks

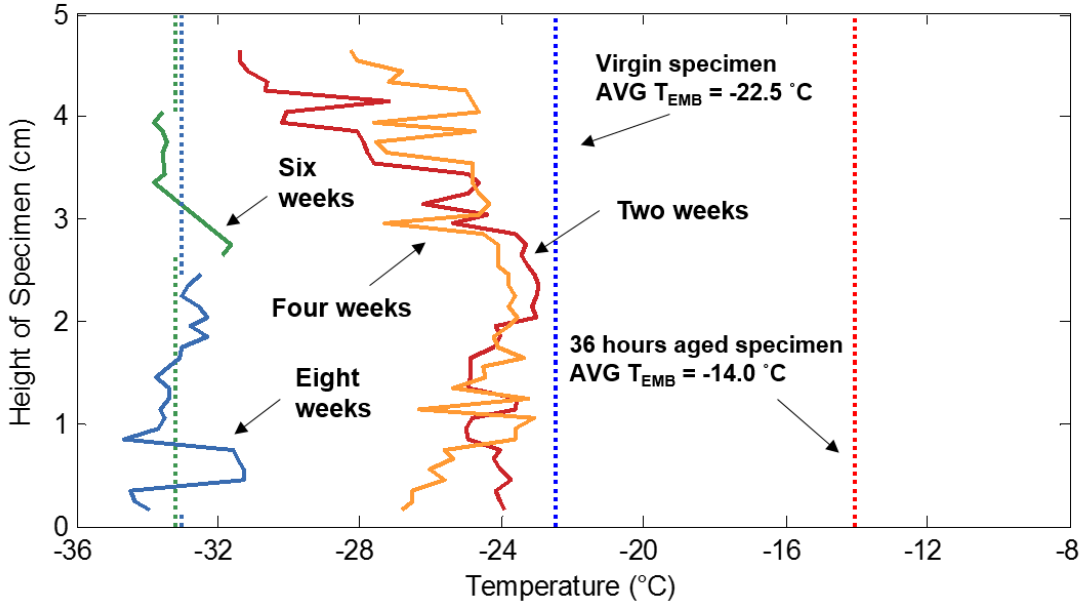

Figure D.6: Combined embrittlement temperature results for the asphalt specimens

D.2 Threshold Increasing Rate: 15 Emissions Per 3 Minutes Per 0.5 cm

If the threshold increasing rate is relaxed from 30 emissions per 3 minutes to 15 emissions per 3 minutes, it can be observed from Figure D.7 that the beginning of the stable crack region (represented by the red dots) shifts to the right with respect to Figure D.2.

The subsequent average embrittlement temperature increases to -12 $^{\circ}C$ for 36-hour aged specimen and -21.2 $^{\circ}C$ for virgin specimen by comparing the embrittlement temperature plots in Figure D.3 and Figure D.8.

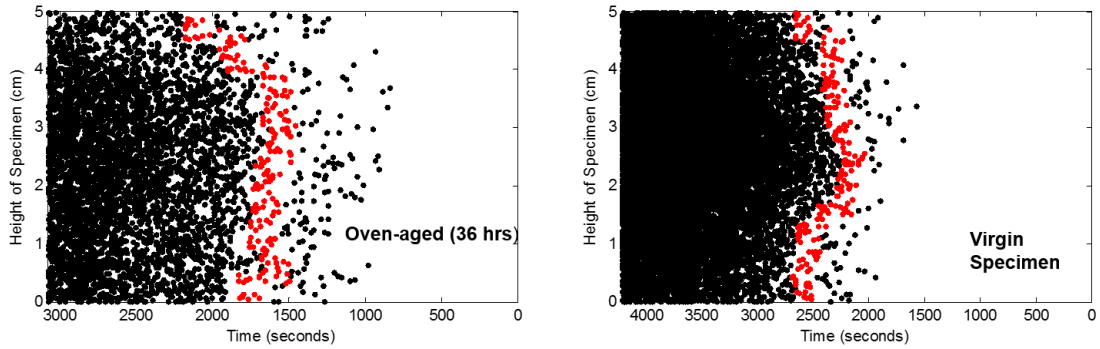

Figure D.7: The beginning of the stable crack region for 36-hour aged and virgin specimen using 15 emissions per 3 minutes per 0.5 cm as the threshold increasing rate

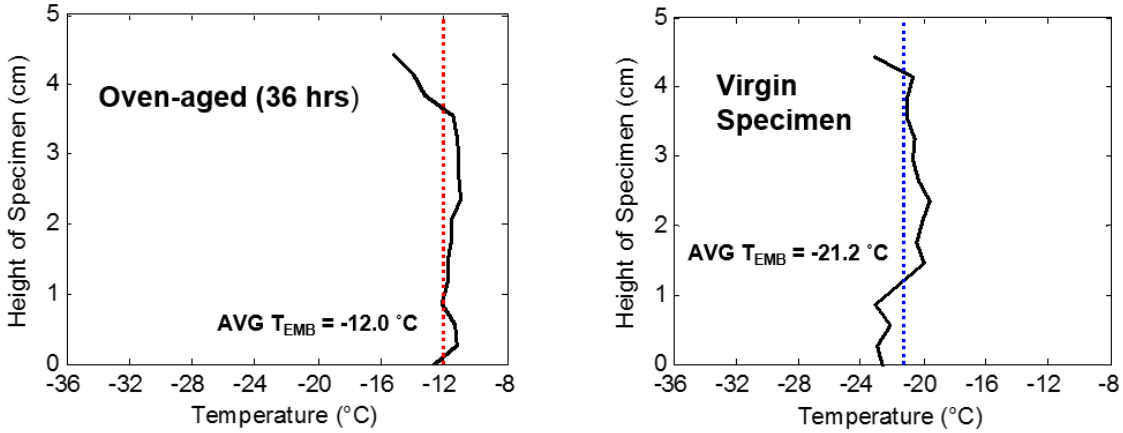

Figure D.8: The estimation of embrittlement temperature using 15 emissions per 3 minutes per 0.5 cm as the threshold increasing rate. (a) Average embrittlement temperature at each height interval of asphalt concrete samples oven-aged for 36-hours. (b) Average embrittlement temperature at each height interval of the virgin asphalt specimens

By averaging the occurring temperatures of the events colored in red in Figure D.9, Figure D.10 shows the relationship between embrittlement temperatures and the height of AE sources for the four rejuvenated specimens. As compared to Figure D.5, the average embrittlement temperature is able to be computed for every portion of the 6-week and 8-week specimens in Figure D.10.

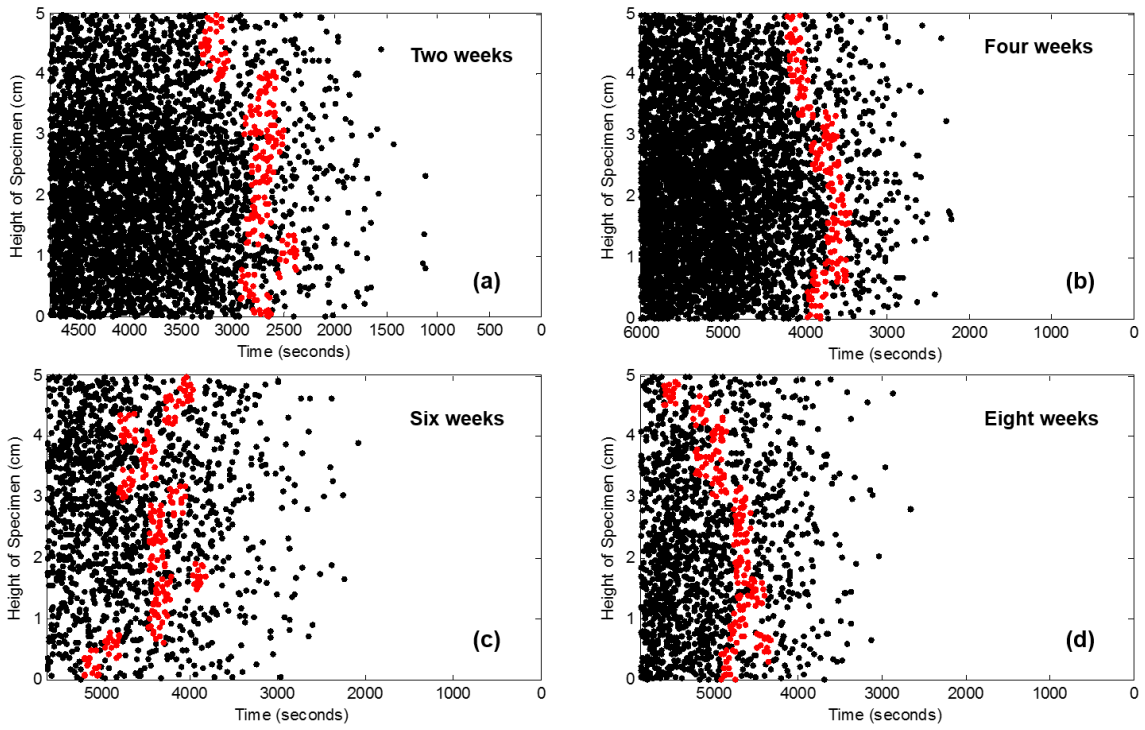

Figure D.9: The beginning of the stable crack region for for 36-hour aged specimens exposed to rejuvenator with a dwell time of (a) two weeks, (b) four weeks, (c) six weeks and (d) eight weeks using 15 emissions per 3 minutes per 0.5 cm as the threshold increasing rate

However, this threshold increasing rate is not ideal. With reference to Figure D.8, the average embrittlement temperatures for 36-hour aged specimen and virgin specimen are -12 $^{\circ}C$ and -21.2 $^{\circ}C$ respectively. These embrittlement temperatures are considered to be too warm as compared to the embrittlement temperatures obtained in previous studies ($\sim$ -15$^{\circ}C$ for 36-hour aged specimen and $\sim$ -25 $^{\circ}C$ for virgin specimen) [10–12, 17, 18, 54].

The comparison among the embrittlement temperature results obtained using different threshold increasing rates in this appendix suggests that a change in the threshold increasing rate will affect the embrittlement temperatures estimated from the source location results. A high threshold increasing rate will result in lower embrittlement temperatures, which may exceed the lowest cooling temperature limit in the cooling test and the results are not reliable anymore. If the threshold increasing rate is too low, the obtained embrittlement temperatures will be too warm to be consistent with the embrittlement temperatures obtained using standard tests.

Therefore, the threshold increasing rate must be chosen carefully to estimate the embrittlement temperatures using the source location results, so that the estimated embrittlement temperatures for 36-hour aged specimen and virgin specimen are not only within the valid range, but close to the values obtained using other standard testing methods as well. In this study, 10 emissions per 1 minute per 0.5 cm interval is considered as a reasonable threshold increasing

rate to be used for estimation of embrittlement temperatures.

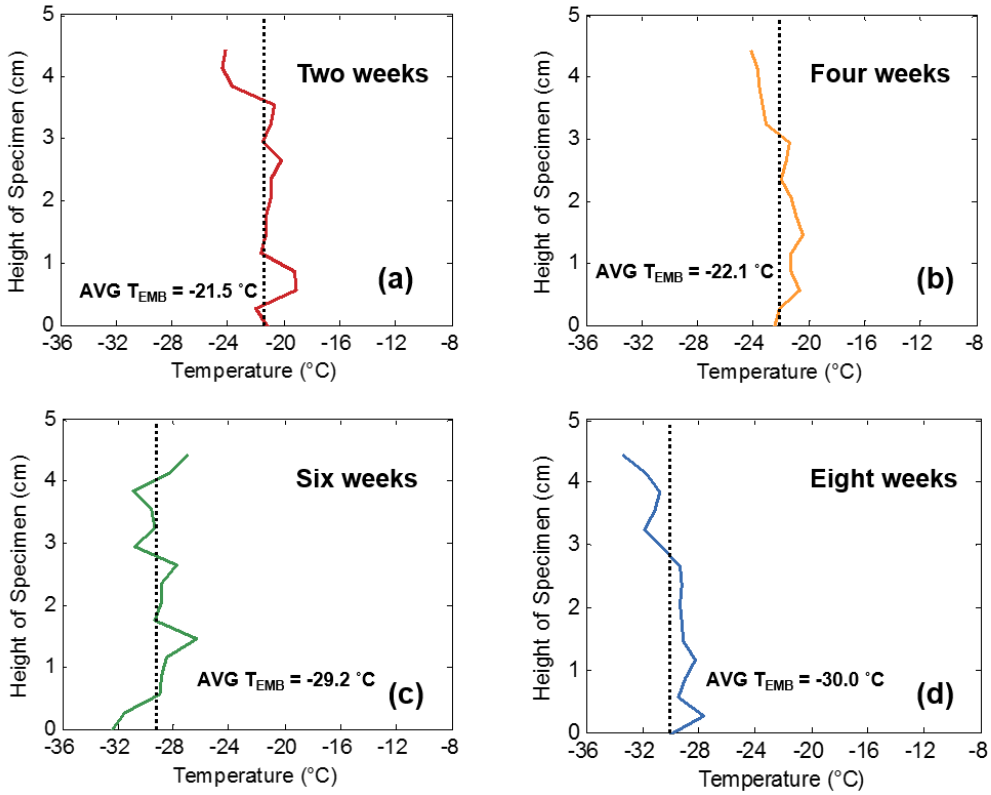

Figure D.10: Embrittlement temperature at each height interval of asphalt samples oven-aged for 36 hours and exposed to rejuvenator with a dwell time of (a) two weeks, (b) four weeks, (c) six weeks and (d) eight weeks

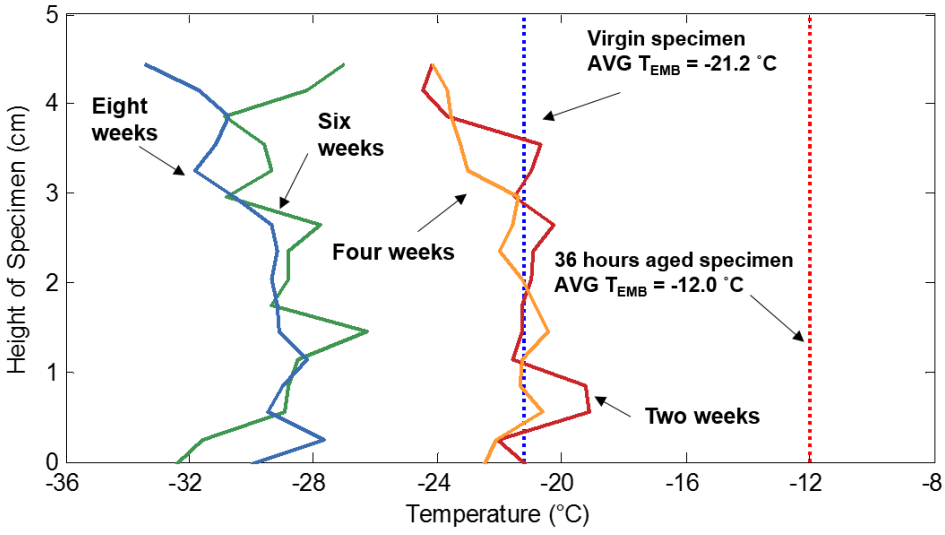

Figure D.11: Combined embrittlement temperature results for the asphalt specimens